A Thesis for the Degree of Ph.D. in Engineering

A Study on Interference Modelling, Management and Avoidance in Wireless Communication Systems

August 2016

Graduate School of Science and Technology
Keio University
Fereidoun H. Panahi

Acknowledgements

I would initially like to express my deepest gratitude to my supervisor Prof. Tomoaki Ohtsuki for all his support, advice and encouragement during my Master and Ph.D. periods. The committee members, Prof. Iwao Sasase, Prof. Yukitoshi Sanada, Prof. Hiroshi Shigeno and Prof. P.Y. Kam deserve a special mention. I would like to thank them for their precious time and advice that helped improve the quality of this dissertation.

I would like to express my appreciation to the Ministry of Education, Culture, Sports, Science and Technology (MEXT) of Japan for the Japanese government (Monbusho) scholarship, which supported my stay at Keio University as Ph.D. student. I would like to thank the JGC-S scholarship foundation (Nikki Saneyoshi/Daisanshu), and the Japanese government for the JASSO Honors scholarship, which supported my stay at Keio University as Master student. I am also very grateful for receiving the Keio graduate School Scholarship, administered by the student affairs center at Keio University. My special thanks are extended to the research development and sponsored project section at Keio University for the Keio University doctorate student grant-in-aid program, which supported most of my research activities in Japan for 2 years; providing research funding to purchase equipment, and research trips to domestic and international conferences. Assistance provided by the following organizations is also greatly appreciated: Keio Leading Edge Laboratory (KLL), for offering a research grant to support my research activities and trips to domestic and international conferences, NEC C&C foundation for funding my attendance to IEEE international conferences. Finally, I would like to express my sincere gratitude to the Japan Society for Promotion of Science (JSPS) for making it possible to be the JSPS Research Fellow (DC2). The financial support and special grant provided by the JSPS is also gratefully acknowledged.

I would also like to thank my lovely sisters and brothers who always take care of me: Farhad, Galavezh, Zhila, and Dr. Farzad H. Panahi. My friends and colleagues also deserve a special thanks and mention: Dr. Jihoon Hong, Dr. Juan Camilo Cornea, Dr. Kentaroh Toyoda and Anthony Beylerian. My final and the most valuable thanks go to two very special people in my entire life. Firstly, to my father, thanks for all your support and love throughout my life. Last but certainly not least, I would like to thank my lovely mother for all her love, support and patience.

Table of Contents

List of Tables

List of Figures

A Study on Interference Modelling, Management and Avoidance in Wireless Communication Systems

Fereidoun H. Panahi
fereidoun@ohtsuki.ics.keio.ac.jp
Keio University, 2016
Supervisor: Prof. Tomoaki Ohtsuki, Ph.D.
ohtsuki@ics.keio.ac.jp

Abstract

The best solution to the spectrum saturation and bandwidth availability problems in wireless networks is to adopt technologies that make the most efficient use of existing spectrum through frequency reuse schemes. For example, in universal frequency reuse schemes, the existing spectrum can be aggressively and effectively reused by all of the coexisting users in the network. This will lead to higher spatial spectrum utilization and network usage capacity at the expense of an increased possibility of interference among network users and of a reduced quality of service (QoS). In other words, interference is increasingly becoming a major performance-limiting factor, and hence, interference modeling, management and avoidance are the primary focus of interest for both the industry and academic communities. This dissertation is concerned with providing mechanisms on interference modeling, management and avoidance to improve performance on both user and network scales. In particular, we will explore and provide solutions to challenges due to interference in different scenarios and networks, namely in cognitive radio (CR) networks,

heterogeneous cellular networks, and multiple-input multiple-output (MIMO) interference channels (ICs).

Chapter 1 presents an introduction to the interference issue of different wireless communication environments, appropriate solutions and troubleshooting procedures of eliminating interference to improve the user experiences and QoS. The chapter ends with the scope and contributions of this dissertation.

Chapter 2 studies the interference management issue in CR networks. In a CR network, the channel sensing scheme used to detect the existence of a primary user (PU) directly affects the performances of both CR and PU. However, in practical systems, the CR is prone to sensing errors due to the inefficiency of the sensing scheme. This may yield PU interference and low system performance. We present a learning-based scheme for channel sensing in CR networks. Specifically, we formulate the channel-sensing problem as a partially observable Markov decision process (POMDP), where the most likely channel state is derived by a learning process called fuzzy Q-learning (FQL). The optimal policy is derived by solving the problem. Using our proposed sensing scheme, the CR-enabled user can significantly improve its own spectral efficiency and reduce the probability of interfering with the PU.

Chapter 3 deals with the interference challenges in heterogeneous cellular networks. We present a CR based statistical framework for a two-tier heterogeneous cellular network (femto-macro network) to model the outage probability at any arbitrary secondary (femto) and primary (macro) user. A system model based on stochastic geometry (utilizing the spatial Poisson point process (PPP) theory) is applied to model the random locations and network topology of both secondary and primary users. A considerable performance improvement can be generally achieved by mitigating interference in result of applying the CR idea over the above model. Novel closed-form expressions are then derived for the downlink outage probability of any typical femto and macro user considering the Rayleigh fading for the desired and interfering links. Some important design factors that their role and importance in the determination of outage and interference cannot be ignored will be also studied. Simulations are conducted to validate our analytical results and evaluate the

proposed schemes in terms of outage probability for different values of signal-to-interference-plus-noise-ratio (SINR) target.

In Chapter 4, we similarly present a CR based statistical framework for a femto-macro network to model the outage probability at any arbitrary secondary and primary user. A system model based on stochastic geometry utilizing the spatial PPP theory is applied to model the random locations and network topology of both secondary and primary users. Unlike the previous chapter that Rayleigh fading assumption is used to relax the difficulty of addressing a closed-form expression for the outage probability, in this chapter novel closed-form expressions are derived for the outage probability of any typical femto and macro user considering the Nakagami-m fading for each desired and interference links. We also study some important design factors, which their important role in the determination of outage and interference cannot be ignored. We conduct simulations to validate our analytical results and evaluate the proposed schemes in terms of outage probability for different values of SINR target.

Chapter 5 focuses on the interference avoidance in MIMO ICs. Interference alignment (IA) has emerged as a viable transmission technique towards mitigating interference that can result in sum-rates that scale linearly with the number of users in the system for high signal-to-noise power ratio (SNR). We present three iterative IA algorithms for the problem of joint power allocation and transmit/receive filter design in a K-user MIMO IC. The optimality criterion is based on the achievable sum-rate and the average per user multiplexing gain in the MIMO IC. By allowing channel state information (CSI) exchanged between base stations (BSs) and a central unit (CU), we design a feedback topology where CU collects local CSIs from all BSs, computes all transmit and receive filters and sends them to corresponding user-BS pairs. Note that the local CSIs at BSs are obtained from the estimation of the channel states during the so-called uplink-training phase. At the CU, we propose iterative algorithms utilizing alternating optimization strategy to design the filters. In most of the studies on the MIMO IC, choice of equal transmit power for all user-BS pairs ignores the essential need to search for the optimal power allocation policy; they do not take the full advantage of the system's total power. Thus, how to

allocate power among all the user-BS pairs in the network based on the sum-rate maximization strategy and under a sum power constraint is another key to this chapter.

Finally, Chapter 6 summarizes the conclusions and possible venues for future research of this work.

Chapter 1

Introduction

1.1 Background

With the great development of telecommunications industry, the radio spectrum shortage has become a more serious problem. However, while reuse of spectral resources, as a key solution of the insufficiency of the electromagnetic spectrum (EMS), yields a spectral capacity increase in the network, it gives rise to co-channel interference. Co-channel interference is considered as one of the main sources of performance degradation in wireless communications, such as the decrease of signal-to-interference-plus-noise-ratio (SINR) or signal-to-interference ratio (SIR) and the increase of bit error rate (BER). In particular, under severe interference conditions, interference power will reach the threshold causing the blockage of the wireless channel and consequently a waste of the frequency spectrum. Therefore, appropriate techniques of interference evaluation are the basis of the interference managements and they should be considered in the design and deployment of any wireless networks. Effective interference evaluation methods provide a scientific basis for scheming out the communication jamming and keeping availability, reliability, maintainability, safety and security of the communication networks, both in civil and military communications fields. Indeed,

the interference phenomenon takes place at the physical layer (PHY) (i.e., PHY interference) of the receiver terminal, as an unwanted (undesired) interfering signal disturbing the reception of a given desired signal. However, the properties of the radio interfering signal and its disturbance effects can be explored and determined by features of the interfering transmission at various layers or domains [1]. According to the analytical assessments and based on the purpose of the interference evaluation at different layers of the wireless networks, the interference evaluation can be classified into two aspects [1]: (i) the evaluation of the characteristics of the interference signal itself, and (ii) evaluation of the impacts of the interference on the networks performance. The focus of the first group is on the parameters of the PHY, such as the probability density function (pdf) of the interference, SIR or SINR, BER, outage probability, and so on. In the second aspects, emphasis is given to the network performance, which is affected by interference and is related to higher layer and the quality of service (QoS) or the quality of experience (QoE) of the networks. In this dissertation, the main focus regarding the evaluation of interference is to provide solutions to interference modeling, coordination, and avoidance issues arising in different wireless communication environments to improve performance on both user and network scales. In particular, we will explore and provide solutions to challenges due to interference in different scenarios and networks, namely in cognitive radio (CR) networks, heterogeneous cellular networks, and multiple-input multiple-output (MIMO) interference channels (ICs).

This chapter is organized as follows: Section 1.2 introduces the cognitive strategies for interference avoidance in CR systems with machine-learning techniques. Section 1.3 presents an introduction to an interference modeling approach to the case of a HetNet. Section 1.4 gives an introduction to an iterative interference management scheme in MIMO networks called "Interference Alignment (IA)". Finally, Section 1.5 provides a summary of the contributions and scope of this dissertation, including the dissertation configuration, an outline chapter by chapter of the research topics, and relation of each chapter to existing research.

1.2 Machine-learning Based Techniques in Cognitive Radios

The term CR refers to a radio device that is capable of learning, being aware of its surroundings and adapting to its environment [2], [3]. Cognition is a term referring to a process involved in gaining knowledge and comprehension. This process includes thinking, knowing, remembering, judging and problem-solving [4]. One of the key aspects of any CR device is the capability of self-programming and the ability to learn autonomously [5]. In facts, CRs are brain-empowered wireless devices aimed at improving the optimal use of the EMS. A CR is assumed to use the methodology of understanding-by-building and is aimed toward the fulfillment of two primary objectives: Permanent reliable communication in which communication takes place as smoothly as possible and no interference occurs, and efficient utilization of the radio spectrum resources [6]. This definition and interpretation of CRs has started a new era, focusing on dynamic spectrum sharing (DSS) techniques to improve the radio frequency (RF) spectrum utilization [6]-[8]. This led to study on different aspects and areas of signal processing and communication theory required for dynamic spectrum access (DSA) networks. These included underlay, overlay and interweave paradigms for spectrum co-existence by secondary CRs in licensed spectrum bands [8]. To perform its cognitive task properly, a CR must have the ability to become aware if its RF environment. In other words, it should have the ability to sense its surrounding radio environment and detect all types of RF activities. Thus, spectrum sensing for the purpose of identifying various types of RF activities was considered as a major ingredient in CRs [6]. A number of spectrum sensing methods have been proposed in literature over the last decade based on matched filter [9], energy detection [10], cyclostationary feature detection [11], detection using wavelet [12] and covariance based detection [13]. A review of the spectrum sensing techniques for CRs is provided in [14]. Surveys on the DSA techniques and the medium access control (MAC) layer operations for the CRs can be found in

[15], [16]. In addition to being aware of its surrounding environment and current situation, a CR should be equipped with learning and reasoning abilities and mechanisms to utilize the acquired information [2], [3]. These capabilities are embedded into a cognitive engine (CE), which is the cognition core of the CR. The CE helps to coordinate the actions of the CR by making use of machine-learning techniques. At the CE, learning schemes can be used to allow efficient adaption of the CRs to their surrounding environment, yet without the full knowledge of the dependence among parameters [17]. For instance, a threshold-learning algorithms was proposed in [17] to allow CR to reconfigure its spectrum sensing process under uncertain RF environment. In heterogeneous CR networks, the problem becomes even more complex. In the case of heterogeneous CR networks, the CR not only has to adapt to the RF environment and uncertainty conditions, but also it has to coordinate its actions with respect to the other radios or nodes available in the network. When there is only a limited cooperation between nodes, and consequently a limited amount of information exchange among them, a CR, in order to select its proper actions, needs to determine and estimate the behavior of other nodes. For instance, in the context of DSA, CRs try to access idle primary channels for communications while avoiding collisions with both licensed and other secondary cognitive users [18]. In addition, conventional solutions to the decision process (i.e. Dynamic Programming in the case of Markov Decision Processes (MDPs) [19]), when CRs are operating in unknown RF environments, may not be feasible since they require full knowledge of the system. On the other hand, specific learning algorithms such as the reinforcement learning (RL) [17], [18], make it possible to arrive at the best possible solutions to the MDP, without the presumed knowledge of the transition probabilities of the Markov model. Thus, given the re-configurability requirements of wireless systems and the need for autonomous operation in heterogeneous and unknown RF environment, CRs may use learning algorithms as tools for coordination with peer radio devices and adaptation to the RF radio environment. Moreover, by applying low-complexity learning algorithms to CRs a reduced system complexity can be always expected. A literature review on CRs shows that both supervised and unsupervised learning

methods have been used and applied to different learning tasks. The authors in [20], [21] have used supervised learning based on support vector machines (SVMs) and neural networks for CR applications. On the other side, unsupervised learning, such as RL, has been used in [22], [23] for DSS applications. QL algorithm, a form of RL, has been shown to be effective in some particular CR applications. For example, in [24], Q-learning (QL) is used by the CRs to improve detection and classification performance of primary signals. Although the RL algorithms (such as QL) may provide a suitable framework for autonomous unsupervised learning, their performance can become unsatisfactory in partially observable non-Markovian and multi-agent systems [24], [25]. On the other hand, most research done in the field of QL has focused on discrete domains, although the environment in which the agent must interact is usually continuous. For instance, the major drawback of the QL algorithm is that the original algorithm cannot deal with continuous and multi-agent domains. In the situations that we deal with a continuous state and also when the input state space dimension is large, the classical approaches such as QL for solving RL problem are not so practical, and are usually intractable to represent since they require mainly large memory tables as "look-up tables". These kinds of problems are called curse of dimensionality and will be treated by means of more advanced RL techniques and generalization approaches over the input state [26], [27]. Generalization techniques allow compact representation of the learned knowledge instead of using look-up tables. In short, as the name suggests they use the concept of generalizing and extending the learned skills over similar situations, states and actions. Generalization methods are based on function approximation techniques from the machine-learning field. One of the generalization techniques that is more accurate and powerful is fuzzy logic. To address the aforementioned difficulties (N-dimensional real-valued domains), in Chapter 2, we propose to employ a fuzzy Q-learning (FQL) algorithm that combines fuzzy logic with the QL algorithm [27], [28]. In summary, the utilization of fuzzy theory in RL is to improve learning with more adaptation of RL for continuous and multi-agent domains and to accelerate the learning process. In the FQL algorithm, the controlled system is presented as a fuzzy inference system

(FIS). The proposed FIS structure is made up of several extended rules. It has been shown that this combination results in an FIS that can learn through its experience without experts' knowledge. As in this way, we can build an FIS (or an agent) that can learn to solve the given problem by itself through the interaction with the given problem, that is through its experience like an animal. Moreover, the proposed structure can resolve the continuous environment problem in QL by virtue of an FIS. Our unique and timely approach of designing advanced machine-learning and computational modeling techniques with CR research can bring about a paradigm shift in the way a CR device to operate efficiently for performance enhancement, rather than just being functional.

Since our proposed technique (FQL) in Chapter 2 is constructed based on the QL algorithm, we now explain the basic idea of QL algorithm and its problems in more details.

The basic idea of QL is that we have a representation of the environmental states s (i.e., primary user (PU)'s states), and possible actions a to choose for those states, and we learn the value of each of those actions for each of those states. This value, q, is referred to as the state-action value. We start by setting all state-action values to 0, and then we go around and explore the state-action space. After an action is tried out by the agent for the observed state, the outcome is evaluated. If it has led to an undesirable outcome, the q-value of that action for that state is reduced so that other actions will have a greater value and therefore a higher chance to be chosen instead the next time we observe that state. Similarly, if the agent is rewarded for taking a particular action, the weight of that action for that state is increased, so the agent is more likely to choose it again the next time we observe the same state. Note that, when q is updated, we are actually updating it for the previous state-action combination, and q will be updated only after we have seen the outcome. Now this system, as is, gives us no foresight further than one time step, and therefore it cannot be useful. To make this more useful we can include a look-ahead value. The look-ahead works as follows. When a given q value is updated for a particular state-action combination the agent just

experienced, we do a search over all the q-values for that observed state. For that observed state, we find the maximum state-action value, and incorporate that into the update equation of the q-value representing the state-action combination the agent just experienced. Specifically, we update the previous state-action value in a simple way using $q(s,a) \leftarrow q(s,a) + \kappa(r(s,a) + \gamma \max(q(s')) - q(s,a))$, where s is the previous state, a is the previous action, s' is the current state, κ is a learning rate and γ is the discount factor. The details of this expression will be discussed later in Chapter 2. In QL at its simplest, state-action values are stored in a look-up table. So, we have a giant table, which is size $N \times M$, where N is the number of different possible states, and M is the number of different possible actions. At the decision time, the agent simply goes to that table, look up the corresponding action values for the observed state, and chooses the maximum.

There exist some other issues that we need to consider. First, we need to cover the case where there are several actions that all have the same value. For this case, the agent has to randomly choose one of them. This helps the agent out of that situation, but now if we ever happen upon a decent action, the agent will always choose that one in the future, even if there is a way better action available. To tackle this problem, we need to introduce an exploration phase by defining the additional term, ε. More detailed information about the exploration phase will be given later in Chapter 2. The other problem now is that even after we have explored all the possible actions and the best action, the agent still sometimes choose a random action, i.e., the exploration phase does not turn off. To overcome this issue, we gradually reduce the value of ε, so that it explores less and less as time passes and the best actions for the majority of situations have been learned.

As mentioned, QL at its simplest uses tables to store data. This very quickly loses viability with increasing sizes of state/action space of the system. In other words, QL suffers from what is called the curse of dimensionality, meaning that its computational requirements grow exponentially with the number of state/action variables. In QL, it is assumed that the domain is discrete, or discretized. Therefore, to deal with a continuous/multi agent domain, QL needs some discretization approaches [17]. To discretize a continuous state and action space is

a challenge, since if a discretization is too rough (i.e., when the look-up table size is chosen to be very small), it will be impossible to find the optimal policy which results in a very low performance; if a grid is too fine (i.e., when the look-up table size is chosen to be large) the generalization will be lost, i.e., the time to converge and time per iteration increases rapidly making this problem computationally intractable. It should be noted that to be able to compare the QL method with other proposed methods in terms of performance (not convergence speed), in this thesis, we will consider the second option i.e., a large q-table.

Thus, more generally, QL can be combined with function approximation techniques (such as fuzzy). This makes it possible to apply the algorithm to larger problems, even when the state space is continuous (therefore, infinitely large), as it is in our case. Furthermore, it may speed up learning, due to the fact that the algorithm can generalize earlier experiences to previously unseen states.

1.3 Modelling and Analysis of Multi-tier and Cognitive Cellular Networks Based on Stochastic Geometry

The number of users using the wireless cellular infrastructure for Internet connectivity as well as the traffic demand per user is increasing dramatically. It has been said that by 2020 there will be more than 50 billion connected devices around the world, makes it necessary to develop the existing cellular infrastructure [29]. The traditional homogenous network expansion techniques relies on cell splitting which are less efficient and proven not to keep up with the rapid increase of user population, and the deployment process is complex and iterative. Moreover, site acquisition for macro base stations (BSs) with towers becomes more challenging especially in dense urban areas. In response to the capacity and cost challenges, new solutions and more flexible deployment models to improve broadband user experience and to accommodate the increased capacity demand, should be developed by the operators. For example, small cells including femtocells have been

added to the 3G, LTE and WiMAX standards, and many cellular service providers have already commercially launched their small cell equipment and services. Small cells are low-powered, low cost radio access nodes that operate in licensed and unlicensed spectrum having a range of 10 meters to 1 or 2 kilometers while a typical mobile macrocell may have a range of a few tens of kilometers. Small cells may encompass femtocells, picocells and microcells [30]. Small cell is viewed as an offload technique (especially in 3G networks) [31]. In other words, small cells are traffic offloading spots in the radio access network to decrease the congestion in macrocells, leading to a higher QoS experience and an increase of the overall system capacity. A multi-tier network (referred to as the coexistence of different networks) where small cells are overlaid on traditional macrocells is referred to as a heterogeneous network (HetNet). As mentioned earlier, due to the scarce wireless spectrum along with the increased capacity demand, the ability to re-use frequencies [32] across the coexisting network tiers to increase both coverage and capacity has become the key characteristic of multi-tier cellular networks. Due to aggressive spectrum reuse among the coexisting network tiers, the increase in spatial spectrum efficiency and network capacity however comes at the expense of increased interference. In multi-tier cellular networks, interference is increasingly becoming a major performance-limiting factor, and hence, interference modeling, coordination, and avoidance are the primary focus of interest for both the industry and academic communities. As explained in the previous sub-section, applying the CR technology in multi-tier cellular networks to be aware of and adapt to communication environments, some of the above challenges can be tackled. In fact, CR is the key enabling technology for interference management and avoidance in multi-tier cellular networks. However, the aggregate interference environment is more complicated to model (i.e., interference modeling is a challenging issue), and evaluating the performance of communication techniques in the presence of heterogeneous interference is challenging. For interference characterization, if the BSs of the cellular network follow a regular grid (e.g., the traditional hexagonal grid model [33]), then the SINR characterization will be either intractable [34], [35] or inaccurate due to unrealistic assumptions [36]. Moreover, as urban areas are

built out, the BS infrastructure is becoming less like points on a hexagonal lattice and more random. Hence, the use of a hexagonal grid to model the BS locations is violated and is considered too idealized [37]. Furthermore, according to [34], [35] and [37] for snapshots of a cellular network at different locations, the positions of the BSs with respect to each other follow random patterns due to the size and unpredictability of the BSs in these kinds of networks. Therefore, the need for a powerful mathematical and statistical tool for modeling, analysis, and design of wireless networks with random topologies is quite obvious. A new modeling approach called "stochastic geometry" has been recently applied to the analysis of multi-tier cellular networks due to its ability to capture the topological randomness in the network and its aim at deriving accurate and tractable expressions for different network metrics [34], [36] (e.g., outage probability, as one of the interference evaluation metrics). Stochastic geometry stems from applied probability and has a wide range of applications in the analysis and design of wireless networks in particular for modeling and analyzing systems with random channel access (e.g., ALOHA [38], [39] and carrier sensing multiple access (CSMA) [40]), single and multi-tier cellular networks [37], and networks with cognitive abilities [38], [41]. Chapter 3 discusses this new theoretical model to provide a better understanding of the heterogeneous cellular networks of tomorrow and their challenges (interference modeling, coordination, and avoidance) that must be tackled in order for these networks to reach their potential.

1.4 Interference Alignment (IA)-Based Networks

As we already explained, interference is a major limiting factor in achieving permanent reliable communication in multi-user wireless networks. Thus, developing effective interference management schemes is always the primary focus of interest for both the industry and academic communities. Traditionally, the interferences can be handled often by granting each user exclusive access to a fraction of the wireless communication resources. For example, frequency-division multiple-access (FDMA) [42] and time-division multiple-access (TDMA) [43] are

two well-known channel access techniques. In FDMA, the bandwidth is divided among users, i.e., non-overlapping frequency bands are allocated to different users on a continuous time basis (i.e., signals assigned to different users are clearly orthogonal, at least ideally); while in TDMA, users take turns to solely use the whole bandwidth for data transmission periodically. In the terminology of wireless interference networks, these solutions correspond to the "cake-cutting" interpretation of spectrum allocation as each user can utilize part of wireless resources free of interference. The performance of these orthogonal access schemes is far from the capacity of interference networks. IA, which is a recently emerging idea for wireless networks, is an effective approach to manage interference and it is known to be a degrees of freedom (DoFs) optimal approach, which means that it can reach the capacity of interference networks at very high signal-to-noise power ratio (SNR). The key idea of IA, as a linear precoding technique, is to align multiple interfering signals in time [44], frequency [45], or space [46] (the IA in space dimension is seen in majority of the more practically oriented studies due to the wide applications of MIMO technique nowadays) in order to reduce the effective interference while still allowing the desired signals to be discerned. The promising performance of IA in interference management has resulted in the development of many IA schemes for different kinds of wireless network topologies [47]-[50]. However, to be able to leverage IA in more practical scenarios and realistic settings, some issues and challenges exist that should be solved, e.g., the global and accurate channel state information (CSI) that are difficult to obtain must be available at each node to calculate the solutions of IA [51], [52]. In addition, the closed-form solutions of the IA problem are generally difficult to obtain, especially when the number of users in the network is larger than 3 [53], [54]. Thus, it is necessary to resort to iterative algorithms where the IA solutions are optimized progressively. Moreover, when SNR becomes lower, IA will fall short of the theoretical maximum [55]. In other words, the observed SINR may decrease in IA-based networks, and thus the minimum requirement of QoS of the systems cannot be satisfied. The SINR decrease is considered as one of the most challenging issues among those mentioned above, because it will directly affect both the QoS

and sum-rate of the network. When using IA, the sum-rate over IC can approach the channel's sum capacity at very high SNR. However, the sum-rates resulting from IA may fall short of the theoretical maximum, particularly at low and moderate SNRs. This is because IA mainly concentrates on mitigating the interference, without paying attention at the quality of the resulting equivalent channel and the desired signal [56]. Many studies have been conducted to improve the sum-rate or QoS of IA-based networks at low SNR through quality enhancement of desired signal. For example, Max-SINR [56] algorithm trades interference mitigation and desired signal enhancement. A Max-SINR algorithm for IA is defined to maximize the SINR of the received signal, which can consequently improve the sum-rate of interference networks especially at low SNR. However, its advantage tends to be lost when SNR becomes larger. Recently, iterative optimizations using the maximum sum-rate criterion have become more favorable for the implementation of IA. As we explain in Chapter 5, it is necessary to design iterative algorithms that directly or indirectly aim at maximizing the achievable sum-rate for users rather than seeking a perfect IA solution and meeting the IA feasibility conditions. Many researchers believe that IA, as a technique that maximizes spectrum efficiency of the network to optimize the performance, can be considered as a promising candidate for interference management into the future generations of wireless technologies.

1.5 Scope and Contributions of the Dissertation

This dissertation consists of six chapters. In Chapters 2, 3, 4 and 5 novel techniques and approaches in different wireless networks are presented to address various problems related to interference management such as interference modeling, coordination and avoidance. Each chapter contains the particular problem description, the relevant existing literature, the proposed methods and their evaluation. The outline of this dissertation is summarized in Fig. 1.1. Content of this thesis is distributed along Chapter 2 that considers the interference management issue in CR networks, Chapters 3 and 4 that deal with the

interference challenges in heterogeneous cellular networks, and Chapter 5 that focuses on the interference management issue in MIMO ICs. The problems in Chapters 3 and 4 are tightly related, they both deal with interference modeling and avoidance in HetNets by presenting a CR based statistical framework for a two-tier heterogeneous cellular network on the basis of the stochastic geometry, and the goal is to find a closed-form expression for outage probability (as an important performance metric for wireless networks) of any typical user in the network. The main difference in both scenarios is that unlike Chapter 3 that uses some assumptions on the channel links to relax the difficulty of addressing a closed-form expression for the outage probability, in Chapter 4 novel closed-form expressions are derived for the outage probability over general Nakagami-m fading channels. Finally, Chapter 6 contains the conclusions of this dissertation. The relation among chapters of this dissertation can be found in Fig. 1.2. The relation among the solutions in each chapter and existing research is presented in separate figures. Figs. 1.3, 1.4 and 1.5 respectively contain the relationship of Chapter 2, Chapters 3 and 4, and Chapter 5 with existing research and our contributions.

As mentioned, Fig. 1.2 shows the relation among chapters of this dissertation. The future wireless networks are likely to be heterogeneous, i.e., a mixture of overlaid networks with different features such as density, transmit power, spectrum, coverage, complexity, and hardware requirements. The main priority is to improve the performance and increase the throughput of tiered networks with resource/interference management methods. Due to the expensive and scarce spectrum resource, CR communication can be an efficient technique to enhance the spectrum efficiency in the context of coexistence of HetNets. In HetNet, the traditional macrocell system can be considered as primary and the small cell system as secondary system. The secondary system should be self-optimized and the interference generated from the secondary system to the primary system should be suppressed as much as possible. Current network configurations use traditional macrocell nodes, and the deployment of new small cells need additional bandwidth, which is scarce and expensive to acquire, as mentioned. In this context, dense cellular networks (i.e., small cells) have to coexist with traditional macrocells to

utilize the existing spectrum resources efficiently. This requirement has led to the concept of CR which allows for the coexistence of two systems, primary and secondary, over the same spectrum. The most common cognitive technique in the literature is the spectrum sensing technique. With the spectrum sensing technique, secondary users will be able to transmit whenever PUs do not use that specific band, or they can have transmission as long as they meet the interference constraint of the PUs. Motivated by this insight, in Chapter 2, we have comprehensively studied the concept of CR on the basis of a learning technique. To see the fundamental performance of the proposed CR scheme in Chapter 2, we consider a simple small-scale network such as wireless personal area network. However, the final goal is to provide an insight into the role of CR in the large-scale and dense networks, i.e., HetNets.

As mentioned, in HetNet, due to spectrum scarcity and the massive use of wireless devices, frequency/time resources are reused and concurrent transmissions are merely separated in space. With multiple concurrent transmissions in HetNets, interference will become one of the main performance-limiting factors. Interference is largely governed by the geometry of the interferers. Due to the critical role of interference in evaluating the network performance in HetNet, the metric of interest has to be SINR or the SIR when network performs in an interference-limited regime. Nevertheless, the statistical characteristics of interference and the SINR have to be analyzed to deepen the understanding of system behavior and network performance. The traditional hexagonal grid based model is rigid, not scalable to a HetNet and highly idealized. However, the stochastic counterpart leads to scalable and tractable solutions for HetNets. Furthermore, for snapshots of a cellular network at different locations, the positions of the BSs with respect to each other follow random patterns due to the size and unpredictability of the BSs in these kinds of networks. Therefore, to accurately assess and analyze the performance of HetNets, there is a vital need for probabilistic models that describe the randomness of the network nodes. This has motivated us to study, in Chapters 3 and 4, the stochastic modeling of the spatial distribution of HetNet nodes based on the rich mathematical toolset of stochastic geometry, which allows us to

capture realistic distributions of users as well as deployment scenarios for BSs. It should be noted that the concept of CR technique, presented in Chapter 2, is also applied in Chapters 3 and 4 for the purpose of interference mitigation in HetNets.

As mentioned earlier, in the context of HetNets, secondary users are allowed to transmit whenever PUs do not use that specific band, or in underlay techniques, SUs are allowed to transmit as long as they meet the interference constraint of the PUs. When the strength of secondary interference to the primary is comparable to the desired signal, treating as noise (which is generally non-capacity achieving) is not an option because of interference constraints while decoding and canceling also requires complex primary receivers with their own security issues. In addition, in HetNet, classical resource management techniques based on frequency/space reuse and power control are not able to cope with the additional interference. Thus, an efficient interference management technique is critical for the successful deployment of HetNets. In this context, IA as an interference management technique tool has received important attention recently in the CR research community. In this direction, in Chapter 5 of this dissertation, we also investigate the concept of IA in MIMO multi-user systems. It should be noted that the coexistence of cognitive small cells and macrocells equipped with IA enabled MIMO transceivers will not be studied in this dissertation. However, for the future work, IA technique can be exploited in HetNets to mitigate the interference of cognitive transmitters towards the primary receivers.

Fig 1.3 contains the relationship of Chapter 2 with existing research and our contributions. As mentioned before, a reliable communication with little or no interference, and efficient utilization of the radio spectrum are the two main goals to achieve in cognitive wireless networks. In an effort to meet these goals, any CR needs some tools and strategies. Firstly, it should have the ability to sense the surrounding radio environment and detect all types of RF activities. Various spectrum sensing methods have been proposed in the literature based on matched filter, energy detection, cyclostationary feature detection, detection using wavelet and covariance based detection [9]-[13]. Energy detection, which detects the presence/absence of a signal just by measuring the received signal power, is the

most common approach to spectrum sensing. This is because of its low implementation complexity. It is therefore used as the main sensing method in Chapter 2. Secondly, CR should decide on the best frequency band (of all bands available) to meet QoS requirements, and make proper decisions in the decision-making process; therefore, spectrum management/control functions are required for CRs. When CRs are operating in unknown and uncertain RF environments, MDP based spectrum management schemes [19], as the conventional decision-making units, may not be feasible. Therefore, in Chapter 2, we instead use a partially observable Markov decision process (POMDP) based framework. Lastly, the CR needs to be equipped with learning and reasoning abilities embedded into a CE. The learning algorithms can be divided in two main categories: supervised [20], [21] (e.g., SVMs) and unsupervised learning methods [22]-[24] (e.g., RL), as mentioned earlier. When we deal with uncertainty and unknown situations, RL methods are the best candidates to be used at the CE. Among the conventional RL methods, QL ([24]) has shown an unsatisfactory performance in continuous, partially observable and multi-agent environments. To improve learning with more adaptation of RL for continuous, unknown and multi-agent domains and to accelerate the learning process, we propose FQL. Thus, in Chapter 2, based on the energy detection and POMDP, a novel FQL based sensing scheme is presented.

Fig 1.4 contains the relationship of Chapters 3 and 4 with existing research and our contributions in the HetNets. As mentioned earlier, the ever increasing number of users, the increased capacity demand and cost challenges, makes it necessary to develop the existing cellular infrastructure [29] (i.e., the traditional homogenous macrocell network deployments). New solutions and more flexible deployment models such as the low powered/cost small cells [30], [31] (small cells may encompass femtocells, picocells and microcells [30]) should be lunched by the network operators to improve user experience and to accommodate the increased capacity demand. Small cells are overlaid on the traditional macrocells. The resulting network is referred to as a HetNet. In these kinds of networks, the ability to re-use frequencies across the coexisting network tiers to increase both coverage and capacity has become the key characteristic. However, due to aggressive

spectrum reuse among the coexisting network tiers, the increase in network capacity comes at the expense of increased interference. Hence, interference management and modeling techniques are the primary focus of interest. In Chapters 3 and 4, cognitive HetNet is a proposed solution for the interference management issue. Most of the existing interference management techniques are developed in idealized and simplified interference network settings (e.g., the grid model/setting [33]). In other words, the existing interference management techniques are mostly considered in settings with a particular number of cooperative transmit-and-receiver pairs, ignoring any potential interference from outside of the cooperative set. The fundamental challenge is to re-evaluate the gains obtained with the interference management techniques using models that can accurately reproduce and capture the impact of the random spatial structure of wireless transmit-and-receiver locations and channel characteristics. As mentioned earlier, the possible direction is to use analytical models for large-scale interference networks via stochastic geometry [34], [36]. This modeling approach facilitates compact and closed-form expressions of outage probability (as the main performance metric used in Chapters 3 and 4) and spatially averaged spectral efficiency of in networks with the effects of out of cell interference and different channel distributions. Based on this modeling approach, closed-form expressions are therefore obtained for any typical user in HetNet considering the Raleigh (in Chapter 3) and Nakagami-m (in Chapter 4) fading assumptions.

Fig 1.5 contains the relationship of Chapter 5 with existing research and our contributions. This figure emphasizes the fact that interference is a fundamental phenomenon in multi-user MIMO communication networks. As mentioned earlier, uncoordinated interference reduces wireless network throughput. As a result, it is essential to understand and manage interference to achieve the highest network performance. Orthogonal access schemes (avoiding interference through orthogonalization of the shared time/frequency resource) has been considered as a conventional approach to deal with interference. It should be noted that treating other transmitters' signals as noise, or decoding interference can be also considered as conventional interference management schemes. FDMA and TDMA, the two

main orthogonal access schemes, have been studied extensively and adapted to contemporary wireless systems [42], [43]. Although these conventional approaches control interference without system overhead, it turns out that they are not optimal in most of the network configurations, except in certain special cases because of their inefficient usage of the spectrum. Recently, a new paradigm for interference management techniques has emerged: interference shaping. This technique has shown to offer a better performance in the interference-limited communication regime than traditionally thought possible. The idea behind the concept of interference shaping is to create a certain interference pattern when transmitting nodes propagate signals so that the aggregated interference effect is dramatically reduced or eliminated at each receiver. IA is a representative interference shaping technique. IA can align multiple interfering signals in time, frequency, or space domains [44]-[46]. However, the IA in space dimension is seen in majority of the more practically oriented studies due to the wide applications of MIMO technique nowadays. As mentioned before, to be able to leverage IA in more practical scenarios and realistic settings, some challenges exist that should be solved, e.g., the global and accurate CSI. Most of the existing studies are based on the assumption that the global and accurate CSI is available at each wireless node in the network [51], [52]. However, in Chapter 5, a central coordinator along with a channel estimation phase are applied to the network to avoid making such unrealistic assumptions. Regarding the existing IA solutions, closed-form solution of the IA problem is a possible candidate [53], [54]. However, in general, it is difficult to obtain closed-form IA solutions, especially when the number of users in the network is quite large. We therefore resort to iterative algorithms where the IA solutions are optimized progressively. We propose iterative IA algorithms based on different criteria such as the conventional leakage minimization and Max-SINR [56], and a newly proposed criterion called the maximum sum-rate [57]. Indeed, as shown in Fig. 1.5, our proposed IA algorithms solve the problem of joint power allocation and transmit/receive filter design in a K-user MIMO IC. Equal power allocation has been considered in most of the related studies (e.g., [56], [57]).

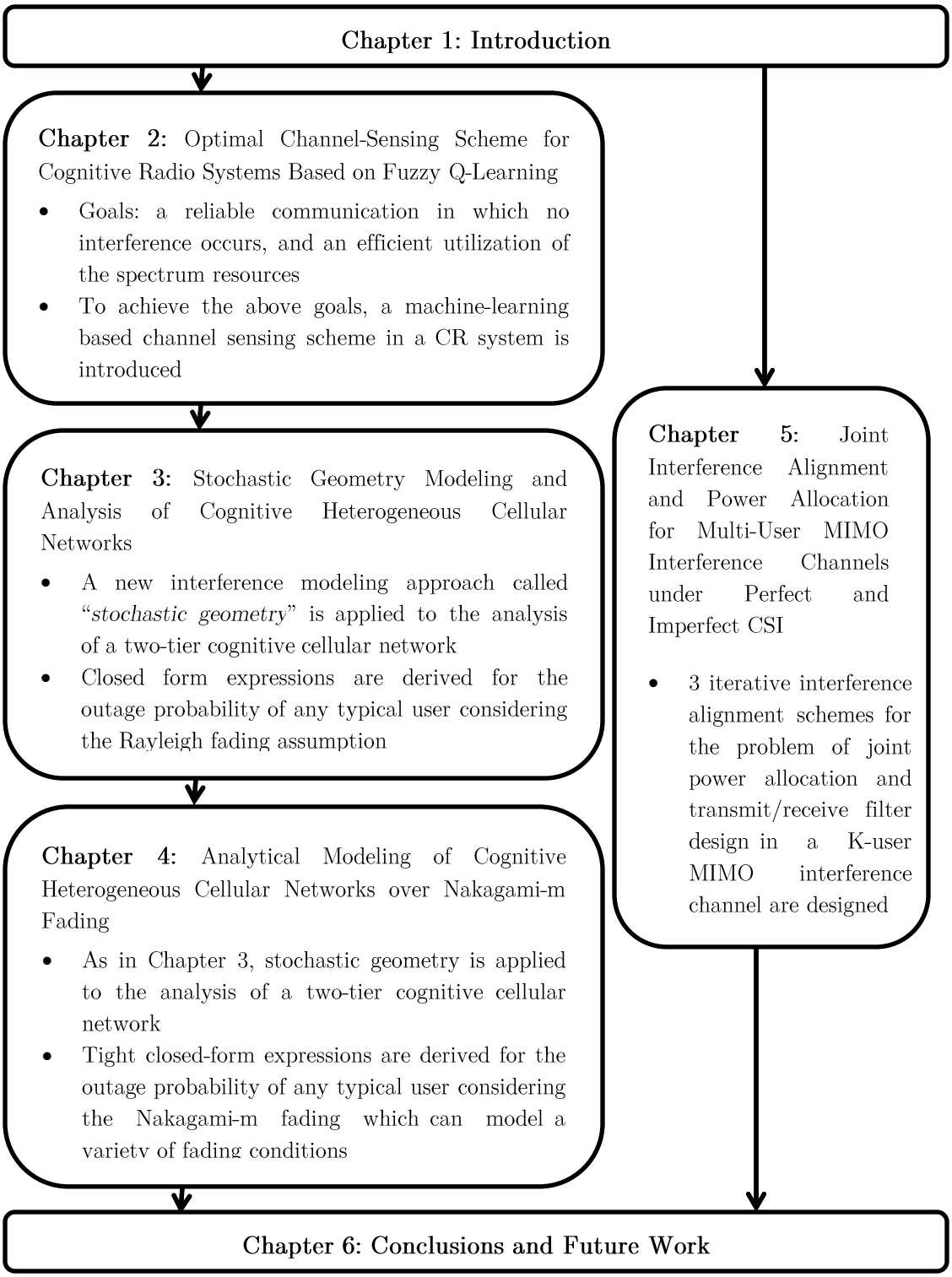

Fig. 1.1: Configuration of this dissertation

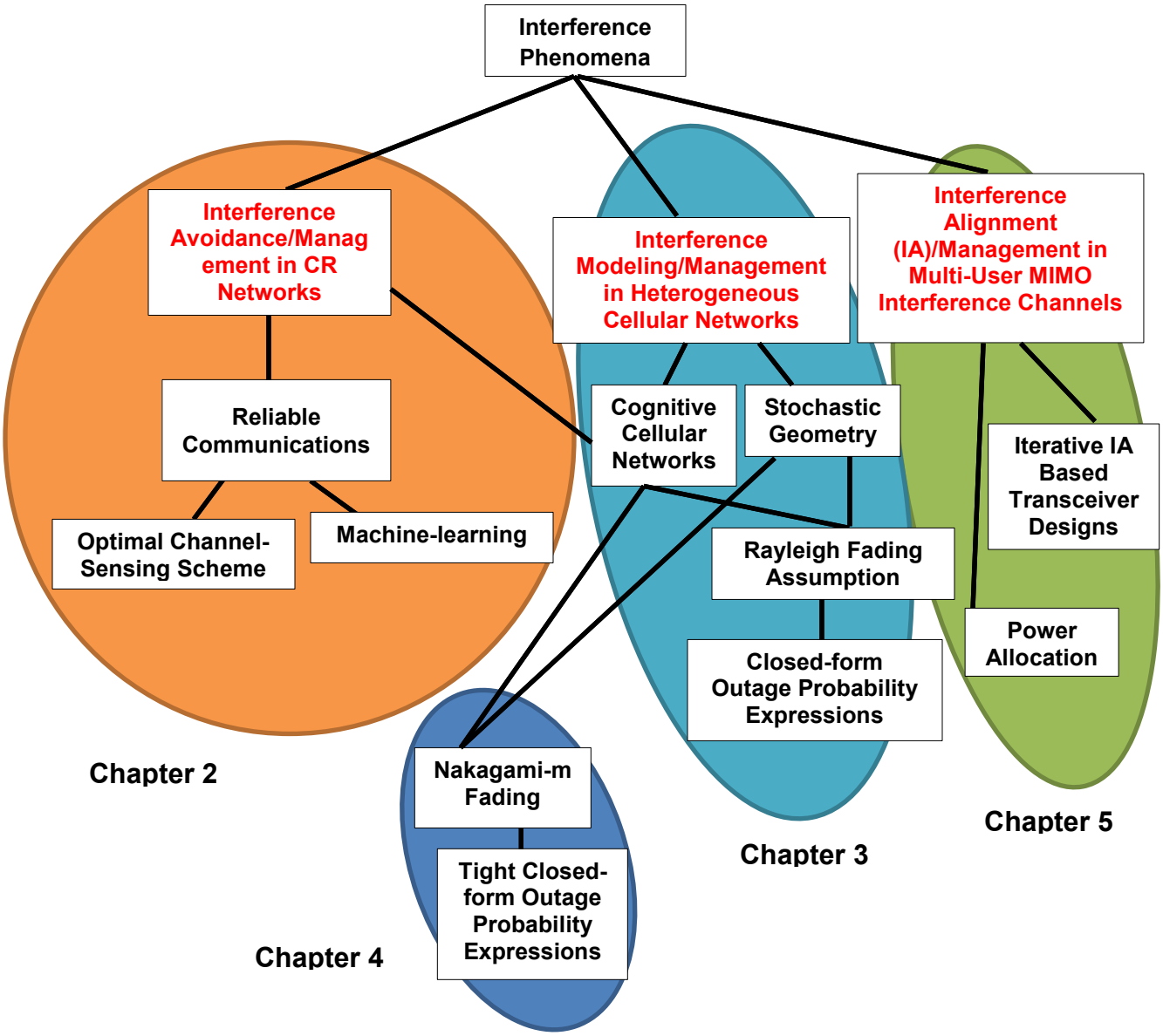

Fig. 1.2: Position in existing research of each chapter

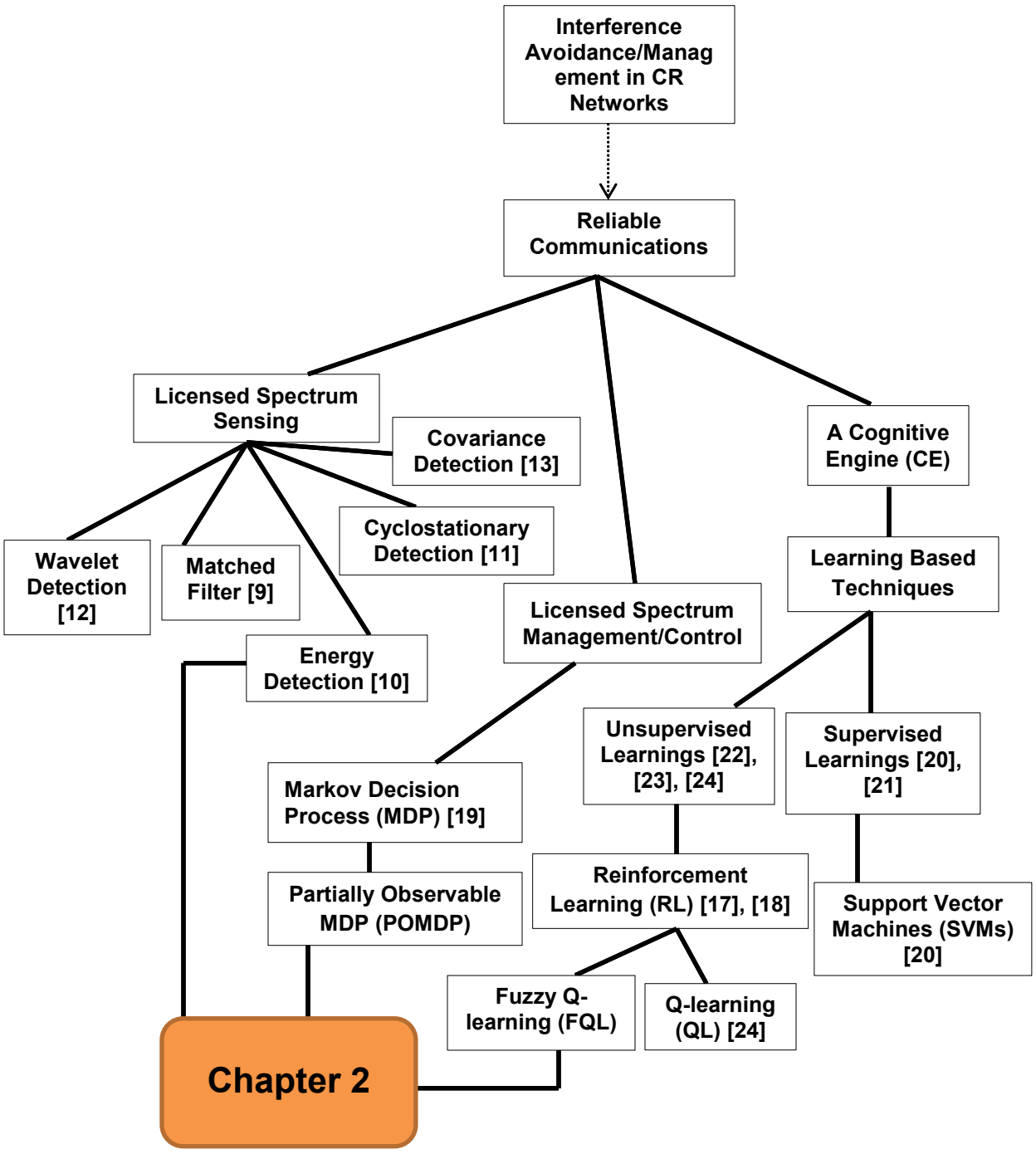

Fig. 1.3: Relation between Chapter 2 and existing research. See Chapter 2 for further details.

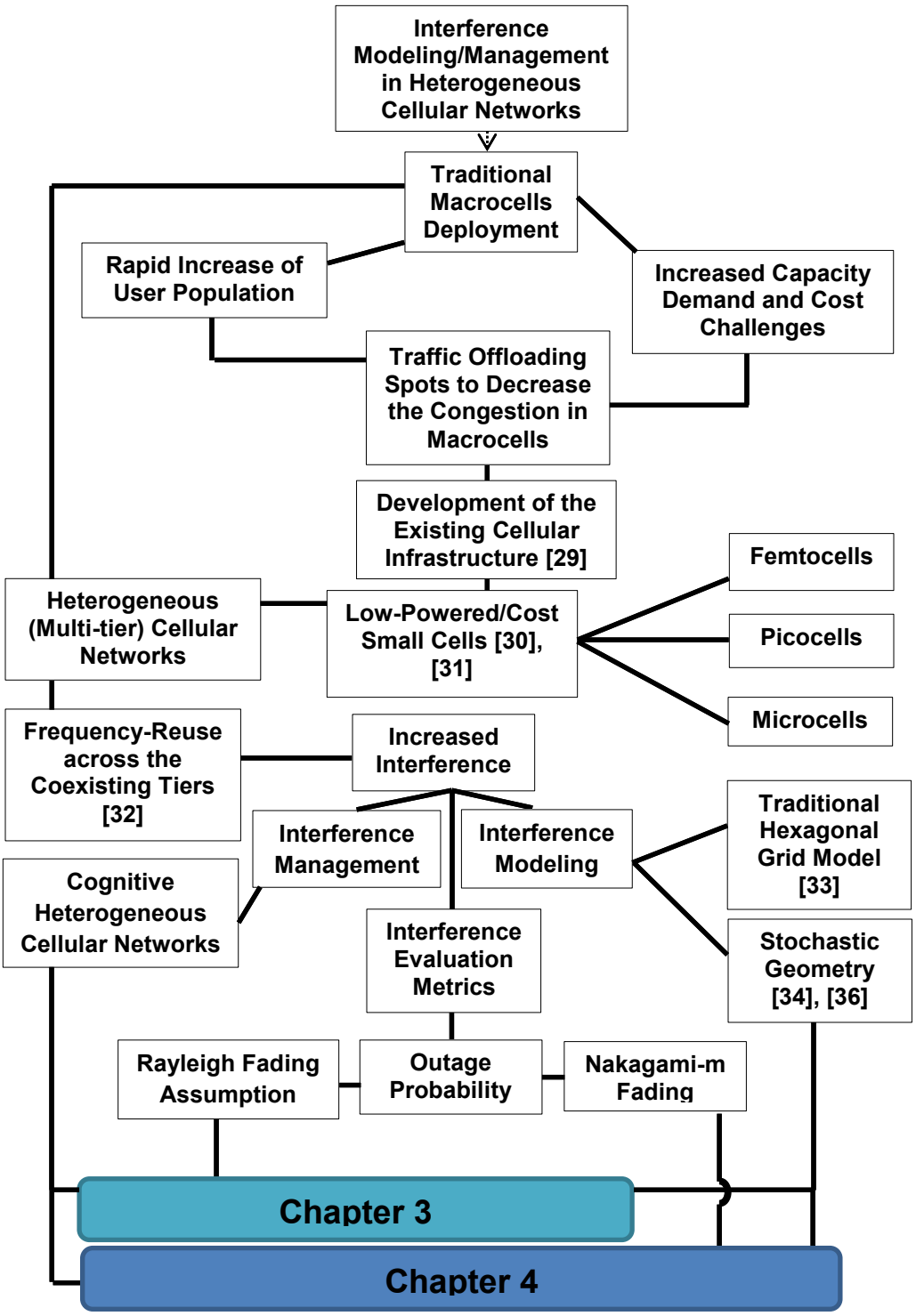

Fig. 1.4: Relation between Chapters 3 and 4 and existing research. See Chapters 3, and 4 for further details.

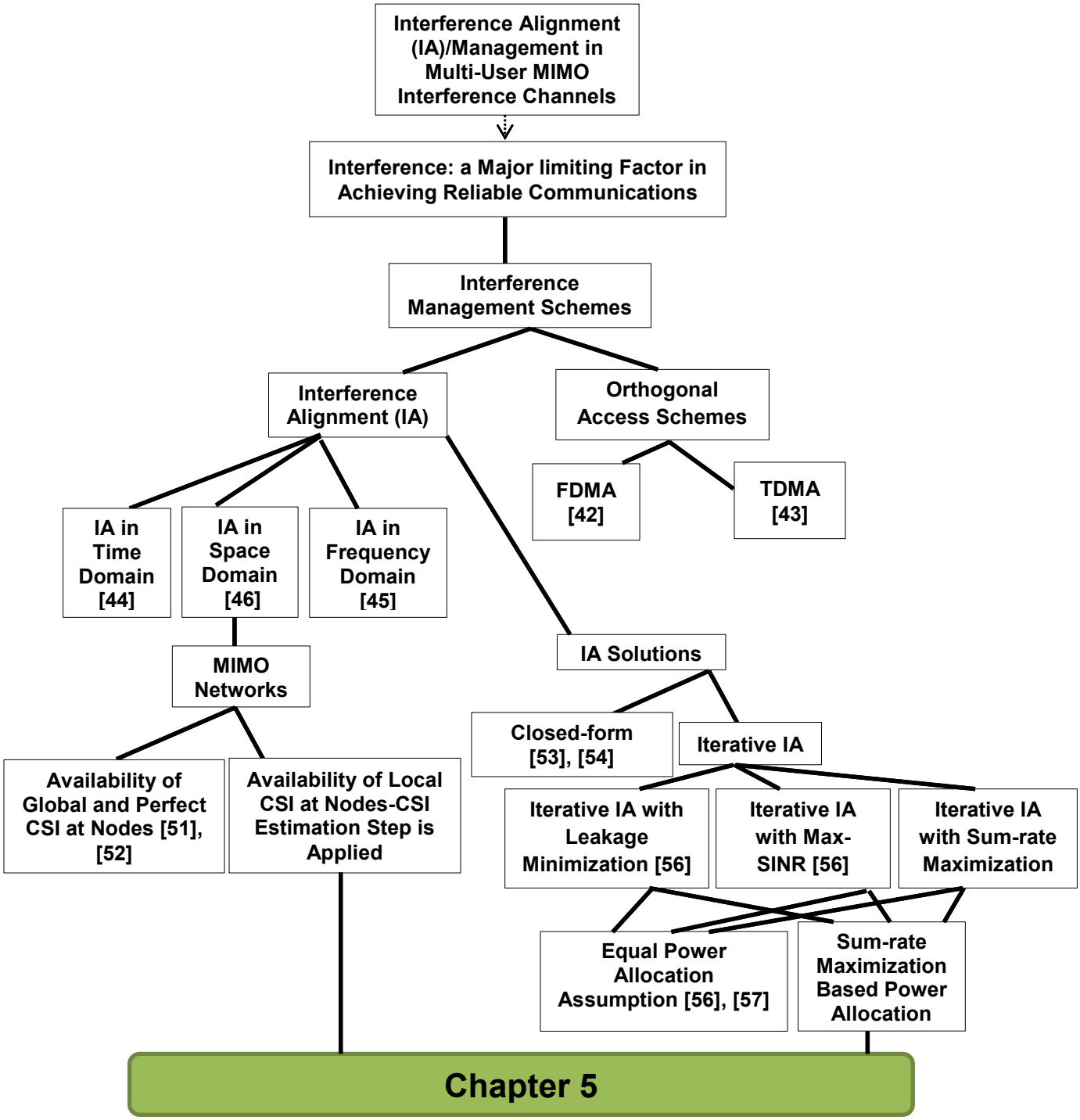

Fig. 1.5: Relation between Chapter 5 and existing research. See Chapter 5 for further details.

Chapter 2

Optimal Channel-Sensing Scheme for Cognitive Radio Systems Based on Fuzzy Q-Learning

2.1 Introduction

Energy detection is the most common approach to channel sensing [58]. This is because of its low implementation complexity. One of the main drawbacks of energy detectors is that they need a large amount of data in order to be able to detect the signals at very low SNR values. This makes the sensing duration very long to guarantee sufficiently low detection error probability [59], [60]. Typically, in the periodic sensing strategy (where CR periodically senses the channel to monitor the PU activity) (e.g., [58], [61], and [62]), after each sensing period T, the energy detector provides a real-valued test statistic as the result of energy detection. CR can make a hard decision on the state of the PU (active or not) by comparing this test statistic with a certain threshold. Thus, period T must be long enough that PU activity can be reliably detected and the final decision of PU activity is correct. Since the CR is not allowed to transmit any data during a sensing period, a long sensing duration results in low channel utilization and QoS for the CR network. Moreover, according to [10], [61], and [63] in some environments, very short spectrum opportunities (spectrum holes)

caused by fast PU state variations are available for the CR to exploit. Therefore, the CR should frequently perform channel sensing in much shorter time intervals to catch the fast variations in the PU state and consequently exploit these short spectrum opportunities. On the other hand, because of the short sensing period, it is difficult for the CR to make an accurate decision on the PU activity only from the single test statistic (provided by the energy detector) over the sensing result. Furthermore, since such sensing results are noisy, the CR has to combine multiple factors (i.e. multiple sensing results) to provide reliable information regarding the PU state after each sensing period and takes the test statistic into account only as a soft "sensing result."

Sequential decision-making is the cognitive process leading to the selection of actions among variations at consecutive decision epochs (see Fig. 2.1). One-way to automate the decision making process is to provide a model of dynamics for the domain in which a machine will make decisions. A reward structure can be used to motivate immediate decision that will maximize the future reward. The aim of the decision-making algorithm is to maximize channel utilization for the CR while restricting interference to the PU. To design the optimal algorithm that achieves such goal, we use POMDP framework [64]. POMDP is an aid in the automated decision-making. POMDP policy informs the CR what action to be executed. It can be a function or a mapping and typically depends upon the channel state.

In summary, in each short sensing interval, the CR uses the energy detection method to obtain knowledge about PU state. However, the CR does not rely only on this knowledge and combines more soft sensing results to enhance adaptability and adaptive decisions at the sequential decision epochs are made by the optimal decision-making algorithm, which was designed by using the POMDP framework. Indeed, a POMDP is equivalent to a MDP with a continuous state space [65], [66]. In this chapter, we formulate the channel sensing in the CR network as a POMDP problem. This statistical-based sensing model uses a probabilistic, rather than deterministic approach to design the optimal decision-making algorithm. In the POMDP model decision, an agent (i.e. CR) tries to maximize some reward function in the

face of limited and noisy information about its surrounding environment (i.e. PU). Although POMDP has emerged as a powerful framework for modeling and optimizing sequential decision making problems under uncertainty, achieving an optimal policy is computationally very challenging [65], [67]. As mentioned before, POMDP is equivalent to MDP with a continuous state space b, called belief state. Thus, a POMDP policy is a mapping from a region in belief state space to an action. Not surprisingly this is extremely difficult to construct and whilst some works make use of POMDP framwork (e.g., [62], and [63]), they do not present solution algorithms for POMDP, or their solutions do not scale to problems with continuous state space and multi-agent domains. RL has now established itself as a major and powerful scheme to address adaptive optimal control of uncertain systems and learn the optimal policy [17]. On the other hand, fuzzy expert systems also have been extensively used in intelligent control problems where mostly traditional methods have poor performance. With the utilization of fuzzy theory in RL, we can enhance learning with more adaptation of RL for continuous and multi-agent domains and speedup learning process [26]. In this chapter, a FIS is also employed for generalizing a continuous belief space POMDP. We propose a FIS-based RL controller with a FQL implementation to solve the POMDP problem. FQL is an approach to learn a set of fuzzy rules by reinforcement. It is an extension of the popular QL algorithm [68]. Learning fuzzy-rules makes it possible to face problems where inputs are described by real-valued variables (continuous state spaces), matched by fuzzy sets. Fuzzy sets play the role of the ordinal values used in QL, thus making possible an analogous learning approach, but overcoming the limitations due to the interval-based approximation needed by QL to face the same type of problems. We will present the simulation results that show how the proposed scheme for channel sensing achieves significant performance in terms of channel utilization while restricting interference to the PU.

2.2 System Model

2.2.1 Model Description

Consider a frequency channel that the PU is licensed to use. The CR network can access the channel whenever it is not occupied by the PU. A collision happens if the CR network sends data on the channel currently being used by the PU. We consider a small-scale network such as the wireless personal area network with a "master node (MN)" in its center and "slave nodes (SNs)" attached to the MN, and assume that all of them are adjusted to the same frequency channel, called "operating channel,". It should be noted that we do not consider the PU activities on frequency channels other than the operating channel, because they are needed only for frequency channel selection, to which we do not pay attention in this chapter. The MN performs channel sensing on the operating channel when it is necessary (not periodically) and the channel sensing process is monitored only by the MN, whereas the SNs do not. If the PU is detected, then the MN switches the operating channel to another channel and directs the SNs to move to the new operating channel [63]. Clearly, based on the sensing results, the MN chooses the next appropriate action at each decision epoch, and it informs the SNs from the chosen action by sending a control signal. As soon as receiving the control signal, the SNs follow the order in it. Indeed, the MN senses the operating channel and provides the SNs with information about the PU activity, while user data are exchanged only by the SNs. To see the fundamental performance of the proposed method and for simplicity of exposition, we ignore fading and shadowing. It should be noted that in real communication environments, fading and shadowing can deteriorate the spectrum sensing performance of the CR user and cause interference to the PU, consequently. To solve this problem, cooperative sensing method (multi-agent scenario) is usually introduced that can be considered as future work.

2.2.2 System Structure

As stated, the MN chooses the next proper action at each decision epoch, which occurs at the end of each action. The decision epoch is indexed by $t(= 1, \cdots)$. The

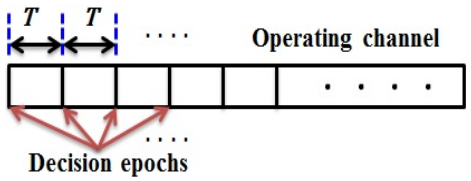

Fig. 2.1. A CR can make channel-sensing decisions over short time intervals

MN selects the appropriate action among "data transmission", "stop data transmission", and "channel switching". In Section 2.3, we explain how this action is selected by the MN. In the following we explain the operating modes of the CR network when each decision is made by the MN.

1) Data Transmission: whenever the MN is convinced that the operating channel is not occupied by the PU, it selects data transmission for the SNs. The SNs will be aware of the MN's decision upon receiving the control signal sent by the MN. Then SNs immediately start to exchange user data by using the time-division multiple-access (TDMA) approach. The SNs perform data transmission during a period T (same as the sensing period for the MN) allocated by the MN in the received control signal. During this period the MN will be quiet.

2) Stop Data Transmission: if the MN is not sure about the PU existence over the operating channel, then it prefers to select stop data transmission. This decision is clearly made to avoid from a probable collision with the PU. Similar to the case which the selected action by the MN is data transmission, a control signal containing the selected action and the allocated time interval is sent to the SNs, and thus the SNs stop data transmission as soon as receiving the control signal and the MN starts to do channel sensing for another T period.

3) Channel Switching: when the MN realizes the PU existence with a high certainty, it selects channel switching and sends a control signal that orders the SNs to switch the operating channel. We assume that it takes T_c to complete the channel-switching process and be ready to choose another action, since the CR nodes should tune their frequency band and perform a synchronization process.

2.3 Decision-Making Configuration

2.3.1 POMDP Formulation

In this section, we formulate the adaptive sensing, in the CR network as a POMDP to design the optimal decision-making algorithm. A POMDP framework has been investigated in [63], [64]. In [61], [62] it is shown that the PU activity can be modeled as a Markov process with two states as $s_t \in \{0, 1\}$ where s_t represents the state of the operating channel (see Fig. 2.2). Empirical measurements taken in the 928-948 MHz paging band [69] and in 802.11b based wireless Local Area Network (WLAN) ([70], [71]) have also validated a Markovian pattern in the spectrum occupancy of the PU. s_t is 0 if the operating channel is vacant at tth decision epoch and 1 if the operating channel is occupied by the PU at tth decision epoch. However, the CR network does not know the true state of the PU and only infers it from noisy sensing results. In such environments where the CR network's information about the PU activity is incomplete, the theory of POMDP will be the best candidate for modeling the situation [64], [72]. To choose the appropriate action at each decision epoch, "belief state" is calculated. Belief state is a probability distribution over the PU state, which is prepared by the MN. In [64], it is shown that the belief state contains all the necessary information for making an optimal decision. As depicted in Fig. 2.1, at each decision epoch having this belief state, the MN selects an action among the possible actions: data transmission, stop data transmission, and channel switching. The belief state at each decision epoch is denoted by $\mathbf{b}^t = (\pi^{0,t}, \pi^{1,t})$, where $\pi^{i,t}$ is the probability of state i ($i \in \{0, 1\}$) at tth decision epoch. Note that the MN performs channel sensing (using energy detection method) on the operating channel during a period of which the length is T and presents its obtained result as the observation probability $Y_{i,e}$ in the belief state formula. We define $Y_{i,e}$ as the probability that the MN receives e as the observation in channel state i. The output of energy detector with the sensing period T immediately after the tth decision epoch is expressed as

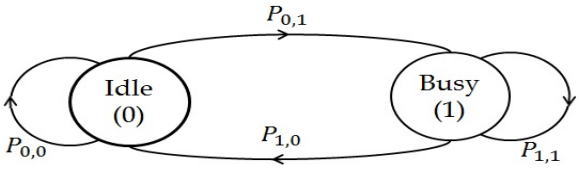

Fig. 2.2. The state-transition diagram of the PU

follows:

$$E_t = \frac{1}{N_0/2} \sum_{j=1}^{WT} |y_{j,t}|^2 \tag{2.1}$$

where $y_{j,t}$ denotes the jth signal sample in the sensing period T after the tth decision epoch, and N_0 is the noise spectral density used for normalization and assumed to be known from the MN viewpoint. W is the bandwidth of the frequency channel. According to [10], [63] the sensing result obtained by the energy detection method follows the chi-square distribution with $2WT$ degrees of freedom if the PU is inactive. If the PU is active, then the sensing result follows the non-central chi-square distribution with the same degrees of freedom as that of the case that PU is inactive and the non-central parameter of $2PT/N_0$, where P is the power of the received PU signal. Fig. 2.3 shows the probability mass functions (pmf's) of the simulation sensing results when the PU is inactive and active. Therefore, the observation probability denoted by $Y_{i,e}$ can be easily calculated from the pmf's of the sensing results. Besides the observation probability that is a soft sensing result, the other factor in the belief state formula is the state transition probability of the PU. Let $P_{i,j}$ $(i, j \in \{0, 1\})$ be the state transition probability of the PU from state i to state j. We may first assume that the MN is aware of the state transition probability as in [62] and [63]. In practice, this may not be achievable. The problem then becomes one of POMDP with unknown transition probability. In Section 2.5, we completely explain how the state transition probability of the PU is estimated. We also assume that the PU's state can change only once during each T period.

From now on, we will explain how the belief state is calculated. As mentioned before, the belief state $\mathbf{b}^t$ is inferred by the MN at the tth decision epoch on the basis of the previous actions and observations. After the tth decision epoch, the decision-making

algorithm updates $\mathbf{b}^t$ to $\mathbf{b}^{t+1}$ on the basis of the selected action at the tth decision epoch and the received observation during the period T after the tth decision epoch. If the selected action is data transmission, then the SNs exchange the user data for the T period and the MN will be quiet in this period and receives a null observation (no sensing result). In this case, the belief state formula evolves according to the state transition probability. That is, the algorithm updates the belief state based on the assumed Markovian evolution as follows:

$$\left(\sum_{i=0}^{1} P_{i,0}\pi^i, \sum_{i=0}^{1} P_{i,1}\pi^i \right). \tag{2.2}$$

If the selected action is stop data transmission, then the SNs stop transmitting data for the T period, and the MN performs sensing (energy detection) during this period. Therefore, besides the state transition, the sensing result of energy detection in the form of the observation probability is also taken into account by using Bayes' theorem as follows:

$$\left(\frac{Y_{0,e} \sum_{i=0}^{1} P_{i,0}\pi^i}{f}, \frac{Y_{1,e} \sum_{i=0}^{1} P_{i,1}\pi^i}{f} \right) \tag{2.3}$$

$$f = Y_{0,e} \sum_{i=0}^{1} P_{i,0}\pi^i + \ Y_{1,e} \sum_{i=0}^{1} P_{i,1}\pi^i. \tag{2.4}$$

From (2.3) and (2.4) and Fig. 2.3, we can see that for example, the belief that the state of PU is 1 (i.e., $\pi^{1,t}$) increases as the quantized value of the sensing result increases. This corresponds to the fact that a high value of the sensing result indicates a high probability that the channel is occupied (clearly, a low probability that the channel is idle). Thus, the soft sensing result (energy detection result) is well taken into account in updating the belief vector and has an important role in making the final decision. The goodness of the POMDP framework is that even in the case of a sensing error observed in the energy detection result, the decision making algorithm can still make a reliable decision (relying on the other soft sensing results) compared

to the case when this energy detection result is used as the only available information in making the final decision. However, it is clear that a better performance of the energy detection method, results in more accurate decisions for the CR. If the action is channel switching, then the CR network moves to the next channel. In this case, the probability distribution over the PU state (belief state) converges to the stationary probability η. The proposed approach is easily applicable to multi-agent POMDP domains (with two or more MNs) wherein each MN maintains a belief simultaneously and communicates it to a central FIS (it can be via communication by wire) at each decision epoch, which forms a fuzzy mapping of the belief space of the underlying multi-agent POMDP. This fuzzy belief mapping is then used to solve a sequence of Bayesian games to generate an approximate optimal joint policy which is executed by each agent (i.e. MN). Under this joint action, each MN updates his own belief and the whole system receives a signal that indicates the goodness of executing the joint action (joint reward). This signal is then used to tune q-values to reflect the consequence of taking that joint action as per standard QL.

2.3.2 Solution to POMDP

We define the total discounted reward of the MN as $\sum_{t=1}^{\infty} \gamma^t \; r^t$, where r^t is considered as the reward of the MN at tth decision epoch and $\gamma \in (0, 1)$ is a discount factor. In the discounted reward model, we are given a discount factor γ, and the goal is to maximize total discounted reward collected, where reward for an action taken at decision epoch t is discounted by γ^t. The discount rate has two roles: (i) it determines the present value of future rewards: a reward received t time steps in the future is worth only γ^t times what it would be worth if it were received immediately (i.e., discounting to prefer earlier rewards), (ii) it keeps the total reward finite which is useful for infinite horizon problems. This modeling approach is motivated by an approximation to a planning problem in the MDP framework under the commonly employed infinite horizon (the number of decision epochs indicates the horizon length) discounted reward optimality criterion [17]. In other words, to encourage the agent to perform the tasks that we want, and to do so in a timely manner, a

commonly employed aggregate reward objective function is the infinite horizon discounted reward. The approximation arises from a need to deal with exponentially large state spaces (i.e., large number of decision epochs). As stated before, to enable an appropriate action by the MN, belief state is calculated at each decision epoch. Each MN's action which is based on the belief state is determined by a "policy". A policy is a mapping between state and action (where state can be belief state as our case). Among the policies, we should exploit the optimal policy that maximizes the total discounted reward. The fact is that actions taken by the MN do not affect the evolution of the channel state. Thus, in finding the optimal policy, no recursive procedures are required. According to the aforementioned references, a POMDP can be seen as a continuous-space "belief MDP" as the MN's belief is encoded through a continuous "belief state". We may solve this belief MDP using dynamic programming (DP) algorithm such as value iteration to extract the optimal policy over a continuous state space [73]. However, it is too difficult to solve the continuous space MDPs with this algorithm. Unfortunately, DP updates cannot be carried out, because there are a huge number of belief states. One cannot enumerate every equation of value function. The QL algorithm, one of the approaches to RL [17], [68] is capable of learning the optimal policy that maps belief state to an action. The major drawback of the QL algorithm is that the original algorithm cannot deal with continuous and multi-agent domains [27].

In the situations that we deal with a continuous state and also when the input state space dimension is large, the classical approaches such as QL for solving RL problem are not so practical, and are usually intractable to represent since they require mainly large memory tables as "look-up tables". These kinds of problems are called curse of dimensionality and will be treated by means of more advanced RL techniques and generalization approaches over the input state [26], [27]. Generalization techniques allow compact representation of learned knowledge instead of using look-up tables. In short as the name suggests they use the concept of generalizing and extending the learned skills over similar situations, states and actions. Generalization methods are based on function approximation techniques from machine-learning field. One of the

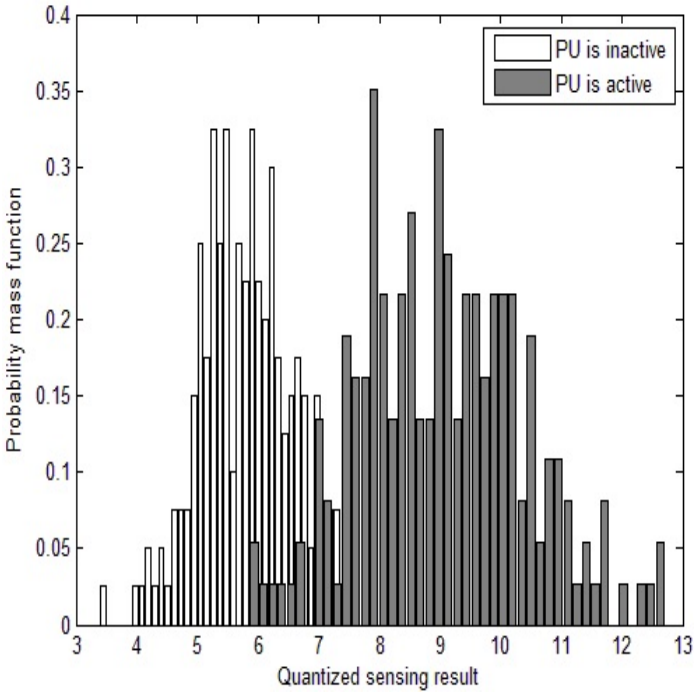

Fig. 2.3. The obtained pmf's for the simulation sensing results when the PU is inactive and active. $W = 1$ MHz, $T = 0.1$ ms, and the SNR of the PU signal is -10 dB

generalization techniques that is more accurate and powerful is fuzzy logic. To address the aforementioned difficulties (N-dimensional real-valued domains), we propose to employ the FQL algorithm that combines fuzzy logic with the QL algorithm [27], [28]. In summary, the utilization of fuzzy theory in RL is to improve learning with more adaptation of RL for continuous and multi-agent domains and to accelerate learning process. In the FQL algorithm, the controlled system is presented as a FIS.

2.3.3 Fuzzy Q-Learning (FQL) Design

Fuzzy approximation architecture plays a crucial role in our approach. It dominates the computational complexity of the FQL, as well as the accuracy of the method. There exist two systems for fuzzy inference, which are denoted as: Takagi-Sugeno type FIS and Mamdani type FIS. A Takagi-Sugeno type FIS has fuzzy inputs and a crisp ouput (i.e., linear combination of the inputs). Mamdani type FIS has fuzzy inputs and a fuzzy output. This study would apply the Takagi-Sugeno type inference to predict the action type taken by the MN. In this chapter, we will refer to zero-order

Takagi-Sugeno FISs, since the other type (first-order) calls for a lot more computational cost than zero-order, besides adding more complexity [74]. In the FQL, the FIS is presented by a set of rules R with a rule $j \in R$ defined as:

IF $(b_1\ is\ L_j^1)$ **...AND** $(b_n\ is\ L_j^n)$ **...AND** $(b_N\ is\ L_j^N)$ **THEN** o_j **with** $q(L_j, o_j)$.

L_j^n is the linguistic label (fuzzy label) of the input variable b_n (nth component of an N-dimensional belief state vector $\mathbf{b} = [b_1, \ldots, b_n, \ldots, b_N]$) participating in the jth rule. o_j is an possible output action of the jth rule while $q(L_j, o_j)$ denotes its corresponding q-value. We build the FIS with competing actions o_j for each rule. A schematic diagram for the FQL architecture and its interaction with the environment can be observed in Fig. 2.4. The learning agent has to find the best conclusion for each rule, i.e. the action with the best q-value among the possible discrete actions for each rule. The q-values are zeroed initially and are not significant in the first stages of the learning process. In order to explore the set of possible actions and acquire experience through the reinforcement signals (rewards), the actions for each rule are selected using an exploration exploitation policy (EEP) as [17]. The ε-greedy method is used as the EEP policy for choosing the actions:

$$\begin{cases} o_j = \underset{k \in A}{\text{argmax}}\ q(L_j,\ o_k) & : \textit{with probability } 1-\varepsilon \\ o_j = \underset{k \in A}{\text{random}}\ (o_k) & : \textit{with probability } \varepsilon \end{cases} \tag{2.5}$$

where ε determines the tradeoff between exploration and exploitation, and A is the set of all possible actions for each rule or for each component b_n of the input belief state vector $\mathbf{b}$. As stated above, the rule j is defined by the intersection (with respect to a T-Norm) of fuzzy sets along each dimension $L_j^1, \ldots, L_j^N$ with the truth degrees $\mu_{L_j^1}(b_1), \ldots, \mu_{L_j^N}(b_N)$ (where $\mu_{L_j^1}(b_1)$ and $\mu_{L_j^N}(b_N)$ are the membership functions, respectively defined on the first and the last component of the input belief state vector $\mathbf{b}$ in rule j) and the T-Norm is implemented by product. Hence, the degree of truth in the fuzzy logic terminology (or the membership of the vector $\mathbf{b}$) for rule j can be

written as follows:

$$\alpha_j(\mathbf{b}) = \prod_{n=1}^{N} \mu_{L_j^n}(b_n). \tag{2.6}$$

Furthermore, the following normalization condition should be satisfied:

$$\sum_{j \in R} \alpha_j(\mathbf{b}) = 1. \tag{2.7}$$

Next, the relation between the inferred action (the output action of the FIS that will be executed at the decision epoch) for an input belief state vector $\mathbf{b}$, and the applied rule actions o_j, is derived as:

$$a(\mathbf{b}) = \sum_{j \in R} \alpha_j(\mathbf{b})\, o_j \tag{2.8}$$

where the summation is performed over all rules. For the obtained inferred action $a(\mathbf{b})$, a Q-function is also approximated by the FIS output, which is inferred from the quality (q-value) of the local discrete actions that constitute the global continuous action $a(\mathbf{b})$. Under the same assumptions used for generation of $a(\mathbf{b})$, the Q-function is calculated as:

$$Q(\mathbf{b}, a(\mathbf{b})) = \sum_{j \in R} \alpha_j(\mathbf{b})\ \ q(L_j, o_j). \tag{2.9}$$

We use the value function for the input belief state vector $\mathbf{b}$ defined here as:

$$V(\mathbf{b}) = \sum_{j \in R} \alpha_j(\mathbf{b})\ \max_{k \in A} q(L_j, o_k). \tag{2.10}$$

In order to update the q-values, ΔQ is defined as the variation of the quality $Q(\mathbf{b}, a(\mathbf{b}))$, in other words, the difference between the old and new values of $Q(\mathbf{b}, a(\mathbf{b}))$. Denote by c the new input belief state vector after taking the action $a(\mathbf{b})$ for the input belief state vector $\mathbf{b}$, and receiving the reward r from the environment (the natural reward for RL methods in CR tasks such as spectrum sensing, is related to the CR user's

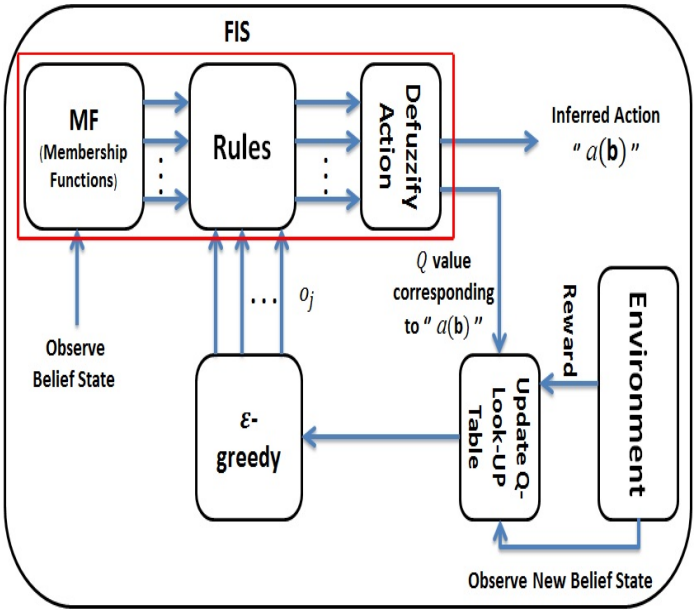

Fig. 2.4. Interaction between the FQL module and the environment ("Environment" is a term that is used to refer to anything outside the sensing device. Here, the received reward is related to the CR user's throughput)

throughput. This information may be easily obtained during the online operation of the CR system). ΔQ is calculated by:

$$\Delta Q = r + \gamma V\left(c\right) - Q(\mathbf{b}, a(\mathbf{b})). \tag{2.11}$$

Now, the update equation for the q-values is given by (2.12). The symbol t is added to highlight the time dependency in the update equation.

$$q^{t+1}\left(L_j, o_j\right) = q^t\left(L_j, o_j\right) + \kappa\alpha_j\left(\mathbf{b}^t\right)\left(r^t + \gamma V^t\left(\mathbf{b}^{t+1}\right)\right. \\ \left. - Q^t(\mathbf{b}^t, a(\mathbf{b}^t))\right. \tag{2.12}$$

where κ is a learning rate. We remind that $q^t\left(L_j, o_j\right)$ are the q-values associated to the chosen actions o_j in all rules. Here, to summarize the FQL-based channel sensing process, an iterative procedure is prepared as can be observed as Table 2.1. Moreover, to clarify the FIS unit structure as well as its rule over the channel sensing process, see the example drawn in Fig. 2.5 which presents the FIS model for a 2-dimensional belief state vector $\mathbf{b} = [b_1,\ b_2]$ as the input for the FIS. As mentioned before, the inferred

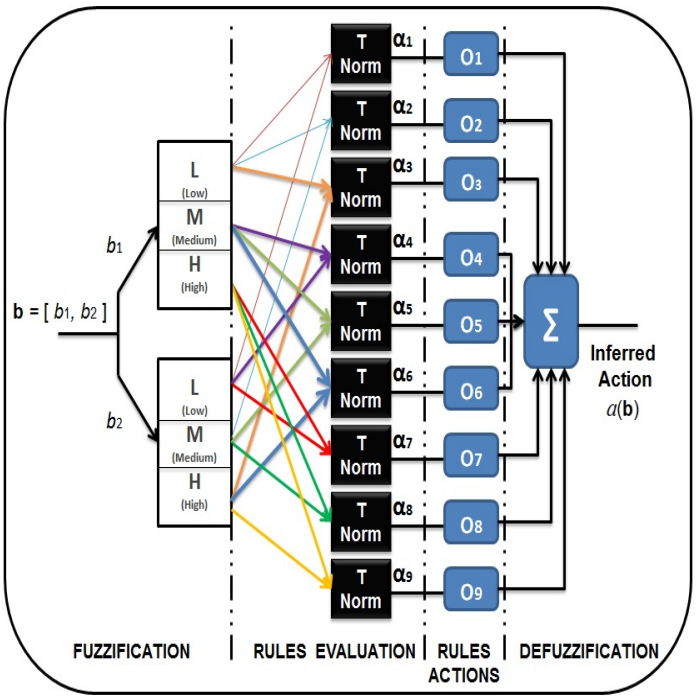

Fig. 2.5. Structure of the FIS model with 2-dimensional belief state vector

action $a(\mathbf{b})$ is the output of the FIS. Obviously, under the same assumptions used for generation of $a(\mathbf{b})$, the other output for the FIS (i.e. the Q-function: $Q(\mathbf{b}, a(\mathbf{b}))$ can be obtained. As shown in Fig. 2.5, for a 2-dimensional belief state vector, 9 fuzzy rules are expected (each color erepresents one rule).

2.4 Simulation Results

2.4.1 FIS Unit Configurations

In this section, we consider a single agent POMDP, including only one MN (and its associated SNs). Therefore, the input belief state vector for the FIS is $\mathbf{b} = [b_1]$. As mentioned, the simulation results can be easily extended to a multi-agent POMDP problem with the input belief state vector $\mathbf{b} = [b_1, \ldots, b_n, \ldots, b_N]$ which requires some consideration about the type of cooperation between the MNs. As stated, we focus on a single agent POMDP with $\mathbf{b} = [b_1]$. The problem has therefore two states, "0" (the PU is inactive in the operating channel) and "1" (the PU is active in the operating channel). Thus, $b_1 = (\pi^{0,t}, \pi^{1,t})$, where as mentioned before, $\pi^{i,t}$ is the probability of state i at tth decision epoch. Since $\pi^{1,t} = 1 - \pi^{0,t}$ we can use only one probability $\pi^{1,t}$

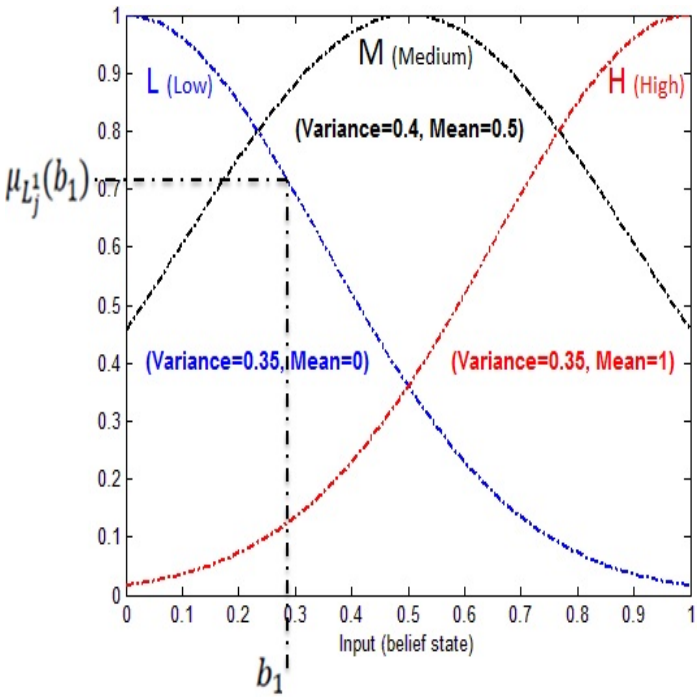

Fig. 2.6. Three fuzzy sets for the belief state

to specify b_1 and the belief state vector is thus specified by $\mathbf{b} = [b_1 = \pi^{1,t}]$. The belief space for the MN is specified by [0 1] (a continuous space). Here, we partition the belief state $\mathbf{b}$ into three fuzzy subsets thereby generating three rules (Note that for a multi-agent POMDP with $\mathbf{b} = [b_1, \ldots, b_n, \ldots, b_N]$, we have 3^N rules). It should be noted that, more detailed partitions yield exponentially growing state space (rule base size), elongating the adaptation time, and dramatically increasing the computational resource demand, while less detailed partitions (containing only a few member fuzzy sets) could cause less approximation accuracy, or unadaptable situation. Therefore, there is a tradeoff between the computational complexity and approximation accuracy, regarding the number of the fuzzy sets.

Linguistic terms for these fuzzy sets are (L, M, H), where L stands for "low", M is "medium" and H stands for "high". As depicted in Fig. 2.6, the membership function (fuzzy sets) for the belief state $\mathbf{b}$ is assumed to be the standard Gaussian membership function [27]. The use of various types of membership functions (e.g., linear functions, triangular, trapezoidal and smoother functions such as the symmetric Gaussian function) can affect the performance of the fuzzy logic controller and corresponding

TABLE 2.1. THE ITERATIVE PROCEDURE ADAPTED FOR FQL-BASED CHANNEL SENSING

*Initialize $q(L_j, o_k)$ for all $j \in R$ and $k \in A$.
For each decision epoch t do the following:
*Observe the belief state vector $\mathbf{b}^t$.
*Calculate the degree of truth of the belief state vector $\alpha_j(\mathbf{b}^t)$ for all rules ((2.6)).
*For each rule select an action o_j using the EEP policy ((2.5)).
*Compute the inferred action $a(\mathbf{b}^t)$ and its corresponding quality $Q(\mathbf{b}^t, a(\mathbf{b}^t))$ ((2.8) and (2.9), respectively).
*Execute the action $a(\mathbf{b}^t)$ and observe the new belief state vector $\mathbf{b}^{t+1}$.
*Receive the reinforcement signal (reward) r^t.
*Calculate the degree of truth of the new belief state vector $\alpha_j(\mathbf{b}^{t+1})$ for all rules ((2.6)).
*Calculate the value function of the new belief state vector ((2.10)).
*Calculate the variation of the quality ΔQ ((2.11)).
*Update the elementary quality $q(L_j, o_j)$ for each rule $j \in R$ and the chosen action o_k, $k \in A$ ((2.12)).

change in the system output (FQL output, i.e., the inferred action learned by the MN) when we change the type of the membership function on the same system. However, the selection of membership function type is out of the scope of this thesis. As mentioned, in this thesis, we use Gaussian function which is more preferable as it provides better smoothness and easy to describe the generation of new fuzzy rules [27]. It should be noted that the inferred action $a(\mathbf{b})$ as the output of the FIS is applied to the environment by the MN. However, since $a(\mathbf{b})$ is a continuous action, its value may not be an integer while this value specifying the action's type (Data Transmission, Stop Data Transmission or Channel Switching) for the MN, should be an integer. Thus, we use the round off principle to quantize the value of $a(\mathbf{b})$ to an integer. A "collision" occurs between the PU and the CR network when the CR nodes (as the SNs related to the MN in the presented model) transmit data while the operating channel is occupied by the PU. Reinforcement signal (reward) r penalizes the CR network whenever a collision occurs between the CR network and the PU. In this case, the CR network is penalized by a negative fixed value, i.e. -5. Accordingly, if the CR network performs channel switching whether the PU is active or inactive over the operating channel, the penalty value is -0.5. Note that if less-frequent channel

switching is preferred for stability, a more negative value can be chosen. The reward r should be a positive value when user data are successfully transmitted by the SNs without collision, i.e. +5. On the other hand, If stop data transmission (regardless the PU state) is chosen, then the time is consumed without transmitting any data, and therefore r should be zero. The values of the rewards can be varied to control the tradeoff between the channel utilization and the collision probability. For example, we can reduce the collision probability at the expense of channel utilization by decreasing the value of r from +5 to +2 [27].

2.4.2 Numerical Evaluations

To show the performance of the FQL algorithm and its supremacy against the QL algorithm, different figures were depicted. The main goal is that the CR network has to avoid any collision with the PU and at the same time achieving the maximum channel utilization. Indeed, the "channel utilization" is defined as the proportion of time in which the CR networks successfully exchange data without collision with the PU. In other words, the final purpose is to maximize the total discounted reward. This value is a figure of merit for the quality of the learned policy, i.e., how much reward the CR accumulates while following the optimal policy. The parameter values used in this chapter are $\kappa = 0.8$, $\gamma = 0.995$, $\varepsilon = 0.3$, $\eta = 0.5$, $T_c = 1$ ms, $T = 0.1$ ms and the SNR of the PU signal is -10 dB (the optimal values of the FQL parameters can be obtained with the help of a genetic algorithm without any prior information as in [75]). The transition probability $P_{i,j}$ is also governed by the following matrix:

$$\begin{pmatrix} P_{0,0} & P_{0,1} \\ P_{1,0} & P_{1,1} \end{pmatrix} = \begin{pmatrix} 0.98 & 0.02 \\ 0.02 & 0.98 \end{pmatrix}. \tag{2.13}$$

Furthermore, in the EEP strategy, we gradually reduce the value of exploration parameter ε after each decision epoch using the following equation:

$$\varepsilon = \varepsilon \times 0.995. \tag{2.14}$$

Fig. 2.7 shows the reward accumulation results for the FQL and QL algorithms as well as a random selection method (where the action regarding the MN's belief state at each decision epoch is selected randomly). As shown in this figure, the FQL achieves the highest sum of discounted reward. Clearly, use of the FIS decision unit allows the agent to quickly and efficiently achieve the optimal policy. Thus, using the FQL, the CR network can accumulate more reward while following the optimal policy. Realization of such high performance is an indicator of the quality of learned policy. Fig. 2.8 illustrates the collision probability between the PU and the CR network. The "collision probability" is defined as the proportion of time in which the CR network transmits data when the operating channel is in use by the PU. Results show that the collision probability when the FQL algorithm is used for discovering the optimal policy is always lower than that when the QL is used. As it is seen in this figure, at the beginning of the learning process (at the initial decision epochs), whenever the PU is in active state or appears in the operating channel, the collision probability is high, and this is because of the wrong decisions made by the CR network from lack of experience regarding the PU state. However, as time goes on and the optimal policy is discovered by the MN (using the RL algorithms), the collision probability is low even in those times that the PU is active or appears in the operating channel. Fig. 2.9 (a), (b) and (c) respectively shows the PU activity on the operating channel (of course, the MN is unaware of the PU activity, but can learn it using the RL), the instantaneous reward gained by the CR network equipped with the QL and the instantaneous reward gained by the CR network equipped with the FQL. Indeed, the instantaneous reward gives more information about the higher performance of the FQL. The FQL based scheme for the CR network got more rewards and fewer penalties, since use of FIS allows the CR network to quickly and stably zero-in on the optimal policy. As a result, higher channel utilization and lower collision probability are achieved.

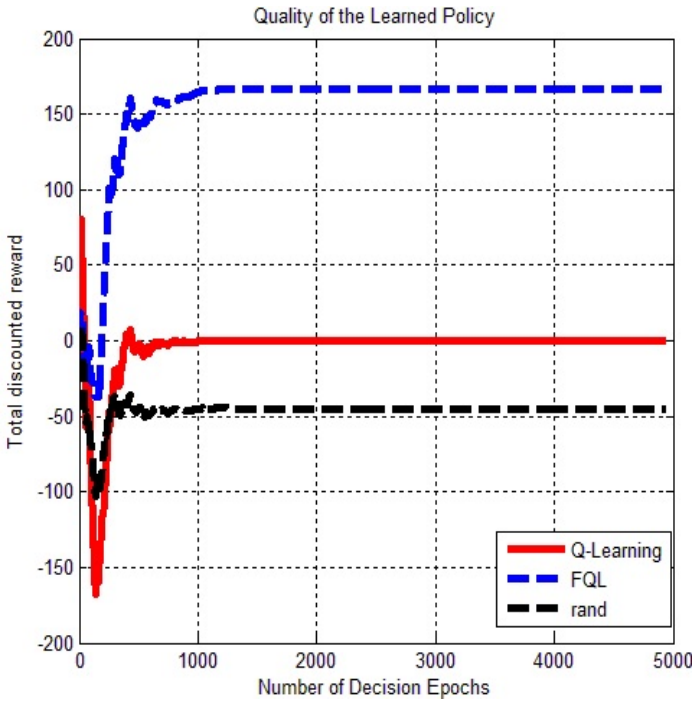

Fig. 2.7. Total discounted reward of different strategies

2.5 Estimation of the State Transition Probabilities

To obtain the simulation results in Figs. 2.7, 2.8 and 2.9, we assumed that the state transition probabilities ($P_{i,j}$) of the PU (in the belief state formula) are known to the CR as in different studies (e.g., [62], and [63]), which is in most cases not true in the real world. Hence, even though the concept of sensing is valid literally, its practical application is severely limited [76], [77]. Thus quite realistically, the channel state transition probabilities are assumed to be unknown. On the other hand, during the whole operation time, the channel state transition probabilities are assumed to be constant; and these values are estimated by the CR network. These transition probabilities can be estimated using the Baum-Welch Algorithm (BWA) [78], which is basically a derived form of the Expectation Maximization (EM) algorithm for hidden Markov models (HMMs) [78]. The concept of an HMM extends directly from Markov models, with the observation being a probabilistic function of the state. An HMM is a doubly embedded stochastic process with an underlying process that is not observable (the hidden state), but can only be observed through another set of stochastic process that produces the sequence of observations [78]. Though a Markov

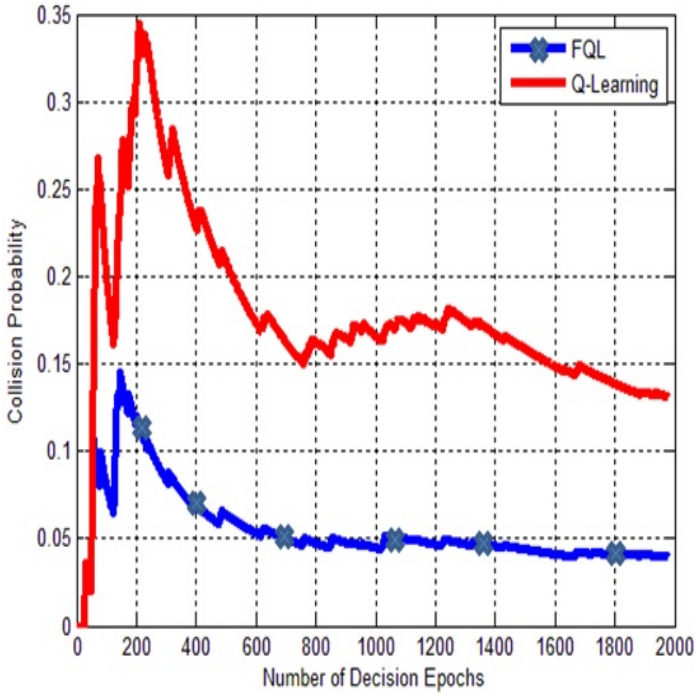

Fig. 2.8. The collision probability comparison: FQL vs. QL.

chain is appropriate in modeling the PU's channel access pattern, the true states of the PU are never known to the CR at any particular sampling instant. What the CR network can observe directly is some signal "emitted" from a particular state (The received PU signal). The received signal fits into a hidden Markov model [79]. The Baum-Welch algorithm can be employed to process input observation sequences (received at the MN) and generate parameters of HMMs. Training is usually done offline. The parameters of the HMM are obtained after the training phase and stored for future use. In other words, the state transition probabilities of the PU (as one of the HMM's parameters) are estimated first, and then it will be used in the POMDP framework, as previously described. The general approach is to train the model with the observation data using some iterative procedure until its convergence. More specifically, the parameter set $\lambda = (A,\ B,\ \pi)$ would be initialized with appropriate guesses at first; a set of transition probabilities $A = \{p_{i,j}\}$, $i, j \in \{0, 1\}$, $B = b_i(Y_t)$ is the observation symbol probability (also called emission probability) distribution in state i ($i \in \{0, 1\}$) which can be easily obtained from the pmf's of the sensing results (we will use Y_t to denote the observation symbol at time t), and finally π is the initial

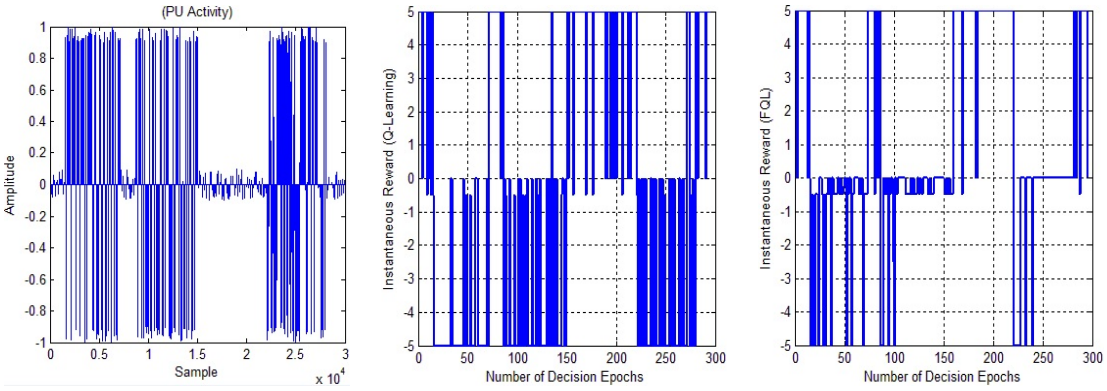

(a) (b) (c)

Fig. 2.9. (a) The PU activity on the operating channel. (b) Instantaneous reward for the QL based CR network. (c) Instantaneous reward for the FQL based CR network.

state probabilities $\pi = \{\pi_i\}$, $i \in \{0, 1\}$. Then a set of re-estimation formula would be repeatedly used in a number of iterations so that the parameter set could gradually approach to the ideal values where the occurrence possibility of the observation sequence is maximized. Let $\xi_t(i, j)$ be the probability of the HMM being in state i at time t and making a transition to state j at time $t+1$, given the appropriate guesses of the model $\lambda = (A,\ B,\ \pi)$ and observation sequence $\mathbf{Y} = \{Y_1,\ Y_2,\ \ldots,\ Y_T\}$ as the partial observation sequence received at the CR network (The signal received at time t (observation symbol, Y_t) at the CR, is a noisy version of the PU's actual signal, i.e., $Y_t = s_t X_t + U_t$ where X_t is the PU's signal, and U_t is modeled as additive white Gaussian noise (AWGN) with mean zero and variance σ^2):

$$\xi_t(i, j) = P(s_t = i, s_{t+1} = j | \mathbf{Y}, \lambda). \tag{2.15}$$

With the first-order Markov assumption, the received samples in the observation sequence are conditionally independent given the state sequence. In other words, the probability distribution of generating current observation symbol depends only on the current channel state, i.e.,

$$P(\mathbf{Y}|\mathbf{s}, \lambda) = \prod_{t=1}^{T} P(Y_t|s_t, \lambda) \tag{2.16}$$

where $\mathbf{s} = \{s_1,\ s_2,\ \ldots\ ,\ s_T\}$ denotes the hidden channel state sequence. Using Bayes law and the independency assumption, (2.15) follows:

$$\frac{\alpha_t(i)\, p_{i,j} b_j(Y_{t+1})\, \beta_{t+1}(j)}{P(\mathbf{Y}|\lambda)} \tag{2.17}$$

$\alpha_t(i) = P\left(s_t = i,\ \mathbf{Y}^{(t)}|\lambda\right)$, $\beta_t(i) = P(\mathbf{Y}^{*(t)}|s_t = i, \lambda)$ and $P(\mathbf{Y}|\lambda)$ are forward probabilities, backward probabilities and observation probability (the pmf's of the observation sequence $\mathbf{Y}$ given the parameter set λ), respectively, where $\mathbf{Y}^{(t)} = \{Y_1,\ \ldots\ ,\ Y_t\}$ is the partial observation sequence up to time t and $\mathbf{Y}^{*(t)} = \{Y_{t+1},\ \ldots\ ,\ Y_T\}$, the partial time series beyond time t. Therefore, $\alpha_t(i)$ is the probability of partial observations up to time t and in state i at time t. $\alpha_t(i)$ is proportional to the likelihood of the past observations and can be solved recursively according to:

$$\alpha_1(i) \ = \ P(Y_1; s_t \ = \ i) \ = \pi_i b_i(Y_1) \tag{2.18}$$

$$\alpha_t(i) \ = \sum_{j\in\{0,1\}} [\alpha_{t-1}(j)\, p_{j,i}] b_i(Y_t) \tag{2.19}$$

for $2 \leq t \leq T$. In a very similar manner, $\beta_t(i)$ is the probability of the partial observation sequence from Y_{t+1} to the end produced by all state sequences that start at the ith state. By definition, $\beta_T(i) = 1$. $\beta_t(i)$ is proportional to the likelihood of the future observations and can be solved recursively according to:

$$\beta_t(i) \ = \sum_{j\in\{0,1\}} \beta_{t+1}(j)\, p_{i,j} b_j(Y_{t+1}) \tag{2.20}$$

for $t = T-1, T-2, ..., 1$. Finally, the normalization factor $P(\mathbf{Y}|\lambda)$ can be calculated in the following ways:

$$P(\mathbf{Y}|\lambda) = \sum_{i\in\{0,1\}} \alpha_T(i) \tag{2.21}$$

$$P\left(\mathbf{Y}|\lambda\right)=\sum_{i\in\{0,1\}}\pi_i b_i\left(Y_1\right)\beta_1\left(i\right) \tag{2.22}$$

$$P\left(\mathbf{Y}|\lambda\right)=\sum_{i\in\{0,1\}}\alpha_t\left(i\right)\beta_t\left(i\right) \tag{2.23}$$

for any $1\leq t\leq T$. Thus the desired probability is simply computed by summing all the forward and backward products as in (2.23). The recursive computation structure of the forward probabilities is illustrated in the trellis of Fig. 2.10. We also define $\gamma_t(i)$ as the probability of being in state i at time t given the observation sequence $\mathbf{Y}$ and the model λ, then it can be proven:

$$\gamma_t\left(i\right)=P\left(s_t=i|\mathbf{Y},\lambda\right)$$

$$\gamma_t\left(i\right)=\frac{P(s_t=i,\mathbf{Y}|\lambda)}{P\left(\mathbf{Y}|\lambda\right)}$$

$$\gamma_t\left(i\right)=\frac{P\left(s_t=i,\mathbf{Y}^{(t)}|\lambda\right)P(\mathbf{Y}^{*(t)}|s_t=i,\lambda)}{P\left(\mathbf{Y}|\lambda\right)}$$

$$\gamma_t\left(i\right)=\frac{\alpha_t\left(i\right)\beta_t\left(i\right)}{P\left(\mathbf{Y}|\lambda\right)}. \tag{2.24}$$

Note that

$$\sum_{t=1}^{T-1}\gamma_t\left(i\right)=\ \textit{expected No. of transitions from state } i. \tag{2.25}$$

$$\sum_{t=1}^{T-1}\xi_t\left(i,j\right)=\ \textit{expected No. of transitions from state } i \textit{ to state } j. \tag{2.26}$$

$\gamma_t(i)$ is shown to be related to $\xi_t(i,j)$ by

$$\gamma_t(i) = \sum_{j=1}^{2} \xi_t(i,j). \tag{2.27}$$

With the above definitions, we can outline the Baum-Welch re-estimation formula:

$$\begin{aligned} \hat{\pi}_i &= \textit{expected frequency in state } i \textit{ at time } t = 1 \\ &= \gamma_1(i) \end{aligned} \tag{2.28}$$

$$\begin{aligned} P_{i,j} &= \frac{\textit{expected No. of transitions from state } i \textit{ to } j}{\textit{expected No. of transitions from state } i} \\ &= \frac{\sum_{t=1}^{T-1} \xi_t(i,j)}{\sum_{t=1}^{T-1} \gamma_t(i)} = \frac{\sum_{t=1}^{T-1} \alpha_t(i)\, p_{i,j} b_j(Y_{t+1})\, \beta_{t+1}(j)}{\sum_{t=1}^{T-1} \alpha_t(i)\, \beta_t(i)} \end{aligned} \tag{2.29}$$

$$\hat{b}_i(m) = \frac{\textit{expected No. of times in state } i \textit{ and observing } U_m}{\textit{expected No. of times in state } i}$$

$$= \frac{\sum_{t=1,\ Y_t=U_m}^{T} \gamma_t(i)}{\sum_{t=1}^{T} \gamma_t(i)} \tag{2.30}$$

where U_m is the mth symbol in the observation alphabet (here we have two observation symbols (active and inactive) in alphabet size representing the PU state). Suppose we have an initial guess of the parameters of the HMM $\lambda_0 = (A_0, B_0, \pi_0)$ and several sequences of observations, then using (2.25) and (2.26), we can calculate the expected values of transition properties of the Markov Chain (the Expectation step of EM algorithm). Then the maximum likelihood estimation of the model is computed through the recursive usage of (2.28)-(2.30) (the Maximization step of EM algorithm). It can be proven [80] that after each iteration and gaining a new parameters of the HMM, the received observation sequences can be better explained by the new model. The λ is iteratively re-estimated until it converges to a limit point. It should be remembered that the Baum-Welch method leads to a local maximum of λ only. In practice, to get

a good solution, the initial guess λ_0 is very important. Usually several sets of starting guesses of λ_0 are used and one with the greatest likelihood value is chosen. Laird suggested a grid search method [80] which divides the searching domain into small grids and starts from each of the intersections. Leroux and Puterman argue that the grid method would generate too many initial points when high dimensional spaces are involved. They suggest a clustering algorithm and a simple implementation can be found in [81]. The independence assumption we made was between the symbols of the single observation sequence $\mathbf{Y} = \{Y_1,\ Y_2,\ \ldots\ ,\ Y_T\}$. We consider a short time window to collect symbols in an observation sequence. Symbols collected within a short time window on the PU activity have negligible correlation as shown in [81]. Therefore, the independence assumption made between the symbols in an observation sequence is to facilitate the mathematical computations and it is a reasonable assumption. However, the major problem with the estimation method is that only a single observation sequence (from a short time window) to train the model is not enough [78]. Hence, in order to have sufficient data to make acceptable estimates of the parameter set λ, we have to use multiple observation sequences. On the other hand, the most important issue is that for a set of observation sequences in a real and practical system, one cannot say these observation sequences are independent from each other [83]. Generally speaking, in real scenarios, these observation sequences are statistically correlated. A controversy can arise if one assumes the independence property while these observation sequences are statistically correlated. Now let us consider a set of observation sequences from a pattern class:

$$\mathbf{O} = \{\mathbf{Y}^{(1)}, \mathbf{Y}^{(2)},\ \ldots\ , \mathbf{Y}^{(L)}\} \tag{2.31}$$

where

$$\mathbf{Y}^{(l)} = \{Y_1^{(l)}, Y_2^{(l)},\ \ldots\ , Y_T^{(l)}\}, 1 \leq l \leq L \tag{2.32}$$

Without loss of generality we have the following expressions

$$\begin{cases} P\left(\mathbf{O}|\lambda\right) = P\left(\mathbf{Y}^{(1)}|\lambda\right) P\left(\mathbf{Y}^{(2)}|\mathbf{Y}^{(1)},\lambda\right) \ ... \ P\left(\mathbf{Y}^{(L)}|\mathbf{Y}^{(L-1)} \ ... \ \mathbf{Y}^{(1)},\lambda\right) \\ P\left(\mathbf{O}|\lambda\right) = P\left(\mathbf{Y}^{(2)}|\lambda\right) P\left(\mathbf{Y}^{(3)}|\mathbf{Y}^{(2)},\lambda\right) \ ... \ P\left(\mathbf{Y}^{(1)}|\mathbf{Y}^{(L)} \ ... \ \mathbf{Y}^{(2)},\lambda\right) \\ ... \\ P\left(\mathbf{O}|\lambda\right) = P\left(\mathbf{Y}^{(L)}|\lambda\right) P\left(\mathbf{Y}^{(1)}|\mathbf{Y}^{(L)},\lambda\right) \ ... \ P\left(\mathbf{Y}^{(L-1)}|\mathbf{Y}^{(L)}\mathbf{Y}^{(L-2)} \ ... \ \mathbf{Y}^{(1)},\lambda\right) \end{cases} \tag{2.33}$$

Based on the above expressions, it is easy to see that the multiple observation sequence probability can be expressed as a combination of individual observation probabilities, i.e.,

$$P\left(\mathbf{O}|\lambda\right) = \sum_{l=1}^{L} w_l P\left(\mathbf{Y}^{(l)}|\lambda\right) \tag{2.34}$$

in which,

$$\begin{cases} w_1 = \frac{1}{L} P\left(\mathbf{Y}^{(2)}|\mathbf{Y}^{(1)},\lambda\right) \ ... \ P\left(\mathbf{Y}^{(L)}|\mathbf{Y}^{(L-1)} \ ... \ \mathbf{Y}^{(1)},\lambda\right) \\ w_2 = \frac{1}{L} P\left(\mathbf{Y}^{(3)}|\mathbf{Y}^{(2)},\lambda\right) \ ... \ P\left(\mathbf{Y}^{(1)}|\mathbf{Y}^{(L)} \ ... \ \mathbf{Y}^{(2)},\lambda\right) \\ ... \\ w_L = \frac{1}{L} P\left(\mathbf{Y}^{(1)}|\mathbf{Y}^{(L)},\lambda\right) \ ... \ P\left(\mathbf{Y}^{(L-1)}|\mathbf{Y}^{(L)}\mathbf{Y}^{(L-2)} \ ... \ \mathbf{Y}^{(1)},\lambda\right) \end{cases} \tag{2.35}$$

are weights. These weights are conditional probabilities and hence they can characterize the dependence-independence property. Based on the above equations, the modification of corresponding re-estimation equations in (2.28), (2.29) and (2.30) are respectively as follows [83]

$$\hat{\pi}_i = \frac{\sum_{l=1}^{L} w_l P\left(\mathbf{Y}^{(l)}|\lambda\right) \gamma_1^l(i)}{\sum_{l=1}^{L} w_l P\left(\mathbf{Y}^{(l)}|\lambda\right)} \tag{2.36}$$

TABLE 2.2. TRANSITION PROBABILITIES ESTIMATION AS A FUNCTION OF THE DATA SET FOR TRAINING MODEL (AT SNR $= -2$ DB)

Original Parameter $P_{i,j}$	Test set 1(300 data)	Test set 2(1000 data)	Test set 3(5000 data)
$\begin{pmatrix} 0.98 & 0.02 \\ 0.02 & 0.98 \end{pmatrix}$	$\begin{pmatrix} 0.7114 & 0.2886 \\ 0.3415 & 0.6585 \end{pmatrix}$	$\begin{pmatrix} 0.8000 & 0.2000 \\ 0.2544 & 0.7456 \end{pmatrix}$	$\begin{pmatrix} 0.9300 & 0.0700 \\ 0.0821 & 0.9179 \end{pmatrix}$

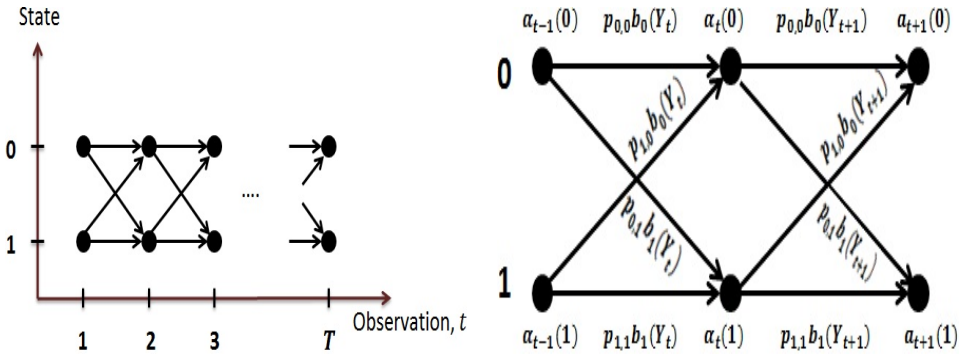

(a) (b)

Fig. 2.10. (a) Implementation of Computation of $\alpha_t(i)$ in terms of a lattice of observations t, and states i. (b) Computing the forward probabilities.

$$P_{i,j} = \frac{\sum_{l=1}^{L} w_l P\left(\mathbf{Y}^{(l)}|\lambda\right) \sum_{t=1}^{T_l-1} \alpha_t^l(i) p_{i,j} b_j\left(Y_{t+1}^{(l)}\right) \beta_{t+1}^l(j)}{\sum_{l=1}^{L} w_l P\left(\mathbf{Y}^{(l)}|\lambda\right) \sum_{t=1}^{T_l-1} \alpha_t^l(i) \beta_t^l(i)} \tag{2.37}$$

$$\hat{b}_i(m) = \frac{\sum_{l=1}^{L} w_l P\left(\mathbf{Y}^{(l)}|\lambda\right) \sum_{t=1,\ Y_t=U_m}^{T_l} \alpha_t^l(i) \beta_t^l(i)}{\sum_{l=1}^{L} w_l P\left(\mathbf{Y}^{(l)}|\lambda\right) \sum_{t=1}^{T_l} \alpha_t^l(i) \beta_t^l(i)} \tag{2.38}$$

However, in [78] the author assumes that each observation sequence is independent from every other sequence, i.e.,

$$P\left(\mathbf{O}|\lambda\right) = \prod_{l=1}^{L} P\left(\mathbf{Y}^{(l)}|\lambda\right) \tag{2.39}$$

Figs. 2.11, 2.12, 2.13 and 2.14 illustrate the following: without any a priori information about the channel characteristics, even in a very transient environment, it is quite possible to achieve reasonable estimates of channel state transition probabilities with a practical and simple implementation. They show the estimates of the channel

transition probabilities as a function of the SNR parameter for the observation set with a length of 1000. It is important to note that the estimates improve by increasing the SNR values, hence allowing better performance for the proposed sensing method in the previous sections. We initialized $\lambda_0 = (A_0, B_0, \pi_0)$ as follows:

$$\lambda_0 = \left(\begin{pmatrix} 0.85 & 0.15 \\ 0.1 & 0.9 \end{pmatrix}, \begin{pmatrix} 1 & 0 \\ 0 & 1 \end{pmatrix}, (\pi_0 = 0.2 \quad \pi_1 = 0.8) \right)$$

Clearly, the estimates also improve as the data set for the training model increases (see Table 2.2). As seen in Table 2.2, the parameter of SNR is not the only factor affecting the accuracy of estimation. Table 2.2 shows the accuracy of the estimates according to the length of the data set. We can see that the estimates become more and more accurate as the data set for the training model increases. In this example, we can get sufficiently accurate estimates from 5,000 training data even at a low SNR value of -2dB.

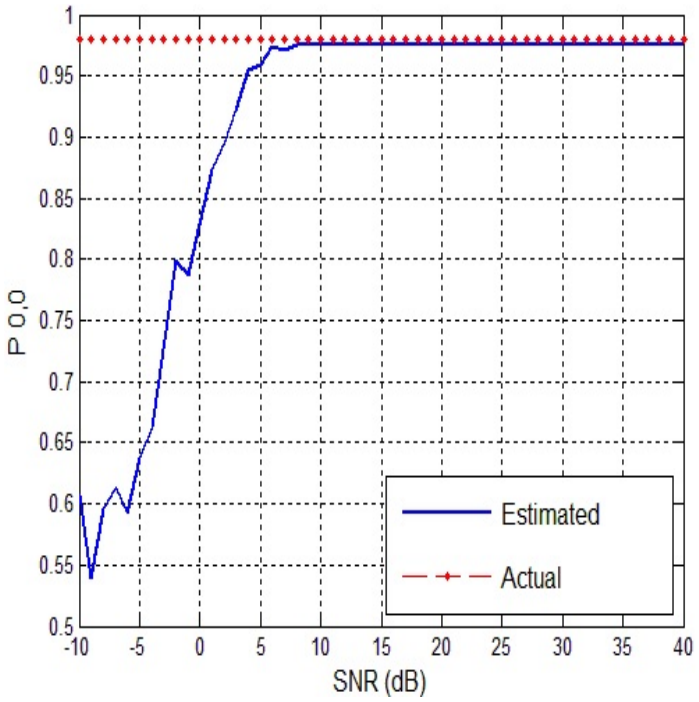

Fig. 2.11. Transition probabilities $P_{0,0}$ estimation

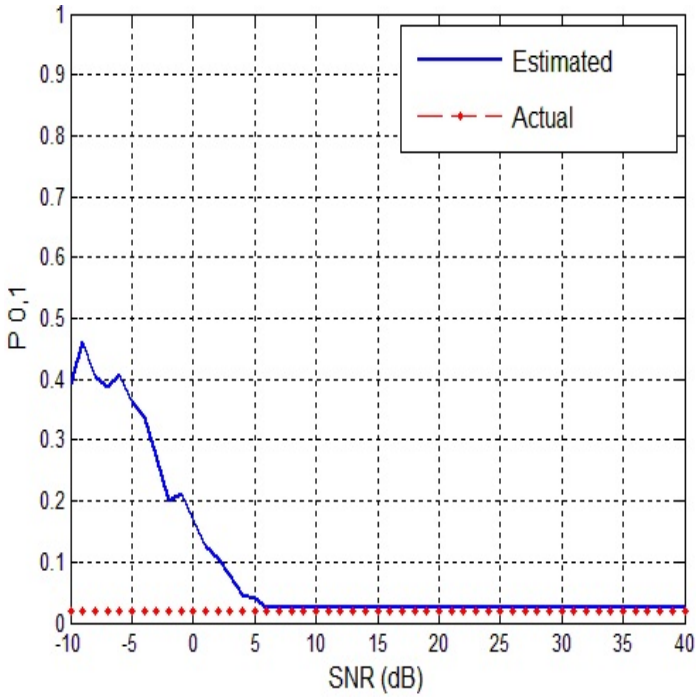

Fig. 2.12. Transition probabilities $P_{0,1}$ estimation

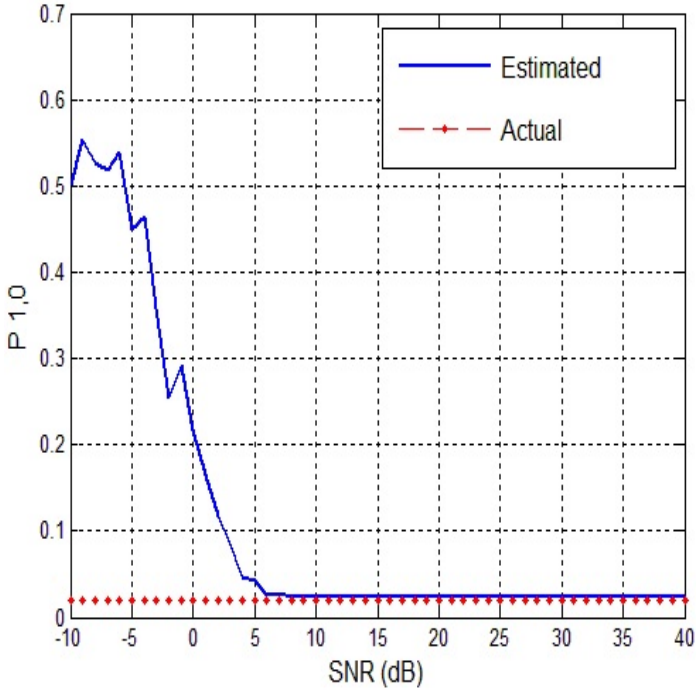

Fig. 2.13. Transition probabilities $P_{1,0}$ estimation

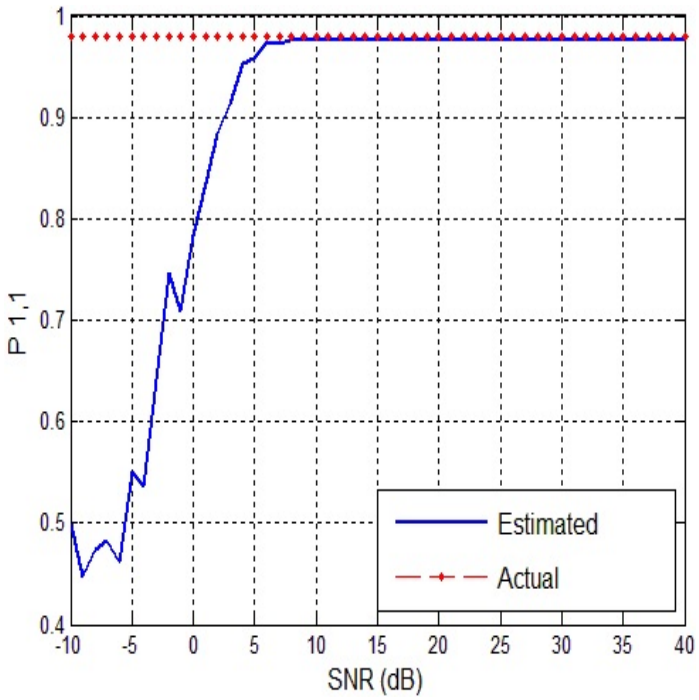

Fig. 2.14. Transition probabilities $P_{1,1}$ estimation

2.6 Conclusion

In this chapter, we have proposed a learning based scheme for channel sensing in partially-sensed CR network. We introduced a novel fuzzy RL control scheme in the POMDP framework to successfully address time and complexity issues. In particular, the CR network's channel sensing scheme is formulated as a POMDP, and the optimal policy is determined by a powerful approach such as the FQL algorithm. Using our proposed sensing scheme, the CR network can significantly improve its own spectral efficiency and reduce the probability of interfering with the PU. Simulation results show that high spectrum utilization and very low sensing error probability are achieved via the maximization of the total discounted reward. We have also shown that without any a priori information about the channel characteristics, even in a very transient environment, it is quite possible to achieve reasonable estimates of channel state transition probabilities.

Chapter 3

Stochastic Geometry Modelling and Analysis of Cognitive Heterogeneous Cellular Networks

3.1 Introduction

Most of the existing interference management techniques in the literature (including the CR technique presented in the previous chapter) are developed in idealized and simplified interference network settings. In other words, most of the interference management techniques are usually considered in settings with a particular number of cooperative transmit-and-receiver pairs, ignoring any potential interference from outside of the cooperative set. Obviously, there exist some limitations in translating the performance gains obtained from the advanced interference management techniques into any practical wireless networks because of their simplified natures. The fundamental challenge is to re-evaluate the gains obtained with the interference management techniques using models that can accurately reproduce and capture the impact of the random spatial structure of wireless transmit-and-receiver locations and channel characteristics. A possible direction is to use analytical models for large-scale interference networks via a new modeling approach called "stochastic geometry". This modeling approach facilitates compact and closed-form expressions of outage probability (as the main

performance metric used in Chapters 3 and 4) and spatially averaged spectral efficiency of in networks with the effects of out of cell interference and different channel distributions. Therefore, for example, by adopting the downlink cellular network model via stochastic geometry [34], it would be possible to analyze the system-level performance of the recent interference management algorithms including the CR technique.

The best solution to the spectrum saturation and bandwidth availability problems in multi-tier cellular networks is to adopt technologies that make the most efficient use of existing spectrum through frequency reuse schemes [30], [84]. In universal frequency reuse scheme, the existing spectrum can be aggressively and effectively reused by all of the coexisting network tiers. This will lead to higher spatial spectrum utilization and network usage capacity at the expense of an increased possibility of interference among network tiers and of a reduced QoS. In multi-tier cellular networks, interference is increasingly becoming a major performance-limiting factor, and hence, interference modeling, coordination, and avoidance are the primary focus of interest for both the industry and academic communities. Applying the CR technology in multi-tier cellular networks to be aware of and adapt to communication environments, some of the above challenges can be tackled. In fact, CR is the key enabling technology for interference management and avoidance in multi-tier cellular networks [34], [84]. On the other hand, the aggregate interference environment is more complicated to model, and evaluating the performance of communication techniques in the presence of heterogeneous interference is challenging. For interference characterization, if the BSs of the cellular network follow a regular grid (e.g., the traditional hexagonal grid model), then the SINR characterization will be either intractable [34], [35] or inaccurate due to unrealistic assumptions [36]. Moreover, as urban areas are built out, the BS infrastructure is becoming less like points on a hexagonal lattice and more random. Hence, the use of a hexagonal grid to model the BS locations is violated and is considered too idealized [37]. Furthermore, according to [34], [35] and [37] for snapshots of a cellular network at different locations, the positions of the BSs with respect to each other follow random patterns due to the size and unpredictability of the BSs in these kinds of networks. Therefore, the need for a powerful mathematical and statistical tool for modeling, analysis, and design of wireless networks with random topologies is quite obvious.

As mentioned, stochastic geometry has been recently applied to the analysis of multi-tier cellular networks due to its ability to capture the topological randomness in the network and its aim at deriving accurate and tractable expressions for outage probability [34], [37]. Stochastic geometry stems from applied probability and has a wide range of applications in the analysis and design of wireless networks in particular for modeling and analyzing systems with random channel access (e.g., ALOHA [38], [39] and CSMA [40]), single- and multi-tier cellular networks [37], and networks with cognitive abilities [38], [41]. Multi-tier cellular networks have been investigated from different perspectives such as power control [85], [86], spectrum allocation [32], [87], and exploiting CR techniques [88], [89], and recently, many works have been done based on the similar concepts to adopt and extend the stochastic geometric approach to different network models and scenarios (see [90]-[93]). This chapter discusses this new theoretical model to provide a better understanding of the heterogeneous cellular networks of tomorrow, and their challenges (interference modeling, coordination, and avoidance) that must be tackled in order for these networks to reach their potential. We focus on a two-tier femto-macro network where low-power and small-coverage local nodes (femto nodes) are distributed in the coverage of macro nodes. We provide an insight into the role of CR in interference mitigation in two-tier HetNets. We derive closed-form expressions for the outage probability of any typical femto and macro user in the network. We also study the effect of several important design factors which play vital roles in the determination of outage and interference.

Our main contributions in this chapter which is an extension of [94] are therefore the following: (i) We analyze the Laplace transforms of all four types of aggregate interference between macro and CR femto networks (including the interference between macro nodes among themselves and femto nodes among themselves, the cross-interference from femto to macro network and vice versa) in perfect and imperfect spectrum sensing CR based femto networks, considering simultaneously the PPP model, and some important design factors (such as spectrum access probability) which can play a major role in determining interference and outage. (ii) This chapter provides an insight into the role of CR in interference mitigation in OFDMA two-tier HetNets. (iii) Closed-form expressions are derived for the outage probability of any typical femto and macro

user considering the Rayleigh fading assumption for the desired and interfering links with the possibility of using the CR ability for the femto network. It should be noted that in most of the available studies in this area none of the network tiers is equipped with the CR capability and they are mostly based on the existence of only one macro-BS (along with the macro users and the femto network) and the effect of considering multiple macro-BSs is ignored in the analysis of outage probability.

Authors in [31], [95]-[97] have considered the two-tier HetNets imposing the CR ability to the femto tier. Different from [95], in our work, we consider both the perfect and imperfect sensing scenarios for the CR femto-BSs, however authors in [95] ignore the effect of sensing errors on the opportunistic channel access probability and consequently the outage probability of each tier. On the other hand, in our work, the mathematical demonstration of the obtained expressions (channel access probability and outage probability expressions) is quite different from the mentioned works.

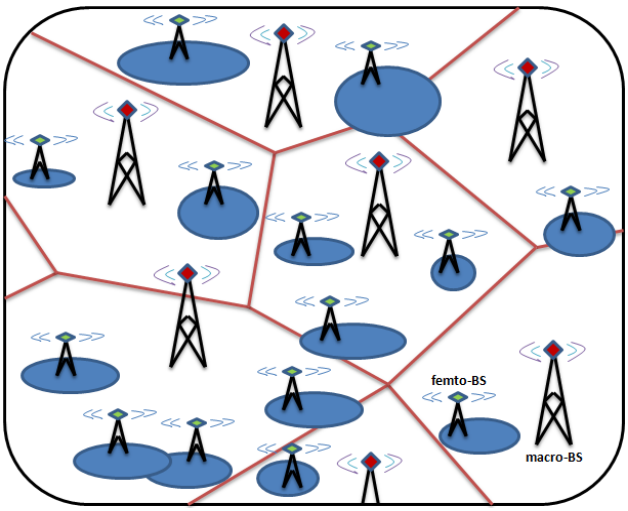

Fig. 3.1. The heterogeneous model (femto and macro BSs)

3.2 Downlink System Model

3.2.1 Model Description

We consider infinite spatially collocated macro-BS and femto-BS node HetNets (see Fig. 3.1). It is assumed that the spatial distribution of the nodes is captured using two collocated and independent homogenous Poisson point processes (HPPPs) [37], [38] i.e., Φ_M and Φ_F with intensities λ_M and λ_F, respectively. In other words, the locations of the macro-BS nodes constitute an HPPP Φ_M, where λ_M is the average number of the macro-BS nodes per unit area. Similar statement can be made for the HPPP formed by the femto-BS nodes Φ_F with intensity λ_F. According to Superposition Theorem [98], the overall node process over the network formed by both the macro-BS and femto-BS nodes also is an HPPP with intensity λ ($\lambda = \lambda_F + \lambda_M$). Furthermore, the macro and femto users are scattered about the plane according to some independent PPPs with different densities compared to λ_M and λ_F, respectively. However, our interference analysis is fundamentally concerned with the distribution of the transmitters (BSs).

Since femto-BSs are installed and maintained by the paying home users for better indoor performance, they are only accessible by their own mobile subscribers (femto users) (known as *closed-access* policy). On the other hand, macro-BSs can be accessed only by unauthorized users (macro users). In practice, macro network is deployed usually without awareness of the distributed femto network. To this end, wireless operators can consider giving priority to the macro users, and the femto network has to be self-optimized to mitigate its interference to the macro users. Motivated by this insight, the macro-BSs (along with the macro users) and the CR enabled femto-BSs (along with the femto users) are analogous to primary and secondary systems in the CR model, respectively.

3.2.2 System Structure

In OFDMA, the spectrum is orthogonally divided into time-frequency resource blocks (RBs), which increases flexibility in resource allocation, thereby allowing high spectral efficiency. As shown in Fig. 2, we consider a spectrum of N RBs, out of which M ($M \leq N$) random RBs are idle or unoccupied by the macro users (primary system). With the CR capability, a femto-BS could actively acquire

knowledge about its environment and access to the RBs without the aid of a macrocell in a decentralized fashion (clearly, no synchronization between the macro and femto network is needed any more) and automatically prevent disturbing the macro users [84].

1) As shown in Fig. 3.2, each femto-BS's transmission strategy is divided into consecutive slots, each having a duration of T. Each slot is divided into two consecutive stages, i.e., sensing and data transmission, with durations of T_S and T_D, respectively. Each femto-BS periodically senses the spectrum to identify which RBs are occupied by the macro network. Indeed, each femto-BS accomplishes sensing one RB in one unit slot T_{SRB} within T_S. Each femto-BS senses N_s RBs in sequence which are randomly selected from the N available RBs, and detects its idle RB set. Clearly, the time required for sensing the N_s RBs is $T_S = T_{SRB}N_s$. Note that the femto-BSs cannot perform data transmission within the sensing time T_S. We assume that all femto-BSs are perfectly synchronized and have the same time as the sensing time. Methods for implementing a perfect synchronization among the femto-BSs are outside the scope of this chapter, however, a set of possible candidates exist, including GPS synchronization, the wired backhaul (IEEE 1588), and leveraging synchronization signals broadcasted by the femto-BSs [99].

2) Each femto-BS senses the received interference power on each RB within the sensing duration.

– If the received interference power on an RB at a typical femto-BS exceeds a certain threshold, the RB is identified as being occupied by one or more macro nodes but not by the femto network since all the femto-BSs have the same sensing time (It should be noted that if an RB is identified as being occupied at a typical femto-BS, it does not necessarily mean that it is also seen as an occupied RB at the other femto-BSs, as this status determination process depends only on the received interference power level on the RB at each individual femto-BS).

–Otherwise, the RB is unoccupied by the macro network.

3) In the data transmission time (T_D), each femto-BS only allocates an unoccupied RB sensed in the sensing time to its user (by only utilizing these unoccupied RBs, *cross-tier* interference can be consequently avoided). Since the determination of each individual RB status as busy/idle is subject to (occasional) error, determined by the probability of (correct) detection of the presence of PUs'

signals P_d and probability of false alarm P_f (probability of falsely declaring an idle RB as busy), we study the effect of both the *ideal* detection, i.e., $P_d = 1$ and $P_f = 0$, and the cases involving imperfect sensing (see [100] and [101]), i.e., $P_d \neq 1$ and $P_f \neq 0$ on the outage probabilities of femto and macro users.

In each realization of the point process, each macro and femto user communicates only with its nearest macro-BS and femto-BS, respectively. As shown in Fig. 3, the macro users' exclusion regions with radius D are used to guarantee that the femto-BSs will, on average, not generate an aggregate interference leading to the outage of macro (primary) users. We assume that the macro users can be localized, e.g., based on pilot signals or transmitted acknowledgments. Therefore, the femto-BSs inside the macro users' exclusion regions may be able to detect the macro signals and cease their transmissions. As shown in the figure, for example, those femto-BSs located in the tagged macro user's exclusion region are not allowed to transmit data whether they pick the same RB as the tagged macro user or a different one. It should be noted that the tagged macro user is not disturbed by the femto-BSs transmitting on different RBs (from that of the tagged macro) even if they are inside its exclusion region. However, we deactivate them to protect the tagged macro user from any harmful interference as a result of possible errors in their sensing and location detection processes (we consider this law throughout the chapter even in the case of the perfect sensing scenario). For instance, if a femto-BS, located at a very close distance from the tagged macro user, wrongly (the cases involving imperfect sensing) picks the occupied RB by the tagged macro user, it will cause a severe interference to the tagged macro user if it is not able to perfectly detect the location of the tagged macro user (e.g., because of the hidden node problem in CR systems [102]) to cease its transmission.

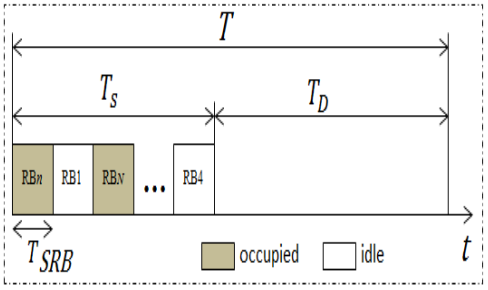

Fig. 3.2. The CR femto-BS's transmission strategy in one time slot

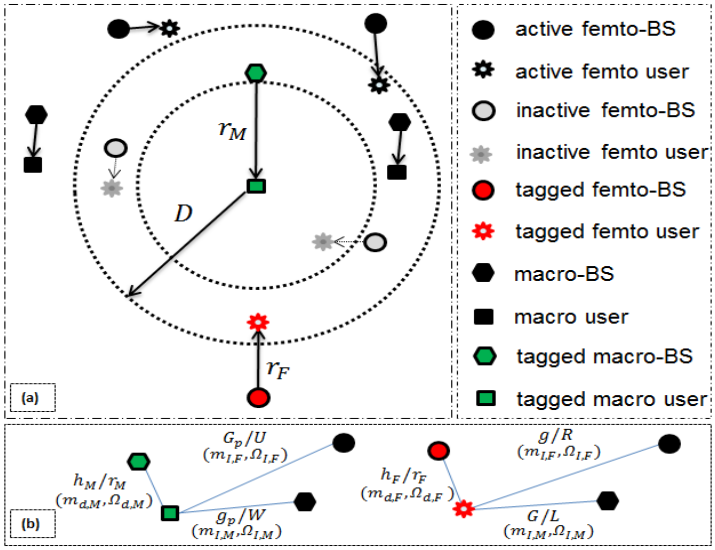

Fig. 3.3. (a) The bipolar network model. (b) The link gains/distances

3.3 Stochastic Geometry Based Network Configuration

3.3.1 Femto Outage Probability Formulation

We derive the probability of outage for a typical femto user (p_{OF}) in a downlink heterogeneous cellular network defined as the probability that a randomly chosen femto user cannot achieve a target SINR θ (or equivalently as the average fraction of femto users who do not achieve a target SINR θ, i.e., the averaged outage probability of all femto users) considering a collocated spectrum sensing CR based femto network and macro-BSs as follows [37]:

$$p_{OF} = 1 - P[\text{SINR} > \theta] \tag{3.1}$$

In fact, the outage probability evaluates the CDF of SINR over the entire network. The experienced SINR by a typical femto user is calculated as

$$\text{SINR} = \frac{P_F h_F r_F^{-\alpha}}{\sigma^2 + I_{FB} + I_{MB}} \tag{3.2}$$

where P_F is the transmission power from the nearest femto-BS (tagged femto-BS) located in the random distance r_F from its tagged femto user (we assume that the tagged femto user under consideration is located at the origin), and α is the path-

loss exponent. I_{FB} and I_{MB} are the aggregate interference power at the origin from the other femto-BSs and macro-BSs, respectively, and σ^2 is the noise power. It should be noted that the transmission power values of all the femto-BSs in the network are kept constant i.e., P_F.

Let $h_F \sim \exp(\mu)$ (with mean $1/\mu$) be a random variable accounting for the random channel gain of the link between the tagged femto user and its corresponding femto-BS, and then we have

$$\begin{aligned} P[\text{SINR} > \theta] &= P\left[\frac{P_F h_F {r_F}^{-\alpha}}{\sigma^2 + I_{FB} + I_{MB}} > \theta\right] \\ &\overset{(\cdot\cdot)}{=} P\left[h_F > (\sigma^2 + I_{FB} + I_{MB})\frac{\theta {r_F}^{\alpha}}{P_F}\right] \\ &\overset{(\cdots)}{=} \mathrm{E}_{I_{FB},I_{MB}}\left[\int_{(\sigma^2+I_{FB}+I_{MB})\frac{\theta {r_F}^{\alpha}}{P_F}}^{\infty} [\mu \exp(-\mu x)]\, \mathrm{d}x\right] \\ &= \mathrm{E}_{I_{FB},I_{MB}}\left[\exp\left[-\mu(\sigma^2 + I_{FB} + I_{MB})\frac{\theta {r_F}^{\alpha}}{P_F}\right]\right] \end{aligned} \tag{3.3}$$

where $(\cdot\cdot)$ is derived by rearranging the terms in SINR; $(\cdots)$ is derived by noting that h_F is an exponential random variable; $\mathrm{E}_{I_{FB},I_{MB}}[\cdot]$ is the expectation operator with respect to the joint distribution of the random variables I_{FB} and I_{MB}.

Note that due to the assumption of independent PPPs for the femto and macro networks, the aggregate interference received from the femto-BSs is independent of the aggregate interference received from the macro-BSs [41], therefore, we can write

$$\begin{aligned} P[\text{SINR} > \theta] &= e^{-\mu\frac{\theta {r_F}^{\alpha}}{P_F}\sigma^2} . \mathrm{E}_{I_{FB}}\left[e^{-\mu\frac{\theta {r_F}^{\alpha}}{P_F} I_{FB}}\right] . \mathrm{E}_{I_{MB}}\left[e^{-\mu\frac{\theta {r_F}^{\alpha}}{P_F} I_{MB}}\right] \\ &= e^{-\mu\frac{\theta {r_F}^{\alpha}}{P_F}\sigma^2} . \mathcal{L}_{I_{FB}}\left(\mu\frac{\theta {r_F}^{\alpha}}{P_F}\right) . \mathcal{L}_{I_{MB}}\left(\mu\frac{\theta {r_F}^{\alpha}}{P_F}\right) \end{aligned} \tag{3.4}$$

where $\mathcal{L}_{I_{FB}}(s)$ and $\mathcal{L}_{I_{MB}}(s)$ are the Laplace transform of random variables I_{FB} and I_{MB} evaluated at s ($s = \mu\frac{\theta {r_F}^{\alpha}}{P_F}$), respectively. Thus, the probability of outage averaged over the plane is derived as

$$p_{OF} = 1 - \mathrm{E}_{r_F}\left[P[\text{SINR} > \theta]\right]$$

$$p_{OF} = 1 - \int_0^{\infty} \left[P[\text{SINR} > \theta]\right] . f_{r_F}(r_F)\, \mathrm{d}r_F \tag{3.5}$$

where $f_{r_F}(r_F) = e^{-\lambda_F \pi {r_F}^2} 2\pi\lambda_F r_F$ (as mentioned before, r_F is the random distance between the tagged femto user and its corresponding femto-BS) is the probability density function (pdf) of r_F [37]. Then, we have

$$p_{OF} = 1 - \int_0^{\infty} e^{-\pi\lambda_F {r_F}^2} . e^{-\mu \frac{\theta {r_F}^{\alpha}}{P_F} \sigma^2} . \mathcal{L}_{I_{FB}}\left(\mu \frac{\theta {r_F}^{\alpha}}{P_F}\right) . \mathcal{L}_{I_{MB}}\left(\mu \frac{\theta {r_F}^{\alpha}}{P_F}\right) . 2\pi r_F \lambda_F \, \mathrm{d}r_F \tag{3.6}$$

Scenario I

Ideal detection ($P_d = 1$ and $P_f = 0$):

Each secondary node (femto-BS) has perfect knowledge of each primary (macro-BS) signaling. In other words, sensing at each femto-BS is done perfectly. Therefore, an RB occupied by a macro-BS is not chosen for data transmission by the nearby femto-BSs. Under this condition, the tagged femto user, during the data transmission time, does not experience any interference from the macro-BSs since it always communicates with its corresponding femto-BS on an idle RB. In fact, we assume that the received interference power from the macro network under this scenario can be neglected if it is measured to be less than a specified threshold (if we do not neglect the received interference power under the explained condition, then the outage probability formulations will be the same as in Scenario II except for the RB selection probability expressions, p_{RB}, as we explain later. Similar arguments can be made for the outage probability of the macro tier as discussed in the next subsection).

Therefore, under this assumption, $\mathrm{E}_{I_{MB}}\left[e^{-\mu \frac{\theta {r_F}^{\alpha}}{P_F} I_{MB}}\right] = 1$ and $\mathcal{L}_{I_{MB}}\left(\mu \frac{\theta {r_F}^{\alpha}}{P_F}\right) = 1$, consequently. Then (3.6) is rewritten as follows

$$p_{OF} = 1 - \int_0^{\infty} e^{-\pi\lambda_F {r_F}^2} . e^{-\mu \frac{\theta {r_F}^{\alpha}}{P_F} \sigma^2} . \mathcal{L}_{I_{FB}}\left(\mu \frac{\theta {r_F}^{\alpha}}{P_F}\right) . 2\pi r_F \lambda_F \, \mathrm{d}r_F . \tag{3.7}$$

The Laplace transform of the aggregate interference from all the active femto-BSs except the tagged femto-BS denoted by fbs_0 is given as follows (Note: some of the femto-BSs located in the macro users' exclusion regions with radius D are deactivated, therefore, $\lambda'_F \leq \lambda_F$ (see Fig. 3.3))

$$\begin{aligned}\mathcal{L}_{I_{FB}}(s) &= \mathrm{E}_{I_{FB}}[\exp(-sI_{FB})] \\ &= \mathrm{E}_{\Phi_F, g_i}\left[\exp\left(-s\sum_{i\in\Phi_F\setminus\{fbs_0\}} P_F g_i R_i^{-\alpha}\right)\right] \\ &= \mathrm{E}_{\Phi_F}\left[\prod\nolimits_{i\in\Phi_F\setminus\{fbs_0\}} \mathrm{E}_{g_i}[\exp(-sP_F g_i R_i^{-\alpha})]\right] \end{aligned} \tag{3.8}$$

where R_i is the distance of the ith interferer from the tagged femto receiver captured by the point process Φ_F. The IC gains g_i are assumed to be mutually independent and have identical pdfs. Each of the active interfering femto-BSs transmits with the same power P_F. Using the definition of the Generating functional [37] for the PPP, which states for some function $f(x)$ that $\mathrm{E}[\prod_{x\in\Phi} f(x)] = \exp(-\int_{\mathbb{R}^d}(1-f(x))\lambda\,\mathrm{d}x)$, (3.8) can be rewritten as

$$\mathcal{L}_{I_{FB}}(s) = \exp\left\{-\mathrm{E}_g\left[\int_{r_F}^{\infty}(1-\exp(-sP_F g R^{-\alpha}))\lambda_I(R)\mathrm{d}R\right]\right\} \tag{3.9}$$

where we flipped the order of integration and expectation. Since the closest interfering femto-BS is at least at distance r_F from the tagged user, the integration limits are from r_F to ∞. In other words, interference is encountered from all the active femto-BSs located in the area $\mathbb{R}^d\backslash b(0, r_F)$ (where $b(x, y)$ is ball of radius y centered at point x). However, not all the femto-BSs will contribute towards the aggregate interference, i.e., only those active femto-BSs located outside the mentioned ball which at minimum satisfy all of the following conditions qualify as potential contributors.

Before explaining these conditions ((a) and (b)), it is useful to translate the point process into polar coordinates. Therefore, according to [38] and [98] the intensity of the HPPP Φ_F is shown as

$$\lambda_I(R) = \lambda'_F d R^{d-1} b_d \tag{3.10}$$

where R is the distance between an arbitrary femto-BS and the tagged femto receiver. b_d is the volume of a unit sphere in $\mathbb{R}^d$ ($b_d = \frac{\sqrt{\pi^d}}{\Gamma(1+d/2)}, \Gamma(x) = \int_0^\infty t^{x-1}e^{-t}\,\mathrm{d}t$ denotes the standard Gamma function).

(a) Satisfying the aforementioned condition, any active femto-BS contributes towards the interference at the tagged femto receiver, if it picks the same RB as the tagged femto-BS to communicate with its user. We show the probability of picking a same RB from a pool of all RBs as p_{RB} (the calculation of p_{RB} for this case is derived in Section 3.4, *Scenario I,* Case 1).

(b) We assume that the CR femto-BSs employ a slotted ALOHA MAC protocol to schedule their transmission. Therefore, they only transmit with probability p_{tx} in the current time slot and defer the transmission with probability $1 - p_{tx}$.

Applying both conditions (a) and (b) which are indeed two independent thinning tools, the thinned point process of Φ_F is formed. In other words, Φ_F is subjected to two thinning processes each presenting an independent deletion/retention of each point of Φ_F with a fixed retention probability. We now formulize this operation, which will in fact result in reducing the number of interferers and hence lowering the outage probability at the tagged femto user. First, Φ_F is reconstructed by p_{RB}-thinning, where each point of Φ_F is retained with probability p_{RB} (to accommodate condition (a)), and then it is thinned again by applying the second independent thinning (to accommodate condition (b)). Thus, the intensity of the process (the number of interfering CR femto-BSs) becomes

$$\lambda_I(R) = \lambda'_F d R^{d-1} b_d p_{RB} p_{tx} \tag{3.11}$$

Now, (3.9) is rewritten as

$$\exp\left\{-E_g\left[\int_{r_F}^{\infty}(1-\exp(-sP_F g R^{-\alpha}))\lambda'_F b_d p_{RB} p_{tx} d R^{d-1} dR\right]\right\}.$$

By using the change of variables $R^d \to x$ and then $x^{\frac{\alpha}{d}} \to y$, and doing some simple calculations, the above expression is simplified as:

$$\mathcal{L}_{I_{FB}}(s) = e^{{r_F}^d b_d p_{RB} p_{tx} \lambda'_F - \frac{d}{\alpha} b_d p_{RB} p_{tx} \lambda'_F (\mu\theta)^{\frac{d}{\alpha}} {r_F}^d M(\theta,\alpha)} \tag{3.12}$$

where

$$M(\theta,\alpha) = \mathrm{E}\left[(g)^{\frac{d}{\alpha}}\left(\Gamma\left(-\frac{d}{\alpha}, \mu\theta g\right) - \Gamma\left(-\frac{d}{\alpha}\right)\right)\right] \tag{3.13}$$

Note that $\Gamma(a,x) = \int_x^\infty t^{a-1}e^{-t}\,\mathrm{d}t$ indicates the incomplete Gamma function. From (3.7) and (3.12), taking $d = 2$, then replacing ${r_F}^2$ with z, we get the final formula for the outage probability of the tagged femto user as follows

$$p_{OF} = 1 - \int_0^\infty e^{\pi z(\lambda'_F p_{RB} p_{tx} - \lambda_F) - \frac{\mu\theta}{P_F}\sigma^2 z^{\frac{\alpha}{2}} - \frac{2}{\alpha}\pi p_{RB} p_{tx} \lambda'_F (\mu\theta)^{\frac{2}{\alpha}} z M(\theta,\alpha)} . \pi\lambda_F \,\mathrm{d}z \tag{3.14}$$

in which $M(\theta,\alpha) = \mathrm{E}\left[(g)^{\frac{2}{\alpha}}\left(\Gamma\left(-\frac{2}{\alpha}, \mu\theta g\right) - \Gamma\left(-\frac{2}{\alpha}\right)\right)\right]$. According to [87], the downlink femtocell networks are assumed to be interference-limited, i.e., the noise can be neglected as the interference dominates the whole performances of the system ($\sigma^2 \to 0$).

Thus, (3.14) reduces to (3.15) as follows ($\alpha = 4$)

$$p_{OF} = 1 - \frac{\lambda_F}{(\lambda_F - \lambda'_F p_{RB} p_{tx}) + \frac{\lambda'_F (p_{RB} p_{tx})}{2}\sqrt{\mu\theta} M(\theta, 4)}. \tag{3.15}$$

Similar with the desired link, we consider the Rayleigh fading model for the femto interfering links as well (Rayleigh fading links with equal parameter μ). Then following the derivation of $M(\theta,\alpha)$ in Appendix A.1, p_{OF} is re-expressed as follows

$$p_{OF} = 1 - \frac{\lambda_F}{(\lambda_F - \lambda'_F p_{RB} p_{tx}) + \sqrt{\pi}\lambda'_F (p_{RB} p_{tx})\mu\left[\sum_{k=0}^\infty \frac{(\mu\theta)^k}{\Gamma\left(k+\frac{1}{2}\right)(\mu+\mu\theta)^{k+1}}\Gamma(1+k)\right]}. \tag{3.16}$$

Scenario II

Imperfect detection ($P_d \neq 1$ and $P_f \neq 0$):

In this scenario, each secondary node (femto-BS) has imperfect knowledge of each primary (macro-BS) signaling. In other words, sensing at each femto-BS is done imperfectly. Therefore, an occupied RB by a macro-BS may also be wrongly considered idle by the femo-BSs, causing collision between the two networks. Two cases can take place under the imperfect sensing scenario:

Case 1. The tagged femto-BS transmits data on an idle RB (for this case, the outage probability formulations can be considered the same as in the perfect sensing scenario except for the calculation of p_{RB} (see Section 3.4, *Scenario II,* Case 1))

Case 2. The tagged femto-BS transmits on an occupied RB (outage probability formulation in this case is explained as follows and the calculation of p_{RB} is presented in Section 3.4, *Scenario II,* Case 2)

In Case 2, the tagged femto user can experience interference from both the active femto-BSs (which pick the same occupied RB as the tagged femto-BS) and macro-BSs. Indeed, the $\mathcal{L}_{I_{MB}}\left(\mu \frac{\theta r_F{}^{\alpha}}{P_F}\right)$ (the Laplace transform of the aggregate interference from the macro-BSs) in (3.6) is not ignored. The Laplace transform of the aggregate interference power generated by the macro-BSs at the tagged femto user is given by

$$\begin{aligned}\mathcal{L}_{I_{MB}}(s) &= \mathrm{E}_{I_{MB}}[\exp(-sI_{MB})] \\ &= \mathrm{E}_{\Phi_M, G_i}\left[\exp\left(-s\sum_{i\in\Phi_M} P_M G_i L_i^{-\alpha}\right)\right] \\ &= \mathrm{E}_{\Phi_M}\left[\prod\nolimits_{i\in\Phi_M} \mathrm{E}_{G_i}[\exp(-sP_M G_i L_i^{-\alpha})]\right] \end{aligned} \tag{3.17}$$

where L_i is the distance of the ith interfering macro-BS from the tagged femto receiver captured by the point process Φ_M. The IC gains G_i are assumed to be mutually independent and have identical pdfs. Each of the active interfering macro-BSs transmits with the same power P_M.

Again, using the definition of the Generating functional for the PPP, we can write

$$\mathcal{L}_{I_{MB}}(s) = \exp\{-\mathrm{E}_G[\int_0^{\infty}(1-\exp(-sP_M G L^{-\alpha}))\lambda_I(L)\mathrm{d}L]\}. \quad (3.18)$$

The interference is encountered from all the macro-BSs located in the area $\mathbb{R}^d \backslash b(0,0)$. It should be noted that not all the macro-BSs in $\mathbb{R}^d$ will contribute towards the aggregate interference, i.e., only those macro-BSs which are transmitting on the same RB as the tagged femto user qualify as potential interferers. The intensity of the HPPP Φ_M process can be therefore written as follows

$$\lambda_I(L) = \lambda'_M \, dL^{d-1} b_d \quad (3.19)$$

where L is the distance between an arbitrary macro-BS and the tagged femto receiver and λ'_M is the intensity of those macro-BSs transmitting on the same RB as the tagged femto user at a time.

Now, (3.18) is rewritten as

$$\exp\left\{-\mathrm{E}_G\left[\int_0^{\infty}(1-\exp(-sP_M G L^{-\alpha}))\lambda'_M L^{d-1} b_d d L^{d-1}\mathrm{d}L\right]\right\}.$$

By using the change of variables and doing some simple calculations, $\mathcal{L}_{I_{MB}}(s)$ is obtained as follows [98]

$$\mathcal{L}_{I_{MB}}(s) = e^{-b_d \lambda'_M \Gamma\left(1-\frac{d}{\alpha}\right)\left(\frac{P_M \mu\theta}{P_F}\right)^{\frac{d}{\alpha}} {r_F}^d \mathrm{E}\left[(G)^{\frac{d}{\alpha}}\right]}. \quad (3.20)$$

From (3.6), (3.12) and (3.20), taking $d = 2$, then replacing ${r_F}^2$ with z, and assuming $\sigma^2 \to 0$, we get the final formula as follows

$$p_{OF} = 1 - \int_0^{\infty} e^{-\pi\left[\left(\lambda_F - \lambda'_F p_{RB} p_{tx}\right) + \frac{2}{\alpha} p_{RB} p_{tx} \lambda'_F (\mu\theta)^{\frac{2}{\alpha}} M(\theta,\alpha) - \lambda'_M \left(\frac{P_M \mu\theta}{P_F}\right)^{\frac{d}{\alpha}} N(\alpha)\right] z} . \pi\lambda_F \, \mathrm{d}z \quad (3.21)$$

in which $M(\theta,\alpha) = \mathrm{E}\left[(g)^{\frac{2}{\alpha}}\left(\Gamma\left(-\frac{2}{\alpha}, \mu\theta g\right) - \Gamma\left(-\frac{2}{\alpha}\right)\right)\right]$ and $N(\alpha) = \Gamma\left(1 - \frac{d}{\alpha}\right)\mathrm{E}\left[(G)^{\frac{d}{\alpha}}\right]$.

Finally, the closed-form expression for the outage probability of the tagged femto user, under the imperfect sensing scenario for all CR femto-BSs, is obtained as follows ($\alpha = 4$)

$$p_{OF} = 1 - \frac{\lambda_F}{(\lambda_F - \lambda'_F p_{RB} p_{tx}) + \frac{\lambda'_F (p_{RB} p_{tx})}{2} \sqrt{\mu\theta} M(\theta,4) + \lambda'_M N(4) \sqrt{\frac{P_M \mu\theta}{P_F}}}. \tag{3.22}$$

Similar with the desired link, we consider the Rayleigh fading model for the femto interfering links as well as the macro interfering links (Rayleigh fading links with equal parameter μ for the femto interfering links and μ_p for the macro interfering links). Following the derivation of $M(\theta, \alpha)$ in Appendix A.1, and after the simplification of $N(\alpha)$ using the definition of expectation and the standard Gamma function, p_{OF} is re-expressed as follows ($\alpha = 4$)

$$p_{OF} = 1 - \frac{\lambda_F}{(\lambda_F - \lambda'_F p_{RB} p_{tx}) + \sqrt{\pi} \lambda'_F (p_{RB} p_{tx}) \mu \left[\sum_{k=0}^{\infty} \frac{(\mu\theta)^k}{\Gamma\left(k+\frac{1}{2}\right)(\mu+\mu\theta)^{k+1}} \Gamma(1+k) \right] + \frac{\pi \lambda'_M}{2\sqrt{\mu_p}} \sqrt{\frac{P_M \mu\theta}{P_F}}}. \tag{3.23}$$

3.3.2 Macro Outage Probability Formulation

We derive the outage probability for a typical macro user (p_{OM}) in a downlink heterogeneous cellular network defined as the probability that a randomly chosen macro user cannot achieve a target SINR γ (or equivalently as the average fraction of macro users who do not achieve a target SINR γ, i.e., the averaged outage probability of all macro users) considering a collocated spectrum sensing CR based femto network and macro-BSs as follows:

$$p_{OM} = 1 - P[\text{SINR} > \gamma] \tag{3.24}$$

The experienced SINR by a typical macro user is calculated as

$$\text{SINR} = \frac{P_M h_M r_M^{-\alpha}}{\sigma^2 + I_{MB} + I_{FB}} \tag{3.25}$$

where P_M is the transmission power from the nearest macro-BS located in the random distance r_M from its tagged macro user located at the origin, and α is the path-loss exponent. I_{FB} and I_{MB} are the aggregate interference power to the tagged macro user (located at the origin) from the surrounding femto-BSs and macro-BSs, respectively, and σ^2 is the noise power. It should be noted that the transmission power values of all the macro-BSs in the network are kept constant i.e., P_M.

Let $h_M \sim \exp(\mu_p)$ (with mean $1/\mu_p$) be a random variable accounting for the random channel gain of the link between the tagged macro user and its corresponding macro-BS, then the similar approach to obtain the outage probability of the tagged femto user is used for the outage probability calculation of the tagged macro user. Therefore, from (3.24) and (3.25) we have

$$p_{OM} = 1 - \int_0^{\infty} e^{-\pi\lambda_M {r_M}^2} . e^{-\mu_p \frac{\gamma {r_M}^{\alpha}}{P_M}\sigma^2} . \mathcal{L}_{I_{FB}}\left(\mu_p \frac{\gamma {r_M}^{\alpha}}{P_M}\right) . \mathcal{L}_{I_{MB}}\left(\mu_p \frac{\gamma {r_M}^{\alpha}}{P_M}\right) . 2\pi r_M \lambda_M \, \mathrm{d}r_M \quad (3.26)$$

where $\mathcal{L}_{I_{FB}}(s)$ and $\mathcal{L}_{I_{MB}}(s)$ are the Laplace transform of random variables I_{FB} and I_{MB} evaluated at $s (s = \mu_p \frac{\gamma {r_M}^{\alpha}}{P_M})$, respectively.

Scenario I

Ideal detection ($P_d = 1$ and $P_f = 0$):

Each secondary node (femto-BS) has perfect knowledge of each primary (macro-BS) signaling. In other words, sensing at each femto-BS is done perfectly. Therefore, an RB occupied by a macro-BS is not chosen for data transmission by any nearby femto-BS. Under this condition, the tagged macro user, during the data transmission time, does not experience any interference (or a negligible interference) from the surrounding femto-BSs, however, those macro-BSs operating on the same RB as the tagged macro user and located in the area $\mathbb{R}^d \backslash b(0, r_M)$ make interference to the tagged macro user. Therefore, (3.26) becomes

$$p_{OM} = 1 - \int_0^{\infty} e^{-\pi\lambda_M {r_M}^2} . e^{-\mu_p \frac{\gamma {r_M}^{\alpha}}{P_M}\sigma^2} . \mathcal{L}_{I_{MB}}\left(\mu_p \frac{\gamma {r_M}^{\alpha}}{P_M}\right) . 2\pi r_M \lambda_M \, \mathrm{d}r_M \quad (3.27)$$

Taking a similar approach to what we had before, $\mathcal{L}_{I_{MB}}(s)$ is obtained as follows

$$\mathcal{L}_{I_{MB}}(s) = \exp\left\{-\mathrm{E}_{g_p}\left[\int_{r_M}^{\infty}\left(1-\exp\left(-sP_M g_p W^{-\alpha}\right)\right)\lambda_I(W)\mathrm{d}W\right]\right\} \tag{3.28}$$

and

$$\lambda_I(W) = \lambda'_M\, dW^{d-1} b_d \tag{3.29}$$

in which W is the distance between an arbitrary macro-BS (captured by the point process Φ_M) and the tagged macro receiver and λ'_M is the intensity of those macro-BSs transmitting on the same RB as the tagged macro user at a time. Similarly, the IC gains g_p (between the interfering macro-BSs and the tagged macro user) are assumed to be mutually independent and have identical pdfs. Each of the active interfering macro-BSs transmits with the same power P_P as for the tagged macro-BS. Same as before, (3.28) is simplified as

$$\mathcal{L}_{I_{MB}}(s) = e^{{r_M}^d b_d \lambda'_M - \frac{d}{\alpha} b_d \lambda'_M (\mu_p \gamma)^{\frac{d}{\alpha}} {r_M}^d V(\gamma,\alpha)}. \tag{3.30}$$

From (3.27) and (3.30), and the previous assumptions, the closed-form formula is expressed as follows

$$p_{OM} = 1 - \frac{\lambda_M}{\lambda_M - \lambda'_M + \frac{\lambda'_M}{2}\sqrt{\mu_p \gamma} V(\gamma,4)} \tag{3.31}$$

in which $V(\gamma,\alpha) = \mathrm{E}\left[(g_p)^{\frac{2}{\alpha}}\left(\Gamma\left(-\frac{2}{\alpha}, \mu_p \gamma g_p\right) - \Gamma\left(-\frac{2}{\alpha}\right)\right)\right]$.

The Rayleigh fading model is also considered for the macro interference links (Rayleigh fading links with equal parameter μ_p). The derivation of $V(\gamma,\alpha)$ is similar to the derivation of $M(\theta,\alpha)$ in Appendix A.1. Therefore, p_{OM} is re-expressed as follows ($\alpha = 4$)

$$p_{OM} = 1 - \frac{\lambda_M}{\lambda_M - \lambda'_M + \sqrt{\pi}\lambda'_M \mu_p \left[\sum_{k=0}^{\infty} \frac{(\mu_p \gamma)^k}{\Gamma\left(k+\frac{1}{2}\right)(\mu_p+\mu_p\gamma)^{k+1}} \Gamma(1+k)\right]} \tag{3.32}$$

Scenario II

Imperfect detection ($P_d \neq 1$ and $P_f \neq 0$):

In this scenario, each secondary node (femto-BS) has imperfect knowledge of each primary (macro-BS) signaling. In other words, sensing at each femto-BS is done imperfectly and subject to (occasional) error. Therefore, an occupied RB by a macro-BS may also be wrongly considered idle by the femto-BSs. In this situation, the tagged macro user can experience interference on its RB, from both the femto and macro BSs. Indeed, the $\mathcal{L}_{I_{FB}}\left(\mu_p \frac{\gamma {r_M}^{\alpha}}{P_M}\right)$ (the Laplace transform of the aggregate interference to the tagged macro user from the surrounding femto-BSs) in (3.26) is not ignored. Using the same approach as described before, $\mathcal{L}_{I_{FB}}(s)$ is also given by

$$\mathcal{L}_{I_{FB}}(s) = \exp\left\{-\mathrm{E}_{G_p}\left[\int_{Kr_M}^{\infty} \left(1 - \exp\left(-sP_F G_p U^{-\alpha}\right)\right)\lambda_I(U)\mathrm{d}U\right]\right\}. \tag{3.33}$$

Since the closest interfering femto-BS is at least at distance Kr_M from the tagged macro user, the integration limits are from Kr_M to ∞. In other words, interference is encountered from all the femto-BSs located in the area $\mathbb{R}^d \setminus b(0, Kr_M)$ (see Fig. 3.3). It should be noted that not all the femto-BSs outside this ball will contribute towards the aggregate interference, i.e., only those femto-BSs which are outside the mentioned ball and at minimum satisfy all of the following conditions are considered as potential contributors

(c) Satisfying the above condition, any arbitrary femto-BS contributes towards the interference at the tagged macro receiver, if it wrongly picks the same RB as the tagged macro-BS to communicate with its user. We show the probability of picking a same RB for data transmission from a pool of all RBs as p_{RB} (the calculation of p_{RB} for this case is seen in Section 3.4, *Scenario II,* Case 2).

(d) Same as the condition (b) in Section 3.3.1.

Applying these two independent thinning, the intensity of the process (the number of the interfering CR femto-BSs at the tagged macro user) becomes

$$\lambda_I(U) = \lambda'_F d U^{d-1} b_d p_{RB} p_{tx} \tag{3.34}$$

Taking the similar approach, (3.33) is simplified as follows

$$\mathcal{L}_{I_{FB}}(s) = e^{K^d r_M{}^d b_d p_{RB} p_{tx} \lambda'_F - \frac{d}{\alpha} b_d p_{RB} p_{tx} \lambda'_F \left(\mu_p \frac{P_F \gamma}{P_M}\right)^{\frac{d}{\alpha}} r_M{}^d O(\gamma,\alpha)} \tag{3.35}$$

in which $O(\gamma,\alpha) = \mathrm{E}\left[(G_p)^{\frac{d}{\alpha}}\left(\Gamma\left(-\frac{d}{\alpha}, \frac{\mu_p \gamma P_F G_p}{K^\alpha P_M}\right) - \Gamma\left(-\frac{d}{\alpha}\right)\right)\right]$.

From (3.26), (3.30) and (3.35), and the previous assumptions, the closed-form expression for the outage probability of the tagged macro user is obtained as follows

$$p_{OM} = 1 - \frac{\lambda_M}{\lambda_M + \lambda'_M\left[\frac{\sqrt{\mu_p \gamma} V(\gamma,4)}{2} - 1\right] + \lambda'_F p_{RB} p_{tx}\left[\frac{\sqrt{\frac{\mu_p \gamma}{P_M}} O(\gamma,4)}{2} - K^2\right]}. \tag{3.36}$$

Similar with the desired link, the Rayleigh fading model for the femto interfering links (with equal parameter μ) as well as the macro interfering links (with equal parameter μ_p) is considered. Considering Appendix A.1, and after replacing $V(\gamma,4)$ and $O(\gamma,4)$ with their expanded versions, p_{OM} can be re-expressed as follows

$$p_{OM} = 1 - \frac{\lambda_M}{\lambda_M - \lambda'_M + \sqrt{\pi}\lambda'_M \mu_p \left[\sum_{k=0}^{\infty} \frac{(\mu_p \gamma)^k}{\Gamma\left(k+\frac{1}{2}\right)(\mu_p + \mu_p \gamma)^{k+1}} \Gamma(1+k)\right] + \lambda'_F p_{RB} p_{tx} K^2 \left[\mu \sqrt{\frac{\pi}{P_F}} \left[\sum_{k=0}^{\infty} \frac{\left(\frac{\mu_p \gamma P_F}{K^4 P_M}\right)^k}{\Gamma\left(k+\frac{1}{2}\right)\left(\mu + \frac{\mu_p P_F}{K^4 P_M}\gamma\right)^{k+1}} \Gamma(1+k)\right] - 1\right]}. \tag{3.37}$$

3.4 Resource Block Selection Probability (p_{RB}) Calculations under Perfect and Imperfect Sensing

In this section, we discuss how the optimal values of the RB selection probability (p_{RB}) for a secondary transmitter (femto-BS) can be determined under each femto-BS's perfect and imperfect sensing scenarios.

Scenario I

Ideal detection for all the CR femto-BSs ($P_d = 1$ and $P_f = 0$) [103], [104]:

- **Case 1.** The tagged femto-BS assigns the ith idle RB to its femto user.
- p_{RB}: The probability that the ith idle RB being selected for data transmission by any of the other active CR femto-BS [104].

$$p_{RB|M_s} = p_{idle}(M_s).\frac{\binom{M-1}{M_s-1}}{\binom{M}{M_s}}.\left(\frac{1}{M_s}\right) \tag{3.38}$$

where

$$p_{idle}(M_s) = \frac{\binom{M}{M_s}\binom{N-M}{N_s-M_s}}{\binom{N}{N_s}}. \tag{3.39}$$

The first term ($p_{idle}(M_s)$) indicates the probability of M_s idle RBs sensed by a femto-BS (during the sensing time, T_S) and the second term is the probability that the ith idle RB is inside the M_s idle RBs, and finally the third term indicates that the probability of selecting the ith idle RB (out of the M_s idle RBs) by that femto-BS is equal to $\frac{1}{M_s}$ (since each of the idle RBs within the M_s idle RBs has an equal probability of being chosen). It should be noted that each CR femto-BS will fail to access when $M_s = 0$ (the maximum value of M_s is equal to $\min\{M, N_s\}$). Therefore, from (3.38),

$$\begin{aligned} p_{RB} &= p_{RB|(M_s \geq 1)} = \frac{1}{M} p_{idle}(M_s \geq 1) \\ &= \frac{1}{M}(1 - p_{idle}(M_s = 0)). \end{aligned} \tag{3.40}$$

If the number of RBs sensed by a CR femto-BS (i.e., N_s) is more than or equal to $N - M + 1$, then at least we have one idle RB within the N_s detected RBs, i.e., $p_{idle}(M_s = 0) = 0$. On the other hand, if N_s is smaller than or equal to $N - M$, the CR femto-BS will fail to access when the RBs within the N_s sensed RBs are all occupied by the macro-BSs. Therefore, we can write

$$p_{idle}(M_s = 0) = \begin{cases} \frac{\binom{N-M}{N_s}}{\binom{N}{N_s}}, & if\ N_s \leq N - M \\ 0, & if\ N_s \geq N - M + 1. \end{cases} \tag{3.41}$$

From (3.40) and (3.41), the probability that a CR femto-BS selects the ith idle RB for data transmission is obtained as follows

$$p_{RB} = \begin{cases} \frac{1}{M}\left(1 - \frac{\binom{N-M}{N_s}}{\binom{N}{N_s}}\right), & if\ N_s \leq N - M \\ \frac{1}{M}, & if\ N_s \geq N - M + 1. \end{cases} \tag{3.42}$$

Scenario II

Imperfect detection for all the CR femto-BSs ($P_d \neq 1$ and $P_f \neq 0$) [103], [104]:

- **Case 1**. The tagged femto-BS assigns the ith idle RB to its femto user.
- p_{RB}: The probability that the ith idle RB being selected for data transmission by any of the other active CR femto-BS [104].

We show the detection result indicator of the nth RBs by D_n ($n \in \{1, 2, \ldots, N\}$). If $D_n = 1$, the nth RB is detected as idle RB, otherwise, $D_n = 0$. The probability of one idle RB detected with no false alarm is $1 - P_f$ and the probability for an occupied RB detected as an idle RB is $1 - P_d$. In other words,

$$\Pr(D_n = 1) = \begin{cases} V_0 = 1 - P_f, & \text{if } n\text{th RB is idle} \\ V_1 = 1 - P_d, & \text{if } n\text{th RB is busy} \end{cases} \tag{3.43}$$

in which P_f is the false alarm probability and can be obtained as follows [58], [104], [105]

$$P_f(\tau) = \mathcal{Q}\left(\sqrt{2\eta + 1}\mathcal{Q}^{-1}(P_d) + \sqrt{\tau f_s}\eta\right) \tag{3.44}$$

($\mathcal{Q}(x) = \frac{1}{\sqrt{2\pi}}\int_x^{\infty} \exp(\frac{-t^2}{2})\,dt$ and P_d is the predefined detection probability. τ is the spectrum sensing time, f_s the sampling frequency, and η the received interference power on an RB to each femto-BS).

Indeed, the probability that the ith idle RB is detected with no false alarm by a CR femto-BS is $\Pr(D_i = 1) = V_0$.

To obtain the probability that the ith idle RB being selected for data transmission by a CR femto-BS (p_{RB}), first, we calculate the probability that the ith idle RB is sensed and included in the M_s idle RBs out of the N_s sensed RBs in the sensing period (T_S), and it is expressed as follows

$$\Pr(\text{the } i\text{th idle RB is sensed} \mid M_s) = p_{idle}(M_s).\frac{\binom{M-1}{M_s-1}}{\binom{M}{M_s}} \tag{3.45}$$

where

$$p_{idle}(M_s) = \frac{\binom{M}{M_s}\binom{N-M}{N_s-M_s}}{\binom{N}{N_s}}. \tag{3.46}$$

Conditioning on M_D (see Table 3.1) and M_s, the probability that the ith idle RB being detected as idle is obtained as follows

$$\begin{aligned}
&\Pr(D_i = 1 \mid M_s, M_D) \\
&= \Pr(D_i = 1)\,.\Pr\left(\sum_{n\neq i, n\in\Phi} D_n = M_D - 1 \mid M_s\right) \\
&= V_0 \times \left[\sum_{m_{ID}=\max\{1, M_D-(N_s-M_s)\}}^{\min\{M_D, M_s\}} \left[\binom{M_s-1}{m_{ID}-1}(V_0)^{m_{ID}-1}(1-V_0)^{M_s-m_{ID}}\right.\right. \\
&\qquad \left.\left.\cdot\binom{N_s-M_s}{m_{OD}}.(V_1)^{m_{OD}}(1-V_1)^{N_s-M_s-m_{OD}}\right]\right]
\end{aligned} \tag{3.47}$$

in which Φ is the set of the detected RBs by a femto-BS (see Table 3.1 for the definitions of m_{ID} and m_{OD}). Replacing m_{OD} with $M_D - m_{ID}$, we have

$$\Pr(D_i = 1 \mid M_s, M_D) = \left[\sum_{m_{ID}=\max\{1, M_D-(N_s-M_s)\}}^{\min\{M_D, M_s\}} \left[\binom{M_s - 1}{m_{ID} - 1} (V_0)^{m_{ID}} (1 - V_0)^{M_s - m_{ID}} \right. \right. \\ \left. \left. \cdot \binom{N_s - M_s}{M_D - m_{ID}} \cdot (V_1)^{M_D - m_{ID}} (1 - V_1)^{N_s - M_s - M_D + m_{ID}} \right] \right] \quad (3.48)$$

Having the M_D detected idle RBs (including the ith idle RB), the probability of a CR femto-BS accessing the ith idle RB is equal to $\frac{1}{M_D}$. Thus, the probability that the ith idle RB is selected for data transmission by any CR femto-BS (under imperfect sensing scenario) is obtained as follows

$$p_{RB|M_s,M_D} = \Pr(\text{the } i\text{th idle RB is sensed} \mid M_s) \times \frac{1}{M_D} \times \Pr(D_i = 1 \mid M_s, M_D). \quad (3.49)$$

Finally,

$$p_{RB} = \sum_{M_s=\max\{1, N_s-(N-M)\}}^{\min\{N_s, M\}} \sum_{M_D=1}^{N_s} p_{RB|M_s,M_D}. \quad (3.50)$$

- **Case 2**. The tagged femto-BS assigns the ith busy RB (occupied by the macro network) to its femto user.
- p_{RB}: The probability that the ith busy RB being selected for data transmission by any of the other active CR femto-BS.

To obtain the probability of the ith busy RB selected for data transmission by a femto-BS (p_{RB}), first, we calculate the probability that the ith busy RB is sensed and included in the $(N_s - M_s)$ busy RBs out of the N_s sensed RBs in the sensing period, and it is expressed as follows

$$\Pr(\text{the } i\text{th busy RB is sensed} \mid (N_s - M_s))$$

$$= \frac{\binom{N-M-1}{N_s-M_s-1}\binom{M}{M_s}}{\binom{N}{N_s}}. \tag{3.51}$$

Conditioning on M_D and $(N_s - M_s)$, the probability that the ith busy RB being detected as idle is obtained as follows

$$\begin{aligned}\Pr(D_i = 1 \mid (N_s - M_s), M_D) &= \Pr(D_i = 1)\,.\Pr\left(\sum_{n\neq i, n\in\Phi} D_n = M_D - 1 \mid (N_s - M_s)\right) \\ &= V_1 \times \left[\sum_{m_{ID}=\max\{1, M_D-(N_s-M_s)\}}^{\min\{M_D,M_s\}} \left[\binom{M_s}{m_{ID}} (V_0)^{m_{ID}} (1-V_0)^{M_s-m_{ID}} \right.\right. \\ &\quad \left.\left. .\binom{N_s - M_s - 1}{m_{OD} - 1}.(V_1)^{m_{OD}-1}(1-V_1)^{N_s-M_s-m_{OD}}\right]\right]\end{aligned} \tag{3.52}$$

in which Φ is the set of the detected RBs by a femto-BS. Again, replacing m_{OD} with $M_D - m_{ID}$, we have

$$\Pr(D_i = 1 \mid (N_s - M_s), M_D) = \left[\sum_{m_{ID}=\max\{1, M_D-(N_s-M_s)\}}^{\min\{M_D,M_s\}} \left[\binom{M_s}{m_{ID}} (V_0)^{m_{ID}} (1-V_0)^{M_s-m_{ID}} .\binom{N_s - M_s - 1}{M_D - m_{ID} - 1}.(V_1)^{M_D-m_{ID}}(1-V_1)^{N_s-M_s-M_D+m_{ID}}\right]\right] \tag{3.53}$$

Having the M_D detected idle RBs (including the ith busy RB), the probability of a CR femto-BS accessing the ith busy RB is $\frac{1}{M_D}$. Thus, the probability that the ith busy RB is selected for data transmission by any CR femto-BS (under imperfect sensing scenario) is obtained as follows

$$\begin{aligned}p_{RB|(N_s-M_s),M_D} &= \Pr(\text{the } i\text{th idle RB is sensed} \mid (N_s - M_s)) \times \frac{1}{M_D} \\ &\quad \times \Pr(D_i = 1 \mid (N_s - M_s, M_D).\end{aligned} \tag{3.54}$$

Finally,

$$p_{RB} = \sum_{M_S=\max\{1,N_S-(N-M)\}}^{\min\{N_S,M\}} \sum_{M_D=1}^{N_S} p_{RB|(N_S-M_S),M_D}\,. \tag{3.55}$$

Table 3.1. Symbols used in Section 3.4

N: Number of RBs
M: Number of idle RBs
N_s: Number of sensed RBs
M_s: Number of idle RBs within the N_s sensed RBs
M_D: Number of RBs detected as idle within the N_s sensed RBs.
m_{ID}: Number of idle RBs (out of the M_D detected idle RBs) detected correctly. ($m_{ID} \in [\max\{1, M_s - (N_s - M_D)\}, \min\{M_s, M_D\}]$)
m_{OD}: Number of busy RBs (out of the M_D detected idle RBs) detected as idle. ($m_{OD} = M_D - m_{ID}$)

3.5 Simulation Results and Discussions

Before we present the obtained results, a brief discussion on the outage probability (as the main performance metric in both Chapters 3 and 4), the spatial distribution of the BSs, and the macro exclusion regions is conducted as follows.

Outage probability is considered as a QoS metric to meet a specific connection data rate requirement, or it can be utilized as a performance measure to evaluate the level of meeting the total demands of users in highly dense networks such as the heterogeneous cellular networks. By obtaining an exact closed-form expression for the system outage probability, we will be able to take a finer look at the system performance with the end goal of better understanding system design principles for the heterogeneous cellular networks.

Outage probability is affected by many parameters that have impact on the system performance. As mentioned before, cognition can be a potential solution for dynamic spectrum allocation which will adapt to the network geometry, solve the interference management issue and reduce the outage probability. Therefore, the primary motivations for the femto-BSs to employ this cognition and hence the p_{RB} and p_{tx} parameters in the cellular network are to provide beneficial coverage improvements for different types of users. In practical heterogeneous cellular networks such as LTE, these parameters are network-specific and not user-specific, thus there needs to be some optimization techniques, which can be considered as future work, used to select parameters that can provide acceptable QoS for the majority of users and to meet the existing outage constraints.

On the other hand, outage probability is significantly affected by the performance of the spectrum sensing. The performance of the spectrum sensing and the determination of each individual RB as busy/idle is determined by two important parameters mentioned before, namely the probability of (correct) detection (P_d) and probability of false alarm (P_f). Considering the fact that p_{RB} is a direct function of P_f and P_d in the practical scenarios (see Section 3.4), a spectrum sensing with high P_f and low P_d results in a lower corresponding QoS and a higher observable outage probability. The ideal sensing procedure is the one with $P_f = 0$ and $P_d = 1$. In practice, however, P_d and P_f are related to each other through a receiver operating characteristic (ROC) curve [90], which is a fundamental attribute of each spectrum sensing system.

We will see later that the outage probability is also an increasing function of the SINR threshold as theoretically can be proved. The SINR threshold θ is generally under the control of the system designer and should be chosen reasonably. Clearly, setting a high value for θ maintains the signal quality but increases the outage probability and reduces the network utilization. Therefore, an upper bound of this threshold can be considered [91] in order to guarantee that outage probability is kept below a maximum value. On the other hand, lowering θ is desirable for better resource utilization. However, small θ allows more users to be admitted per RB which can make the system infeasible if the number of admitted users per RB exceeds a certain limit.

Talking about the femto outage probability, each femto user suffers from two sources of interference, i.e., macro and femto networks. For the macro network, the aggregate interference results from all macro-BSs that use the same RB as the tagged femto user (i.e., we define a homogenous PPP with intensity λ'_M). For the femto network, the aggregate interference results only from the other femto-BSs that (i) pick the same RB as the tagged femto, (ii) are allowed to transmit in the current time slot and (iii) are not inside the macro users' exclusion regions. Hence, the interfering femto-BSs do not constitute a homogeneous point process anymore, and analytical characterization of interference and outage in this case is hard to characterize (the resulting point process is called Poisson hole process). In the analysis, to keep the modeling tractable, we ignored the possible correlation between the locations of the interfering femto-BSs and approximated the spatial distribution of them by a homogeneous PPP of intensity $\lambda'_F p_{RB} p_{tx}$. Authors in [41] and [106] use the same approximation approach, where its accuracy is also justified by simulation in [41]. Similar arguments and approximations were considered for the macro tier outage probability.

As interferences are experienced at receivers, we centered the macro exclusion regions around the macro users. The femto-BSs inside these areas may be able to detect the macro signals and cease their transmissions. The exclusion regions are usually chosen to be centered at the location of the macro-BSs not the macro receivers based on the argument that it is easier to detect the macro-BSs than the macro receivers especially if the receivers are passive like TV receivers. However, if the macro receivers (users) can be localized, e.g., based on pilot signals or transmitted acknowledgments, our obtained results directly apply and the exclusion regions around macro users can make sense. If the macro users cannot be localized, the exclusion regions have to be formed around the macro-BSs. This scenario can be evaluated with slight changes in the proposed model. It should be noted that the location detection of the macro users is outside the scope of this chapter, however, many schemes have been already proposed. Measuring the power leakage of local oscillator is a possible way to detect the presence of the macro passive users (see [14], and [41]). The hidden node problem in CR systems which makes it difficult to detect the macro users can be also tackled, e.g., by adding a margin to the RB access detection threshold accounting for shadow fading, and receiver location uncertainty for worst-case scenarios [102].

First, the accuracy of our analytical results for the downlink analysis in the proposed model is validated by simulations, as shown in Figs. 3.4 and 3.5. The simulations which are built on Matlab platform are carried out to plot the curves of outage probability versus the SINR threshold for the tagged femto and macro user, as shown in Figs. 3.4 and 3.5, respectively. The considered scenario is a two-tier network (exactly following the network model described in Sections 3.2 and 3.3) over an approximately 1×1 km square with the locations of different classes of BSs as realizations of independent PPPs of given densities, and the tagged users located at the center. To have an estimate of the outage probability at the tagged users, the simulation results are averaged over both the spatial PPP (500 different positions) and fading distribution (300 realizations), and are conducted using the parameters mentioned in the figures' captions. Analytical curves are compared with the simulations under both perfect and imperfect sensing. It is observed that the simulation results closely match our analytical model and the curves of analytical and simulation results match fairly well, which confirms our analysis. The plots exhibit slight discrepancies between analytical results and the corresponding simulation results which are mainly due to the independence assumption used in Section 3.3.

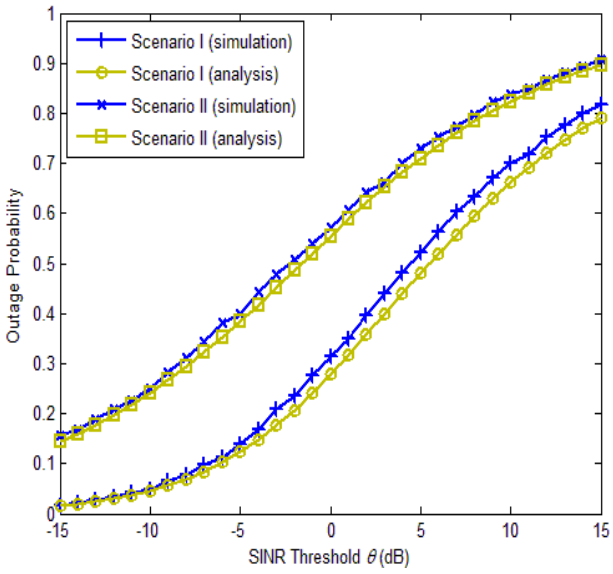

Fig. 3.4. Outage probability of the tagged femto user (or any randomly chosen femto user) under perfect and imperfect sensing scenarios. The system parameters are set as $P_F = 22$ dBm, $P_M = 42$ dBm, $\alpha = 4$, $p_{RB} = 0.8$, $p_{tx} = 0.7$, $\mu = 0.2$, $\mu_p = 1$, $K = 1$, $\lambda'_M = 12$, $\lambda_F = 800$ and $\lambda'_F = 700$.

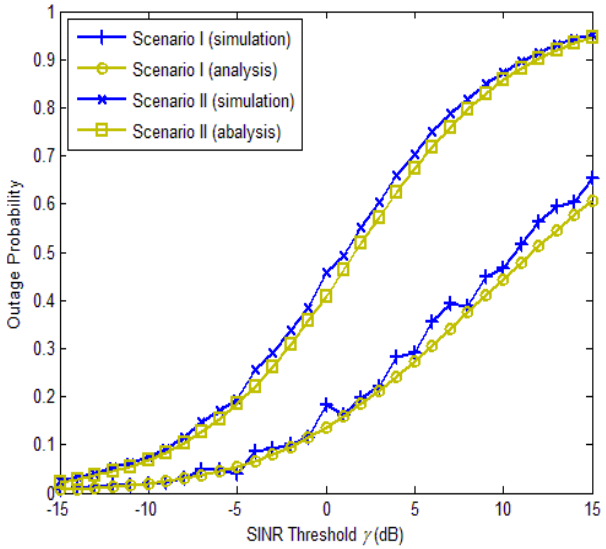

Fig. 3.5. Outage probability of the tagged macro user (or any randomly chosen macro user) under perfect and imperfect sensing scenarios for the CR femto-BSs. The system parameters are set as $P_F = 22$ dBm, $P_M = 42$ dBm, $\alpha = 4$, $p_{RB} = 0.8$, $p_{tx} = 0.7$, $\mu = 0.2$, $\mu_p = 1$, $K = 1$, $\lambda'_F = 700$, $\lambda'_M = 12$ and $\lambda_M = 50$.

In Fig. 3.6, the outage probability of the tagged femto user under perfect and imperfect spectrum sensing abilities for the CR femto-BSs is shown for different values of the target SINR θ on the horizontal axis. Our results show that the outage probability at the tagged femto receiver in the absence of a perfect spectrum sensing ability is considerably increased. In either the Scenario I, when all the femto-BSs employ perfect sensing to sense the RBs, or in *Scenario II*, Case 1, the tagged femto user does not experience any interference from the macro-BSs owing to the correct detection at the tagged femto-BS or choice of idle RBs for data transmission (RBs not occupied by the macro network). In this case, the interference seen by the tagged femto user is only the aggregate interference from the other femto-BSs which are transmitting on the same idle RB as the tagged femto. Clearly, the lowest outage probability is achieved for this case (see the red curve). Now, let's consider the imperfect sensing scenario for the CR femto-BSs. Obviously, the tagged femto user is now subject to sensing error and therefore picking an occupied RB for its data transmission period. Under this condition, it may receive interference not only from the other femto-BSs which pick the same busy RB (due to the imperfect sensing) as the tagged femto, but

also from those macro-BSs communicating with their own users on the same RB as the tagged femto. Therefore, the tagged femto user experiences an interference larger than before, and consequently a significant increase in the outage probability. Moreover, the tagged femto user will face an outage with a higher probability whenever it picks an RB (occupied RB) already used by a larger number of macro users (a larger λ'_M) (see Fig. 3.6).

Fig. 3.7 depicts the outage probability of the tagged macro user for different values of the target SINR γ and different situations. Considering the results obtained in Fig. 3.6, here, we also investigate the effect of employing the two different sensing scenarios for the CR femto-BSs on the outage probability of the tagged macro user. In the case of perfect sensing, the tagged macro user does not experience any interference from the femto-BSs because only those RBs sensed to be idle (RBs not occupied by the macro network) are always chosen for data transmission by the femto network.

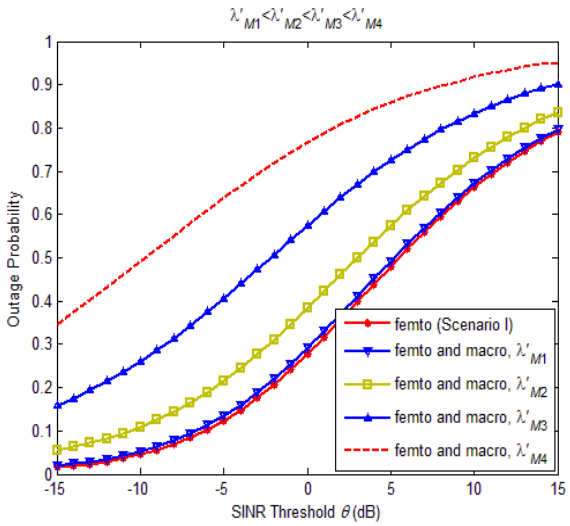

Fig. 3.6. Outage probability of the tagged femto user with different values of λ'_M. Outage probability of the tagged femto user (or any randomly chosen femto user) under perfect and imperfect sensing scenarios with different values of λ'_M. The system parameters are set as $P_F = 22$ dBm, $P_M = 42$ dBm, $\alpha = 4$, $p_{RB} = 0.8$, $p_{tx} = 0.7$, $\mu = 0.2$, $\mu_p = 1$, $K = 1$, $\lambda_F = 800$ and $\lambda'_F = 700$.

In this case, the interference observed at the tagged macro user is only the aggregate interference received from those macro-BSs transmitting on the same RB as the tagged macro. Clearly, the lowest outage probability is obtained for this case (see the red curve). Now, the case of imperfect sensing of the CR femto-BS nodes is considered when the femto-BSs are subject to sensing error and therefore the possibility of transmitting on the RB occupied by the tagged macro. Under this condition, the tagged macro user may receive interference not only from the other macro-BSs communicating with their own users over the same RB (due to the lack of RBs) as the tagged macro, but also from those femto-BSs which pick the same RB. Therefore, the tagged macro user experiences an interference larger than before and consequently a significant increase in the outage probability. Moreover, the tagged macro user will face an outage with a higher probability whenever its own RB is wrongly selected for data transmission by a larger number of femto-BSs (a larger λ'_F).

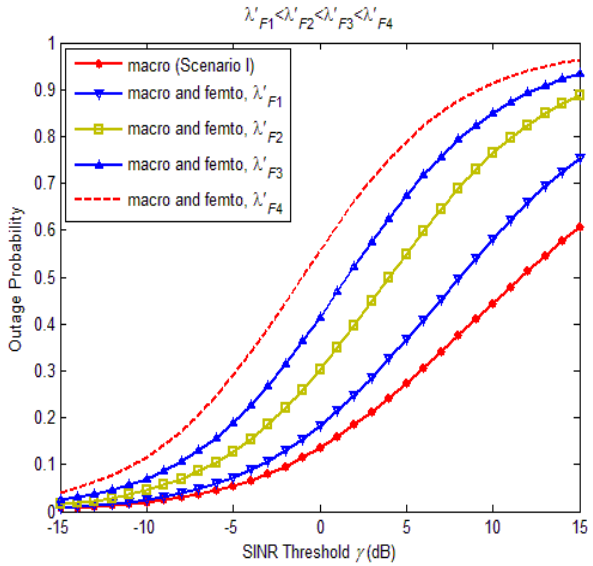

Fig. 3.7. Outage probability of the tagged macro user with different values of λ'_F. Outage probability of the tagged macro user (or any randomly chosen macro user) under perfect and imperfect sensing scenarios for the CR femto-BSs with different values of λ'_F. The system parameters are set as $P_F = 22$ dBm, $P_M = 42$ dBm, $\alpha = 4$, $p_{RB} = 0.8$, $p_{tx} = 0.7$, $\mu = 0.2$, $\mu_p = 1$, $K = 1$, $\lambda'_M = 12$ and $\lambda_M = 50$.

Fig. 3.8 illustrates the effect of K (in $D = Kr_M$) on the observed outage probability at the tagged macro user in the presence of both the macro and femto networks. Considering the previous explanations and Fig. 3.3, let Φ'_F include all the points (representing the femto-BSs) in Φ_F except the points inside the exclusion region D of the tagged macro user. Since $\Phi'_F \subset \Phi_F$, the potential aggregate interference at the tagged macro user, caused by the active (considering slotted ALOHA) CR femto-BSs is less than that in the case with no D. Furthermore, as the exclusion region D becomes larger (when $K = 10$, for example), the probability of outage is significantly reduced. Indeed, the bigger the value of D, the closer the outage probability curve becomes to the black curve which represents the outage probability in the case when no overall interference from the femto network is observed at the tagged macro user due to the perfect sensing ability of the CR femto-BSs. However, the reduction in the outage probability can be less when the number of macro-BSs transmitting on the same RB as the tagged macro is larger (see Fig. 3.8 (b)).

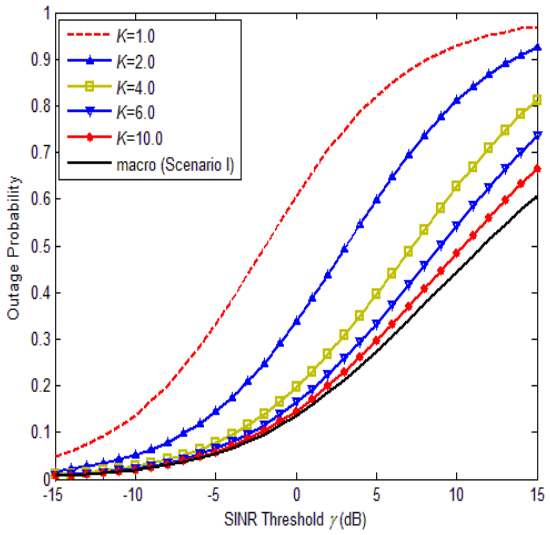

(a)

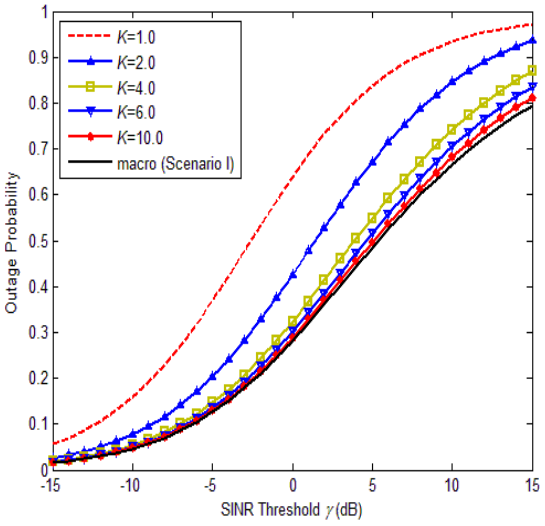

(b)

Fig. 3.8. Effect of D (the defined exclusion region around the tagged macro user) on outage probability of the tagged macro user in the presence of both the macro and femto-BSs. The system parameters are set as $P_F = 22$ dBm, $P_M = 42$ dBm, $\alpha = 4$, $p_{RB} = 0.8$, $p_{tx} = 0.7$, $\mu = 0.2$, $\mu_p = 1$, $\lambda_M = 50$, $\lambda'_M = 12$ (in (a)) and $\lambda'_M = 25$ (in (b)).

For a commercial network, designers must find a way to achieve a lower probability of outage for a certain SINR as the minimum quality needed for a typical femto or macro user to experience an acceptable QoS. A common way to decrease the outage probability is to reduce the number of interfering BSs encountered at the users. This can be done through applying both the (a) and (b) conditions in the perfect sensing scenario (or both the (c) and (d) in the imperfect sensing scenario). As shown in Fig. 3.9, under these constraints the outage probability is significantly reduced at the tagged femto user (note that the number of interfering macro-BSs at the tagged femto user is considered equal for all curves in the figure). The goal is to see the effect of both p_{RB} and p_{tx} (these two parameters are employed at each CR femto-BS) on the outage probability of the tagged femto user. As can be seen, for the case when $p_{RB} = 1$ and $p_{tx} = 1$, outage occurs with higher probability. In other words, when all the existing femto-BSs (except those who are inside the macro users' exclusion regions) pick the same RB as the tagged femto ($p_{RB} = 1$) and when they all have data to transmit in the current time slot ($p_{tx} = 1$), the tagged femto user will experience the maximum value for the outage probability derived for different SINR targets. Clearly, a significant reduction in the outage probability is occurred for the

smaller values of p_{RB} and p_{tx} (see Fig. 3.9) (the smaller the values of p_{RB} and p_{tx}, the closer the outage probability becomes to the outage probability in the case when the received interference at the tagged femto user is only the aggregate interference from the macro network). Indeed, this validates that many studies which do not consider these constraints over-estimate the interference encountered by a typical femto user.

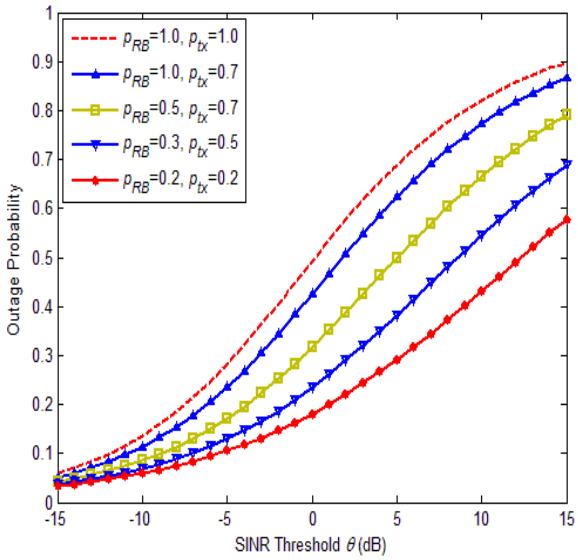

Fig. 3.9. Effect of p_{RB} and p_{tx} on outage probability of the tagged femto user. Effect of p_{RB} and p_{tx} (the defined parameters for the CR femto-BSs) on outage probability of the tagged femto user in the presence of both the macro and femto-BSs. The system parameters are set as $P_F = 22$ dBm, $P_M = 42$ dBm, $\alpha = 4$, $\mu = 0.2$, $\mu_p = 1$, $K = 1$, $\lambda_F = 800$, $\lambda'_F = 700$ and $\lambda'_M = 12$.

It can be seen that even for high values of p_{tx}, the outage probability is relatively less than that in the case where there is no constraint on the femto-BS's transmission schedule ($p_{tx} = 1$). Also, it is obvious that in the presence of multiple RBs where each RB is picked with probability p_{RB}, the outage probability is further decreased. Hence, any practical HetNet designed to satisfy both of the mentioned conditions can reap the benefit of opportunistic exploitation of spectrum, while possibly causing little or no harmful interference. The same story exists when the outage probability of the tagged macro user is investigated. Fig. 3.10 shows the effect of p_{RB} and p_{tx} (parameters which are

related to the CR femto-BSs) on the outage probability of the tagged macro user. For instance, when all the active femto-BSs select the same RB as the tagged macro ($p_{RB} = 1$) and when they all have data to transmit (on this busy RB) in the current time slot ($p_{tx} = 1$), the tagged macro user will experience the maximum value for the outage probability. It should be noted that the number of interfering macro-BSs at the tagged macro is considered equal for all curves in this figure.

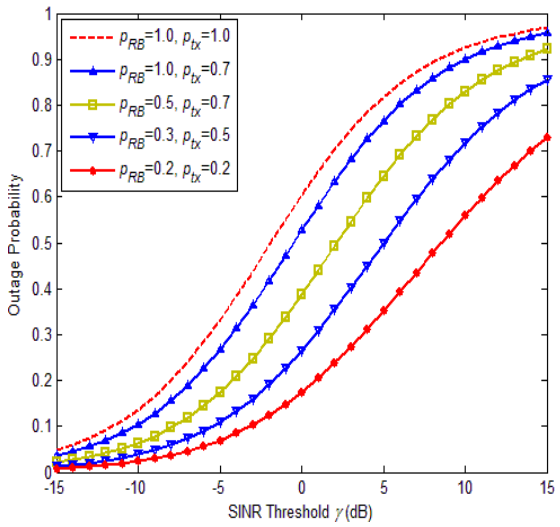

Fig. 3.10. Effect of p_{RB} and p_{tx} on outage probability of the tagged macro user. Effect of p_{RB} and p_{tx} (the defined parameters for the CR femto-BSs) on outage probability of the tagged macro user in the presence of both the macro and femto-BSs. The system parameters are set as $P_F = 22$ dBm, $P_M = 42$ dBm, $\alpha = 4$, $\mu = 0.2$, $\mu_p = 1$, $K = 1$, $\lambda'_F = 700$, $\lambda_M = 50$ and $\lambda'_M = 12$.

In Figs. 3.11 and 3.12, we analyze the performance of the authorized links (femto links) in terms of throughput (achievable with a simple ARQ scheme with error-free feedback) under both the perfect and imperfect sensing scenarios. Considering the slotted ALOHA scheme, we define the following terms [107], [108],

Probabilistic link throughput (τ) of a femto user:

(i) in the half-duplex (HD) communication scenario: it is defined to be the success probability of a femto user (i.e., $1 - p_{OF}$) multiplied by the probability that the corresponding femto-BS actually transmits over a

specific RB (i.e., $p_{RB}p_{tx}$), and the probability that the femto receiver actually receives over that RB (i.e., $1 - p_{RB}p_{tx}$)

(ii) in the full-duplex (FD) communication scenario: it is defined to be the success probability of a femto user (i.e., $1 - p_{OF}$) multiplied by the probability that the corresponding femto-BS actually transmits over a specific RB (i.e., $p_{RB}p_{tx}$).

Femto link throughput (T):

The femto link throughput is defined as the product of the probabilistic link throughput (τ) and the rate of transmission, i.e., $T = \tau \log(1 + \theta)$. Therefore, the femto link throughput for the half and full duplex cases is written as follows

$$\begin{aligned} T^{(half)} &= p(1-p)(1-p_{OF}) \log(1 + \theta) \\ T^{(full)} &= p(1-p_{OF}) \log(1 + \theta) \end{aligned} \tag{3.56}$$

in which $p = p_{RB}p_{tx}$.

In Fig. 3.11, the performance of half and full duplex systems are presented for the femto users. More specifically, the link throughput of any typical femto user (e.g. the link between the tagged femto user and its corresponding femto-BS) under perfect and imperfect spectrum sensing abilities for the CR femto-BSs is shown as a function of the transmission probability over a specific RB (i.e., $p = p_{RB}p_{tx}$). It can be seen that the throughput achieved by the FD system is significantly higher, particularly when p is high. Regarding the performance of the HD system, for both the perfect and imperfect sensing cases, there is a unique optimal p which achieves the maximum throughput ($p = 0.3$ for the perfect and $p = 0.35$ for the imperfect sensing scenario). However, for high p, both throughput curves converge to zero due to over many transmissions and interferences on the RB. Obviously, for both the half and full duplex communications, a higher per-link throughput is achieved when the CR femto-BSs employ perfect sensing.

In Fig. 3.12, the performance of half and full duplex systems are presented for femto users. More specifically, the link throughput of any typical femto user (e.g. the link between the tagged femto user and its corresponding femto-BS) under perfect and imperfect spectrum sensing abilities for the CR femto-BSs is shown as

a function of the target SINR θ. It can be seen that the per-link throughput achieved by the FD system, for both the perfect and imperfect sensing scenarios, is significantly higher than the HD one. As it is seen, the link throughput curves are concave and there is an optimal point in each curve. With a high target SINR, we can transmit the user data with high spectral efficiency; however, the outage probability of this transmission is high, too. In contrast, with a low target SINR, we can send many packets that include little information. In other words, a high reliable transmission can be experienced at low target SINRs, while the minimum requirements for the transmission rate cannot be met.

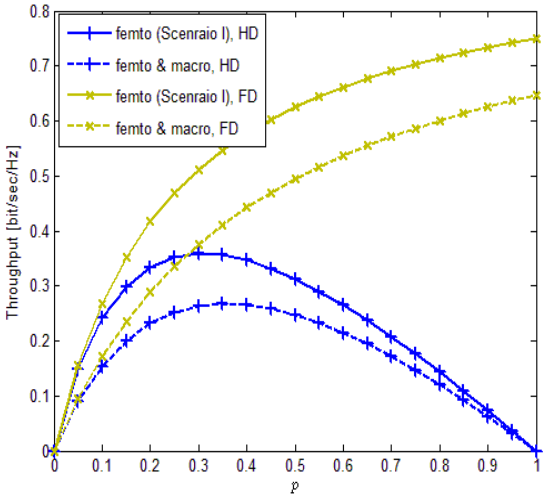

Fig. 3.11. The femto link throughput of half and full duplex systems as a function of the transmission probability. The femto link throughput of half and full duplex systems under perfect and imperfect sensing scenarios as a function of the transmission probability over a specific RB (p). The system parameters are set as $P_F = 22$ dBm, $P_M = 42$ dBm, $\alpha = 4$, $\mu = 0.2$, $\mu_p = 1$, $K = 1$, $\lambda'_M = 12$, $\lambda_F = 800$ and $\lambda'_F = 700$, and $\theta = 11$dB.

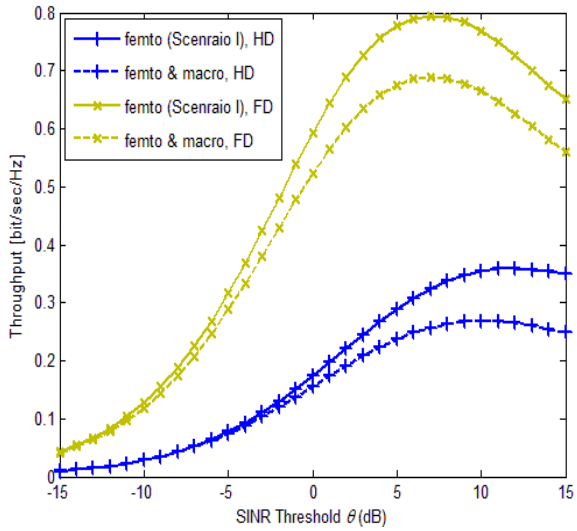

Fig. 3.12. The femto link throughput of half and full duplex systems as a function of the target SINR. The femto link throughput of half and full duplex systems under perfect and imperfect sensing scenarios as a function of the target SINR. The system parameters are set as $P_F = 22$ dBm, $P_M = 42$ dBm, $\alpha = 4$, $\mu = 0.2$, $\mu_p = 1$, $K = 1$, $\lambda'_M = 12$, $\lambda_F = 800$ and $\lambda'_F = 700$, and for each curve the optimal value of p obtained in Fig. 3.11 is applied.

3.6 Conclusion

In this Chapter, utilizing the spatial PPP theory, we presented a tractable model to derive the outage probability of a typical femto and macro user in a two-tier HetNet which provides insight into system design guidelines. In other words, for the case of the node locations modeled by a PPP and the desired and interfering channels are subject to Rayleigh fading, we demonstrated the use of the CR based framework to evaluate the outage probability at any arbitrary user. Exact closed-form expressions were obtained as a result. In addition, we observed that in the downlink analysis, the outage probability is a function of the network topology and several important system design parameters such as SINR target, exclusion regions, MAC mechanisms such as ALOHA (p_{tx}), and the RB selection constraint (p_{RB}) which is controlled by the spectrum sensing measurements.

Chapter 4

Analytical Modelling of Cognitive Heterogeneous Cellular Networks over Nakagami-m Fading

4.1 Introduction

The problems in Chapters 3 and 4 are tightly related, they both deal with interference modeling and avoidance in HetNets by presenting a CR based statistical framework for a two-tier heterogeneous cellular network on the basis of the stochastic geometry, and the goal is to find a closed-form expression for the outage probability (as an important performance metric for wireless networks) of any typical user in the network. The main difference in both scenarios is that unlike Chapter 3 that uses the Rayleigh assumptions on the channel links to relax the difficulty of addressing a closed-form expression for the outage probability, in Chapter 4, novel closed-form expressions are derived for the outage probability over general Nakagami-m fading channels. Thus, in an effort to generalize all previously mentioned analysis in Chapter 3, in this chapter, we extend the proposed model by characterizing the fading for all the communication links (desired and interference links) as Nakagami-m fading. Nakagami-m distribution has gained a lot of attention. It is a very versatile fading model, which by varying the values of the fading parameter "m", it can be modeled as either as Rayleigh model or Rician model. In other words, it is able to model a wider class of fading

channel conditions and fit well the empirical data in a more convenient way. Obviously, a closed-form expression for the outage probability under this fading model will be more and more difficult to obtain.

The main contributions of this chapter are therefore the following: (i) Similarly, we analyze the Laplace transforms of all four types of aggregate interference between macro and CR femto networks (including the interference between macro nodes among themselves and femto nodes among themselves, the cross-interference from femto to macro network and vice versa) in perfect and imperfect spectrum sensing CR based femto networks, considering simultaneously the Nakagami fading, the PPP model, and some important design factors which play vital roles in determination and mitigation of outage and interference. (ii) As in the previous chapter, this chapter also provides an insight into the role of CR in interference mitigation in OFDMA two-tier HetNets. (iii) Tight closed-form expressions are derived for the outage probability of any typical femto and macro user considering the Nakagami fading (as mentioned, Rayleigh fading assumption is used in many studies to relax the difficulty of addressing a closed-form expression for the outage probability (see, e.g., [39] and [40])) for all the communication links (desired and interference links) with the possibility of using the CR ability for the femto network.

To the best of our knowledge, no closed-form expressions for the outage probability of the femto and macro users exist in the current literature without imposing the Rayleigh fading assumption. On the other hand, most of the available studies in this area are based on the existence of only one macro-BS (along with the macro users and the femto network) and the effect of considering multiple macro-BSs is ignored in the analysis of outage probability.

4.2 System Model

As mentioned earlier, the contributions of this chapter are constructed based on the same model description and structure argued in Chapter 3. In an effort to generalize all previously mentioned analysis in Chapter 3, in this chapter, we extend the previously proposed model by characterizing the fading for all the communication links as Nakagami-m fading. Next section gives a complete

explanation of the detailed procedure. We refer the reader to the previous chapter where the details of the system model are given.

4.3 Stochastic Geometry Based Network Configuration

4.3.1 Femto Outage Probability

In this subsection, similarly, we derive the probability of outage for a typical femto user (p_{OF}). For that, we need to remember the definition of the outage probability (see (3.1)) and expression given for the experienced SINR by a typical femto user (see (3.2)) in the previous chapter. When the fading distribution is Nakagami-$m_{d,F}$ for the communication channel between the tagged femto user and its corresponding femto-BS, the pdf of the power fading coefficient $x = h_F$ is as follows

$$p(x) = \frac{{m_{d,F}}^{m_{d,F}}}{{\Omega_{d,F}}^{m_{d,F}}\Gamma(m_{d,F})}(x)^{m_{d,F}-1}e^{-\frac{m_{d,F}x}{\Omega_{d,F}}} \tag{4.1}$$

where $m_{d,F}$ describes the severity of the fading for the desired link, and $\Omega_{d,F}$ is the average SNR. By changing $m_{d,F}$, we can get a variety of fading conditions. For example, if $m_{d,F} = 1$, then the desired link suffers from Rayleigh fading, and $m_{d,F} = \infty$ means that there is no fading. Note that we will represent the Nakagami fading parameters for each communication link, separately (see Fig. 3.3. (b)). Even though the fading power gain distributions are identical, we will still use different symbols to distinguish all the existing links for the sake of analytical convenience.

Here, we derive the complementary CDF (CCDF) of SINR as follows

$$\begin{aligned} P[\text{SINR} > \theta] &= P\left[\frac{P_F h_F {r_F}^{-\alpha}}{\mathfrak{6}^2 + I_{FB} + I_{MB}} > \theta\right] \\ &= P\left[h_F > (\mathfrak{6}^2 + I_{FB} + I_{MB})\frac{\theta {r_F}^{\alpha}}{P_F}\right] \\ &= \mathrm{E}_I\left[P\left[h_F > (I)\frac{\theta {r_F}^{\alpha}}{P_F}\right]\right]. \end{aligned} \tag{4.2}$$

Considering the pdf of the power fading coefficient h_F and the incomplete Gamma function (Note that $\Gamma(a,x) = \int_x^\infty t^{a-1}e^{-t}\,\mathrm{d}t$ indicates the incomplete Gamma function), we have

$$P\left[h_F > (I)\frac{\theta {r_F}^\alpha}{P_F}\right] = \int_{\frac{\theta {r_F}^\alpha}{P_F}(I)}^{\infty} p(x)\,\mathrm{d}x$$
$$= \frac{-{m_{d,F}}^{m_{d,F}}(-1)^{m_{d,F}-1}}{\left(-m_{d,F}\right)^{m_{d,F}}}\left[\frac{\Gamma\left[m_{d,F}, \frac{m_{d,F}}{\Omega_{d,F}}\left(\frac{\theta {r_F}^\alpha}{P_F}(I)\right)\right]}{\Gamma\left(m_{d,F}\right)}\right] \tag{4.3}$$

where $I = \mathfrak{6}^2 + I_{FB} + I_{MB}$.

We know that $\frac{\Gamma[m,my]}{\Gamma(m)} = e^{-my}\sum_{k=0}^{m-1}\frac{m^k}{k!}y^k$ (m is a positive integer). Therefore, $P\left[h_F > (I)\frac{\theta {r_F}^\alpha}{P_F}\right]$ is simplified as follows

$$\left[e^{-\frac{m_{d,F}}{\Omega_{d,F}}\left(\frac{\theta {r_F}^\alpha}{P_F}\right)I}\sum_{k=0}^{m_{d,F}-1}\frac{\left(\frac{m_{d,F}}{\Omega_{d,F}}\frac{\theta {r_F}^\alpha}{P_F}\right)^k}{k!}I^k\right]$$

From the above expression and (4.2) we have

$$P[\mathrm{SINR} > \theta] = \int_0^\infty\left[e^{-\frac{m_{d,F}}{\Omega_{d,F}}\left(\frac{\theta {r_F}^\alpha}{P_F}\right)I}\sum_{k=0}^{m_{d,F}-1}\frac{\left(\frac{m_{d,F}\theta {r_F}^\alpha}{\Omega_{d,F}P_F}\right)^k}{k!}I^k\right]f_I(i)\,\mathrm{d}i. \tag{4.4}$$

Finally, the CCDF of SINR when the fading distribution is Nakagami-$m_{d,F}$ for the communication channel between the tagged femto user and its corresponding femto-BS is given by

$$P[\mathrm{SINR} > \theta] = \left[\sum_{k=0}^{m_{d,F}-1}\frac{(s)^k}{k!}(-1)^k\frac{d^k\mathcal{L}_I(s)}{ds^k}\right] \tag{4.5}$$

where $I = \mathfrak{6}^2 + I_{FB} + I_{MB}$ and $s = \frac{m_{d,F}\theta {r_F}^{\alpha}}{\Omega_{d,F} P_F}$.

Proof: See Appendix B.1.

Note that due to the assumption of independent PPPs for the femto and macro networks, the aggregate interference received from the femto-BSs is independent of the aggregate interference received from the macro-BSs [41], therefore, we can write

$$\begin{aligned}\mathcal{L}_I(s) = F_I(s) &= E[e^{-sI}] \\ &= \mathrm{E}\left[e^{-s\left(\mathfrak{6}^2 + I_{FB} + I_{MB}\right)}\right] \\ &= \mathrm{E}[e^{-sI_{FB}}]\mathrm{E}[e^{-sI_{MB}}]\mathrm{E}\left[e^{-s\mathfrak{6}^2}\right] \\ &= \mathcal{L}_{I_{FB}}(s)\mathcal{L}_{I_{MB}}(s)e^{-s\mathfrak{6}^2} \end{aligned} \tag{4.6}$$

where $\mathcal{L}_{I_{FB}}(s)$ and $\mathcal{L}_{I_{MB}}(s)$ are the Laplace transform of random variables I_{FB} and I_{MB} evaluated at s ($s = \frac{m_{d,F}\theta {r_F}^{\alpha}}{\Omega_{d,F} P_F}$), respectively. Therefore, (4.5) can be rewritten as follows

$$P[\mathrm{SINR} > \theta] = \left[\sum_{k=0}^{m_{d,F}-1} \frac{(s)^k}{k!}(-1)^k \frac{d^k\left(\mathcal{L}_{I_{FB}}(s)\mathcal{L}_{I_{MB}}(s)e^{-s\mathfrak{6}^2}\right)}{ds^k}\right]. \tag{4.7}$$

4.3.1.1 Computation of $\mathcal{L}_{I_{FB}}(s)$ and $\mathcal{L}_{I_{MB}}(s)$ at the Tagged Femto User

We now calculate the closed-form expressions for $\mathcal{L}_{I_{FB}}(s)$ and $\mathcal{L}_{I_{MB}}(s)$ (at $s = \frac{m_{d,F}\theta {r_F}^{\alpha}}{\Omega_{d,F} P_F}$). Based on the information given in the previous chapter (Section 3.3.1), the Laplace transform of the aggregate interference (from all the active femto-BSs except the tagged femto-BS) is given as follows

$$\mathcal{L}_{I_{FB}}(s)_{\left|s=\frac{m_{d,F}\theta {r_F}^{\alpha}}{\Omega_{d,F} P_F}\right.} = e^{{r_F}^{d} b_d p_{RB} p_{tx} \lambda'_F - \frac{d}{\alpha} b_d p_{RB} p_{tx} \lambda'_F \left(\frac{m_{d,F}}{\Omega_{d,F}}\theta\right)^{\frac{d}{\alpha}} {r_F}^{d} M(\theta,\alpha)} \tag{4.8}$$

where

$$M(\theta,\alpha)=\mathrm{E}\left[(g)^{\frac{d}{\alpha}}\left(\Gamma\left(-\frac{d}{\alpha},\frac{m_{d,F}}{\Omega_{d,F}}\theta g\right)-\Gamma\left(-\frac{d}{\alpha}\right)\right)\right]. \tag{4.9}$$

Similar with the desired link, we consider the Nakagami power fading model for the femto interfering links as well (Nakagami fading links with equal parameters $m_{I,F}$ and $\Omega_{I,F}$). Then following the derivations in Appendix B.2, $M(\theta,\alpha)$ is expressed as

$$M(\theta,\alpha)=\left(\frac{-\Gamma\left(-\frac{d}{\alpha}\right){m_{I,F}}^{m_{I,F}}\left(\frac{m_{d,F}}{\Omega_{d,F}}\theta\right)^{-\frac{d}{\alpha}}}{{\Omega_{I,F}}^{m_{I,F}}\Gamma(m_{I,F})}\right)\left[\sum_{k=0}^{\infty}\frac{\left(\frac{m_{d,F}}{\Omega_{d,F}}\theta\right)^{k}\left(\frac{\Omega_{I,F}\Omega_{d,F}}{m_{I,F}\Omega_{d,F}+\Omega_{I,F}m_{d,F}\theta}\right)^{m_{I,F}+k}}{\Gamma\left(k+1-\frac{d}{\alpha}\right)}\Gamma(m_{I,F}+k)\right]. \tag{4.10}$$

Using the similar approach, the Laplace transform of the aggregate interference generated by the macro-BSs at the tagged femto user is obtained and expressed as follows

$$\mathcal{L}_{I_{MB}}(s)_{|s=\frac{m_{d,F}\theta {r_F}^{\alpha}}{\Omega_{d,F}\ P_F}}=e^{-b_d\lambda'_M\Gamma\left(1-\frac{d}{\alpha}\right)\left(\frac{P_M\frac{m_{d,F}}{\Omega_{d,F}}\theta}{P_F}\right)^{\frac{d}{\alpha}}{r_F}^{d}\mathrm{E}\left[(G)^{\frac{d}{\alpha}}\right]}. \tag{4.11}$$

Same as the desired link, we consider the Nakagami power fading model for the macro interfering links as well (Nakagami fading links with equal parameters $m_{I,M}$ and $\Omega_{I,M}$). Below, $\mathrm{E}\left[(G)^{\frac{d}{\alpha}}\right]$ is obtained using the definition of expectation and the standard Gamma function

$$\mathrm{E}\left[(G)^{\frac{d}{\alpha}}\right]=\frac{1}{{\Omega_{I,M}}^{m_{I,M}}}\left[\left(\frac{\Omega_{I,M}}{m_{I,M}}\right)^{\frac{d}{\alpha}+m_{I,M}}\left(\frac{{m_{I,M}}^{m_{I,M}}}{\Gamma(m_{I,M})}\right)\right]\Gamma\left(\frac{d}{\alpha}+m_{I,M}\right). \tag{4.12}$$

4.3.1.2 Closed-Form Femto Outage Probability Expression

Finally, from the outage probability definition (see (3.1), (4.7), (4.8), and (4.11)) and by replacing $z = {r_F}^{\alpha}$, the closed-form expression for the outage probability of the tagged femto user is obtained as follows

$$p_{OF} = 1 - \overbrace{\left[\sum_{k=0}^{m_{d,F}-1} \frac{(z)^k}{k!}(-1)^k \frac{d^k\left(\exp\left(l(z)\right)\right)}{dz^k}\right]}^{P[\text{SINR}>\theta]} \tag{4.13}$$

where

$$\exp\left(l(z)\right) = e^{[\mathrm{A}]z^{\frac{d}{\alpha}} - \frac{m_{d,F}\theta_6{}^2}{\Omega_{d,F}P_F}z}, \text{ and } z = {r_F}^{\alpha} \tag{4.14}$$

and A is given by (4.15).

Note: $m_{d,F}$ is constrained to take integer values only, while $m_{I,F}$ and $m_{I,M}$ can take any value (bigger than 0.5). The restriction on $m_{d,F}$ is because of $m_{d,F} - 1$, as an upper limit for the summation in (4.13). However, for non-integer $m_{d,F}$, by using the infinite series representation of incomplete gamma function, we also obtain an exact but infinite summation expression for the outage probability of the tagged femto user as in Appendix B.3.

The probability of outage averaged over the plane is derived as

$$\begin{aligned} \overline{p_{OF}} &= 1 - \mathrm{E}_{r_F}\left[P[\text{SINR} > \theta]\right] \\ \overline{p_{OF}} &= 1 - \int_0^{\infty} \left[P[\text{SINR} > \theta]\right] f_{r_F}(r_F)\, \mathrm{d}r_F \end{aligned} \tag{4.16}$$

where $f_{r_F}(r_F) = e^{-\lambda_F \pi {r_F}^2} 2\pi\lambda_F r_F$ is the pdf of r.

Here, for example, we present the $\overline{p_{OF}}$ in closed-form expressions for three different values of $m_{d,F}$:

$$m_{d,F} = 1, \alpha = 4: \qquad \overline{p_{OF}} = 1 + \frac{\lambda_F \pi}{(\mathrm{A} - \lambda_F \pi)} \tag{4.17}$$

$$\mathrm{A} = \overbrace{b_d p_{RB} p_{tx} \lambda'_F + \frac{d}{\alpha} b_d p_{RB} p_{tx} \lambda'_F \left(\frac{\Gamma\left(-\frac{d}{\alpha}\right) {m_{I,F}}^{m_{I,F}}}{{\Omega_{I,F}}^{m_{I,F}} \Gamma(m_{I,F})} \right) \left[\sum_{k=0}^{\infty} \frac{\left(\frac{m_{d,F}}{\Omega_{d,F}}\theta\right)^k \left(\frac{\Omega_{I,F}\Omega_{d,F}}{m_{I,F}\Omega_{d,F}+\Omega_{I,F}m_{d,F}\theta}\right)^{m_{I,F}+k}}{\Gamma\left(k+1-\frac{d}{\alpha}\right)} \Gamma(m_{I,F}+k) \right]}^{\mathrm{A}_1}$$

$$\underbrace{-b_d \lambda'_M \Gamma\left(1-\frac{d}{\alpha}\right) \left(\frac{P_M \frac{m_{d,F}}{\Omega_{d,F}} \theta}{P_F} \right)^{\frac{d}{\alpha}} \frac{1}{{\Omega_{I,M}}^{m_{I,M}}} \left[\left(\frac{\Omega_{I,M}}{m_{I,M}} \right)^{\frac{d}{\alpha}+m_{I,M}} \left(\frac{{m_{I,M}}^{m_{I,M}}}{\Gamma(m_{I,M})} \right) \right] \Gamma\left(\frac{d}{\alpha}+m_{I,M}\right)}_{\mathrm{A}_2} \quad (4.15)$$

****

$$m_{d,F} = 2, \alpha = 4: \qquad \overline{p_{OF}} = 1 + \frac{\lambda_F \pi [(\mathrm{A} - \lambda_F \pi) + \frac{\mathrm{A}}{2} \Gamma(2,0)]}{(\mathrm{A} - \lambda_F \pi)^2} \quad (4.18)$$

$m_{d,F} = 3, \alpha = 4$:

$$\overline{p_{OF}} = 1 + \frac{\lambda_F \pi [(\mathrm{A} - \lambda_F \pi)^5 + \frac{5\mathrm{A}}{8} \Gamma(2,0)(\mathrm{A} - \lambda_F \pi)^4 + \frac{\mathrm{A}^2}{8} \Gamma(3,0)(\mathrm{A} - \lambda_F \pi)^3]}{(\mathrm{A} - \lambda_F \pi)^6}. \quad (4.19)$$

It should be noted that in all the above expressions $(\mathrm{A} - \lambda_F \pi) < 0$, and $\mathfrak{6}^2 \to 0$ (operating in an interference-limited regime). For $m_{d,F} \geq 4$, obtaining $\overline{p_{OF}}$ is also quite easy due to the fact that $\exp(l(z))$ is a factor common to every term of the all derivatives of $\exp(l(z))$.

4.3.2 Macro Outage Probability

We now derive the outage probability for a typical macro user (p_{OM}) defined as the probability that a randomly chosen macro user cannot achieve a target SINR γ. When the fading distribution is Nakagami-$m_{d,M}$ for the communication channel between the tagged macro user and its corresponding macro-BS, the pdf of the power fading coefficient $y = h_M$ is as follows

$$p(y) = \frac{{m_{d,M}}^{m_{d,M}}}{{\Omega_{d,M}}^{m_{d,M}} \Gamma(m_{d,M})} (y)^{m_{d,M}-1} e^{-\frac{m_{d,M} y}{\Omega_{d,M}}} \quad (4.20)$$

where $m_{d,M}$ (a positive integer) is the fading parameter for the desired link, and $\Omega_{d,M}$ is the average SNR. Next, the similar approach to obtain the outage probability of the tagged femto user is used for the outage probability calculation of the tagged macro user. Therefore, from the expressions given for the outage probability (see (3.24)) and SINR (see (3.25)) we have

$$P[\text{SINR} > \gamma] = \left[\sum_{k=0}^{m_{d,M}-1} \frac{(s)^k}{k!} (-1)^k \frac{d^k \left(\mathcal{L}_{I_{FB}}(s) \mathcal{L}_{I_{MB}}(s) e^{-s\sigma^2} \right)}{ds^k} \right] \tag{4.21}$$

where $\mathcal{L}_{I_{FB}}(s)$ and $\mathcal{L}_{I_{MB}}(s)$ are the Laplace transform of random variables I_{FB} and I_{MB} evaluated at s ($s = \frac{m_{d,M}}{\Omega_{d,M}} \frac{\gamma {r_M}^{\alpha}}{P_M}$), respectively. We now calculate the closed-form expressions for $\mathcal{L}_{I_{FB}}(s)$ and $\mathcal{L}_{I_{MB}}(s)$ (at $s = \frac{m_{d,M}}{\Omega_{d,M}} \frac{\gamma {r_M}^{\alpha}}{P_M}$).

4.3.2.1 Computation of $\mathcal{L}_{I_{MB}}(s)$ and $\mathcal{L}_{I_{FB}}(s)$ at the Tagged Macro User

Taking a similar approach to what we had before, $\mathcal{L}_{I_{MB}}(s)$ is obtained as follows

$$\mathcal{L}_{I_{MB}}(s)_{|s=\frac{m_{d,M}\gamma {r_M}^{\alpha}}{\Omega_{d,M} P_M}} = e^{{r_M}^d b_d \lambda'_M - \frac{d}{\alpha} b_d \lambda'_M \left(\frac{m_{d,M}}{\Omega_{d,M}} \gamma \right)^{\frac{d}{\alpha}} {r_M}^d V(\gamma,\alpha)} \tag{4.22}$$

in which $V(\gamma, \alpha) = \mathrm{E}\left[(g_p)^{\frac{d}{\alpha}} \left(\Gamma\left(-\frac{d}{\alpha}, \frac{m_{d,M}}{\Omega_{d,M}} \gamma g_p \right) - \Gamma\left(-\frac{d}{\alpha} \right) \right) \right]$.

The Nakagami power fading model is also considered for the interference links (Nakagami fading links with equal parameters $m_{I,M}$ and $\Omega_{I,M}$). The derivation of $V(\gamma, \alpha)$ is similar to the derivation of $M(\theta, \alpha)$ in Appendix B.2. Therefore, $V(\gamma, \alpha)$ is expressed as follows

$$V(\gamma,\alpha) = \frac{-\Gamma\left(-\frac{d}{\alpha}\right) {m_{I,M}}^{m_{I,M}} \left(\frac{m_{d,M}}{\Omega_{d,M}} \gamma \right)^{-\frac{d}{\alpha}}}{{\Omega_{I,M}}^{m_{I,M}} \Gamma(m_{I,M})} \left[\sum_{k=0}^{\infty} \frac{\left(\frac{m_{d,M}}{\Omega_{d,M}} \gamma \right)^k \left(\frac{\Omega_{I,M}\Omega_{d,M}}{m_{I,M}\Omega_{d,M} + \Omega_{I,M} m_{d,M} \gamma} \right)^{m_{I,M}+k}}{\Gamma\left(k + 1 - \frac{d}{\alpha}\right)} \Gamma(m_{I,M} + k) \right]. \tag{4.23}$$

Based on the same approach as described before, $\mathcal{L}_{I_{FB}}(s)$ is also given by

$$\mathcal{L}_{I_{FB}}(s) = e^{\mathrm{K}^d {r_M}^d b_d p_{RB} p_{tx} \lambda'_F - \frac{d}{\alpha} b_d p_{RB} p_{tx} \lambda'_F \left(\frac{m_{d,M} P_F \gamma}{\Omega_{d,M}\, P_M}\right)^{\frac{d}{\alpha}} {r_M}^d T(\gamma,\alpha)} \tag{4.24}$$

in which $T(\gamma,\alpha) = \mathrm{E}\left[(G_p)^{\frac{d}{\alpha}}\left(\Gamma\left(-\frac{d}{\alpha}, \frac{\frac{m_{d,M}}{\Omega_{d,M}}\gamma P_F G_p}{\mathrm{K}^\alpha P_M}\right) - \Gamma\left(-\frac{d}{\alpha}\right)\right)\right]$.

The Nakagami power fading model is also applied to the interference links (Nakagami fading links with equal parameters $m_{I,F}$ and $\Omega_{I,F}$). The mathematical derivation of $T(\gamma,\alpha)$ is quite similar to the derivation of $M(\theta,\alpha)$ and $V(\gamma,\alpha)$ (see Appendix B.2). Hence, $T(\gamma,\alpha)$ is expressed as follows

$$T(\gamma,\alpha) = \frac{-\Gamma\left(-\frac{d}{\alpha}\right) {m_{I,F}}^{m_{I,F}} \left(\frac{m_{d,M}}{\Omega_{d,M}\mathrm{K}^\alpha P_M}\gamma\right)^{-\frac{d}{\alpha}}}{{\Omega_{I,F}}^{m_{I,F}}\Gamma(m_{I,F})} \left[\sum_{k=0}^{\infty} \frac{\left(\frac{\frac{m_{d,M}}{\Omega_{d,M}}\gamma P_F}{\mathrm{K}^\alpha P_M}\right)^k \left(\frac{\mathrm{K}^\alpha P_M \Omega_{d,M} \Omega_{I,F}}{m_{I,F}\Omega_{d,M}\mathrm{K}^\alpha P_M + m_{d,M}\Omega_{I,F} P_F \gamma}\right)^{m_{I,F}+k}}{\Gamma\left(k+1-\frac{d}{\alpha}\right)} \Gamma(m_{I,F}+k)\right]. \tag{4.25}$$

4.3.2.2 Closed-Form Macro Outage Probability Expression

Finally, from the outage probability definition (see (3.24), (4.21), (4.22), and (4.24)) and by replacing $z = {r_M}^\alpha$, the closed-form expression for the outage probability of the tagged macro user is obtained as follows

$$p_{OM} = 1 - \left[\sum_{k=0}^{m_{d,M}-1} \frac{(z)^k}{k!}(-1)^k \frac{d^k\left(\exp\left(l(z)\right)\right)}{dz^k}\right] \tag{4.26}$$

where

$$\exp\left(l(z)\right) = e^{[\mathrm{B}] z^{\frac{d}{\alpha}} - \frac{m_{d,M}\gamma_6^2}{\Omega_{d,M}\, P_M} z} \text{ and } z = {r_M}^\alpha \tag{4.27}$$

and B is given by (4.28).

$$\mathrm{B} = \overbrace{\mathrm{K}^{d} b_d p_{RB} p_{tx} \lambda'_F + \frac{d}{\alpha} b_d p_{RB} p_{tx} \lambda'_F \left(\frac{m_{d,M}}{\Omega_{d,M}} \frac{\gamma}{P_M}\right)^{\frac{d}{\alpha}} \left(\frac{\Gamma\left(-\frac{d}{\alpha}\right) {m_{I,F}}^{m_{I,F}} \left(\frac{m_{d,M}}{\Omega_{d,M} \mathrm{K}^{\alpha} P_M} \gamma\right)^{-\frac{d}{\alpha}}}{{\Omega_{I,F}}^{m_{I,F}} \Gamma\left(m_{I,F}\right)}\right) \left[\sum_{k=0}^{\infty} \frac{\left(\frac{m_{d,M}}{\Omega_{d,M}} \gamma P_F\right)^{k} \left(\frac{\mathrm{K}^{\alpha} P_M \Omega_{d,M} \Omega_{I,F}}{m_{I,F} \Omega_{d,M} \mathrm{K}^{\alpha} P_M + m_{d,M} \Omega_{I,F} P_F \gamma}\right)^{m_{I,F}+k}}{\Gamma\left(k+1-\frac{d}{\alpha}\right)} \Gamma\left(m_{I,F}+k\right)\right]}^{\mathrm{B}_1}$$
$$+ \overbrace{b_d \lambda'_M + \frac{d}{\alpha} b_d \lambda'_M \left(\frac{\Gamma\left(-\frac{d}{\alpha}\right) {m_{I,M}}^{m_{I,M}}}{{\Omega_{I,M}}^{m_{I,M}} \Gamma\left(m_{I,M}\right)}\right) \left[\sum_{k=0}^{\infty} \frac{\left(\frac{m_{d,M}}{\Omega_{d,M}} \gamma\right)^{k} \left(\frac{\Omega_{I,M} \Omega_{d,M}}{m_{I,M} \Omega_{d,M} + \Omega_{I,M} m_{d,M} \gamma}\right)^{m_{I,M}+k}}{\Gamma\left(k+1-\frac{d}{\alpha}\right)} \Gamma\left(m_{I,M}+k\right)\right]}^{\mathrm{B}_2} \quad (4.28)$$

****

The probability of outage averaged over the plane can also be derived as

$$\overline{p_{OM}} = 1 - \mathrm{E}_{r_M}\left[P[\mathrm{SINR} > \gamma]\right]$$
$$\overline{p_{OM}} = 1 - \int_0^{\infty} \left[P[\mathrm{SINR} > \gamma]\right] . f_{r_M}(r_M)\, \mathrm{d}r_M \quad (4.29)$$

where $f_{r_M}(r_M) = e^{-\lambda_M \pi {r_M}^2} 2\pi\lambda_M r_M$ is the pdf of r_M. Such as before, $\overline{p_{OM}}$ can be easily obtained for different integer values of $m_{d,M}$.

4.3.3 Outage Probability Formulation under Perfect and Imperfect Sensing

We now study the effect of both the *ideal* detection, i.e., $P_d = 1$ and $P_f = 0$, and the cases involving imperfect sensing, i.e., $P_d \neq 1$ and $P_f \neq 0$ on the outage probabilities of femto and macro users.

Scenario I

Ideal detection ($P_d = 1$ and $P_f = 0$):
(*femto and macro outage probabilities*)

Each secondary node (femto-BS) has perfect knowledge of each primary (macro-BS) signaling. In other words, sensing at each femto-BS is done perfectly. Therefore, RBs occupied by the macro network are not chosen by any femo-BS for data transmission. In this case, the tagged femto user does not experience any interference from the macro-BSs. This assumption ($P_d = 1$ and $P_f = 0$) is

reasonable in the scenarios where interference from other systems is assumed to be negligible.

Therefore, under this assumption, $\mathrm{E}[e^{-sI_{MB}}] = 1$ and $\mathcal{L}_{I_{MB}}(s) = 1$ (in (4.6)), consequently. Then for the outage probability of the tagged femto user in (4.13), A is only equal to A_1 (see (4.15)). It should be noted that the calculation of p_{RB} for this case was presented in the previous chapter: Section 3.4, *Scenario I,* Case 1.

Clearly, under this scenario, and considering the above explanations, the tagged macro user does not experience any interference from the surrounding femto-BSs. Therefore, for the outage probability of the tagged macro user in (4.26), B is only equal to B_2 (see (4.28)).

Scenario II

Imperfect detection ($P_d \neq 1$ and $P_f \neq 0$):
(*femto and macro outage probabilities*)

In this scenario, each secondary node (femto-BS) has imperfect knowledge of each primary (macro-BS) signaling. In other words, sensing at each femto-BS is done imperfectly and subject to (occasional) error. Therefore, RBs occupied by the macro network may be wrongly chosen by the femo-BSs, as well. Two cases can take place under the imperfect sensing scenario:

Case 1. The tagged femto-BS transmits data on an idle RB (in this case, the outage probability formulations (for both the tagged femto and macro users) are the same as in the perfect sensing scenario except for the calculation of p_{RB} (see Chapter 3: Section 3.4, *Scenario II,* Case 1))

Case 2. The tagged femto-BS transmits on an occupied RB (in this case, the outage probability formulations for both the tagged femto and macro users are explained as follows and the calculation of p_{RB} was presented in the previous chapter: Section 3.4, *Scenario II,* Case 2)

In Case 2, the tagged femto user can experience interference from both the active femto-BSs (which pick the same occupied RB as the tagged femto-BS) and macro-BSs. Then for the outage probability of the tagged femto user in (4.13), A

is equal to $\mathtt{A}_1 + \mathtt{A}_2$ (see (4.15)). Clearly, under this scenario, and in Case 2, the tagged macro user can experience interference on its RB, from both the femto-BSs and macro-BSs. Indeed, for the outage probability of the tagged macro user in (4.26), $\mathtt{B}$ is equal to $\mathtt{B}_1 + \mathtt{B}_2$.

4.4 Simulation Results and Discussions

Before we present the obtained results, we should note that the discussions regarding the outage probability, spatial distribution of the BSs and the macro exclusion regions in the previous chapter apply here as well.

First, the accuracy of our analytical results for the downlink analysis in the proposed model is validated by simulations, as shown in Figs. 4.1 and 4.2. As before, the simulations which are built on Matlab platform are carried out to plot the curves of outage probability versus the SINR threshold for the tagged femto and macro user, as shown in Figs. 4.1 and 4.2, respectively. The considered scenario is a two-tier network (exactly following the network model described in the previous chapter) over an approximately 1×1 km square with the locations of different classes of BSs as realizations of independent PPPs of given densities, and the tagged users located at the center. To have an estimate of the outage probability at the tagged users, the simulation results are averaged over both the spatial PPP (500 different positions) and fading distribution (300 realizations), and are conducted using the parameters mentioned in the figures' captions (note that the parameters applied here are slightly different from those seen in the previous chapter). In the same way as in Chapter 3, the analytical curves are compared with the simulations under both perfect and imperfect sensing. It is observed that the simulation results again closely match our analytical model and the curves of analytical and simulation results match fairly well, which confirms our analysis in this chapter as well. The plots exhibit slight discrepancies between analytical results and the corresponding simulation results which are mainly due to the boundary effect and the independence assumption discussed in Section 4.3.

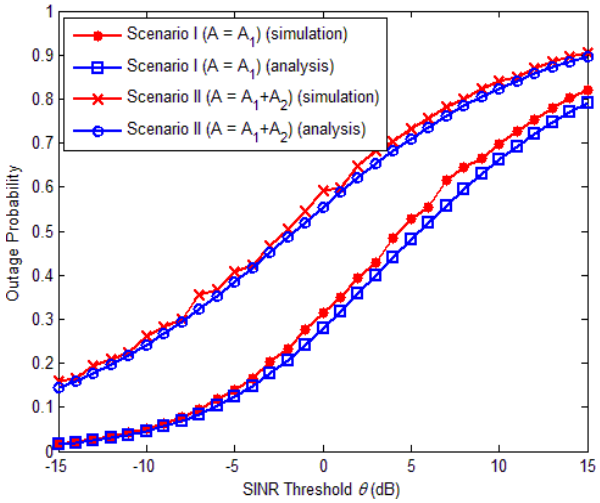

Fig. 4.1. Outage probability of the tagged femto user (or any randomly chosen femto user) under perfect and imperfect sensing scenarios. The system parameters are set as $P_F = 23$ dBm, $P_M = 43$ dBm, $\alpha = 4$, $m_{d,F} = m_{I,F} = m_{I,M} = 1$, $p_{RB} = 0.8$, $p_{tx} = 0.7$, K = 1, $\lambda'_M = 10$, $\lambda_F = 800$ and $\lambda'_F = 700$.

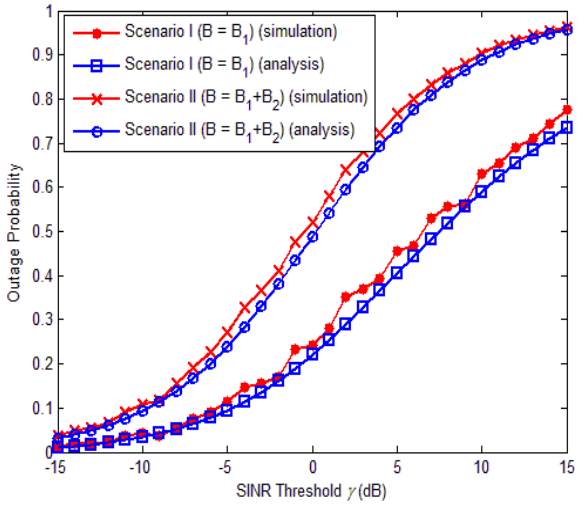

Fig. 4.2. Outage probability of the tagged macro user (or any randomly chosen macro user) under perfect and imperfect sensing scenarios for the CR femto-BSs. The system parameters are set as $P_F = 23$ dBm, $P_M = 43$ dBm, $\alpha = 4$, $m_{d,M} = m_{I,M} = m_{I,F} = 1$, $p_{RB} = 0.8$, $p_{tx} = 0.7$, K = 1, $\lambda'_F = 700$, $\lambda'_M = 10$ and $\lambda_M = 50$.

In Fig. 4.3, the outage probability of the tagged femto user under perfect and imperfect spectrum sensing abilities for the CR femto-BSs is shown for different values of the target SINR θ on the horizontal axis. The results show that the outage probability at the tagged femto receiver in the absence of a

perfect spectrum sensing ability is considerably increased. In either the *Scenario I*, when all the femto-BSs employ perfect sensing to sense the RBs, or in *Scenario II*, Case 1, the tagged femto user does not experience any interference from the macro-BSs owing to the correct detection at the tagged femto-BS or choice of idle RBs for data transmission. In this case, the interference seen by the tagged femto user is only the aggregate interference from the other femto-BSs which are transmitting on the same idle RB as the tagged femto. Clearly, the lowest outage probability is for the case of perfect sensing ($\mathsf{A} = \mathsf{A_1}$ in (4.15)). Now, let's consider the imperfect sensing scenario for the CR femto-BSs. Obviously, the tagged femto user is now subject to sensing error and therefore picking an occupied RB for its data transmission period. Under this condition, it may receive interference not only from the other femto-BSs which pick the same busy RB (due to the imperfect sensing), but also from those macro-BSs communicating with their own users on the same RB as the tagged femto. Therefore, the tagged femto user experiences an interference larger than before, and consequently a significant increase in the outage probability. Moreover, the tagged femto user will face an outage with a higher probability whenever it picks an RB (occupied RB) already used by a larger number of macro users (a larger λ'_M) (see Fig. 4.3).

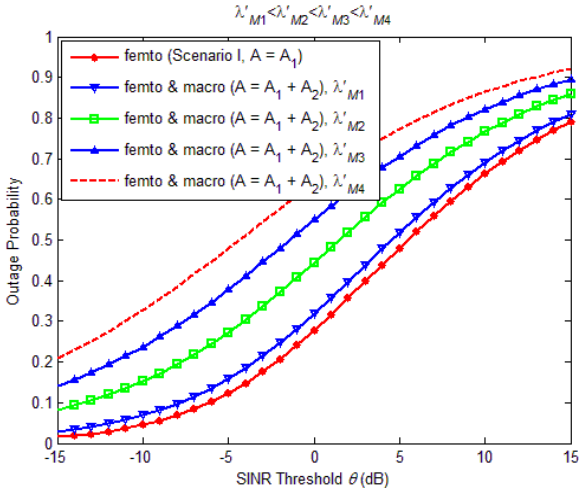

Fig. 4.3. Outage probability of the tagged femto user with different values of λ'_M. Outage probability of the tagged femto user (or any randomly chosen femto user) under perfect and imperfect sensing scenarios with different values of λ'_M. The system parameters are set as $P_F = 23$ dBm , $P_M = 43$ dBm , $\alpha = 4$, $m_{d,F} = m_{I,F} = m_{I,M} = 1$, $p_{RB} = 0.8$, $p_{tx} = 0.7$, $\mathrm{K} = 1$, $\lambda_F = 800$ and $\lambda'_F = 700$.

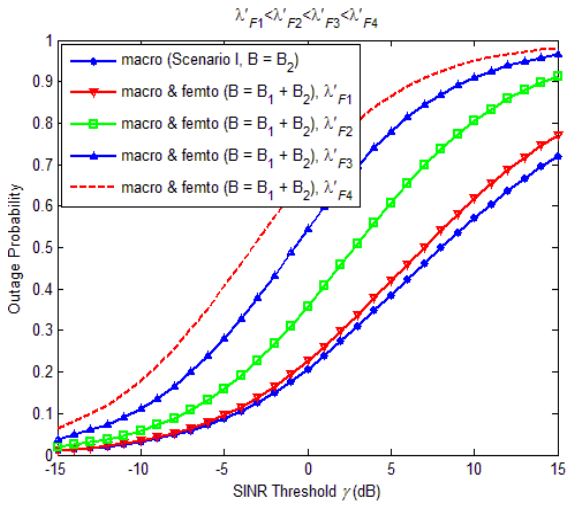

Fig. 4.4. Outage probability of the tagged macro user with different values of λ'_F. Outage probability of the tagged macro user (or any randomly chosen macro user) under perfect and imperfect sensing scenarios for the CR femto-BSs with different values of λ'_F. The system parameters are set as $P_F = 23\,\text{dBm}$, $P_M = 43\,\text{dBm}$, $\alpha = 4$, $m_{d,M} = m_{I,M} = m_{I,F} = 1$, $p_{RB} = 0.8$, $p_{tx} = 0.7$, $\text{K} = 1$, $\lambda'_M = 10$ and $\lambda_M = 50$.

Fig. 4.4 depicts the outage probability of the tagged macro user for different values of the target SINR γ and different situations. Considering the results obtained in Fig. 4.3, here, we also investigate the effect of employing the two different sensing scenarios for the CR femto-BSs on the outage probability of the tagged macro user. In the case of perfect sensing, the tagged macro user does not experience any interference from the femto-BSs because only those RBs sensed to be idle (RBs not occupied by the macro network) are always chosen for data transmission by the femto network. In this case, the interference observed at the tagged macro user is only the aggregate interference received from those macro-BSs transmitting on the same RB as the tagged macro. Clearly, the lowest outage probability is obtained for this case ($\text{B} = \text{B}_2$ in (4.28)). Now, the case of imperfect spectrum sensing of the CR femto-BS nodes is considered, when the femto-BSs are subject to sensing error and therefore the possibility of transmitting on the RB occupied by the tagged macro. Under this condition, the tagged macro user may receive interference not only from the other macro-BSs communicating with their own users over the same RB (due to the lack of RBs) as the tagged macro, but also from those femto-BSs which pick the same RB. Therefore, the tagged macro user experiences an interference larger than before and consequently a

significant increase in the outage probability. Moreover, the tagged macro user will face an outage with a higher probability whenever its own RB is wrongly selected for data transmission by a larger number of femto-BSs (a larger λ'_F).

Fig. 4.5 illustrates the effect of K (in $D = \mathrm{K}r_M$) on the observed outage probability at the tagged macro user in the presence of both the macro and femto networks. Considering the previous explanations in Chapter 3, and since $\Phi'_F \subset \Phi_F$, the potential aggregate interference at the tagged macro user, caused by the active (considering slotted ALOHA) CR femto-BSs is less than that in the case with no D.

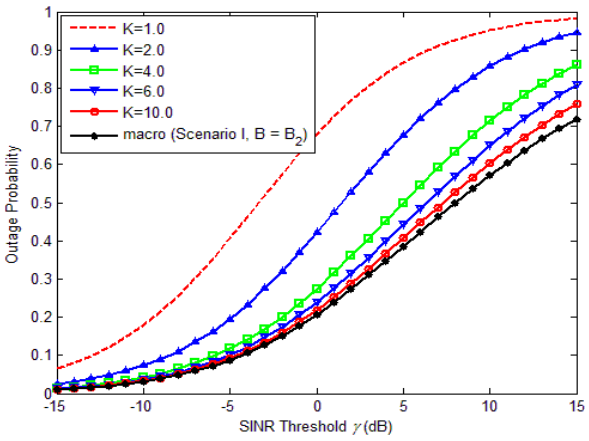

(a)

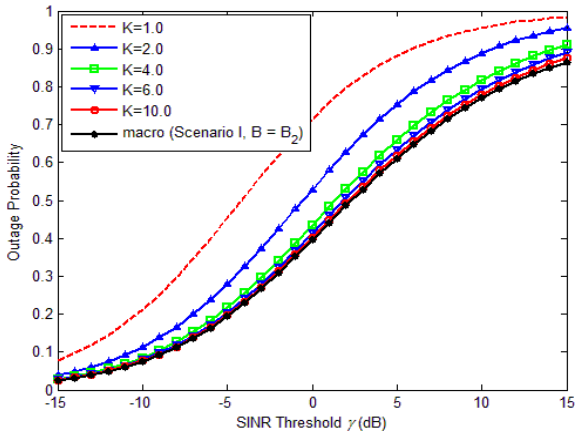

(b)

Fig. 4.5. Effect of D ($D = \mathrm{K}r_M$, the defined exclusion region around the tagged macro user) on outage probability of the tagged macro user in the presence of both the macro and femto-BSs. The system parameters are set as $P_F = 23$ dBm, $P_M = 43$ dBm, $\alpha = 4$, $m_{d,M} = m_{I,M} = m_{I,F} = 1$, $p_{RB} = 0.8$, $p_{tx} = 0.7$, $\lambda_M = 50$, $\lambda'_M = 10$ in (a) and $\lambda'_M = 25$ in (b).

Furthermore, as the exclusion region D becomes larger, the probability of outage is significantly reduced. Indeed, the bigger the value of D, the closer the outage probability curve becomes to the black curve which represents the outage probability in the case when no overall interference from the femto network is observed at the tagged macro user due to the perfect sensing ability of the CR femto-BSs. However, the reduction in the outage probability can be less when the number of macro-BSs transmitting on the same RB as the tagged macro is larger (see Fig. 4.5 (b)).

Same as before, to decrease the outage probability and experience an acceptable QoS, we need to reduce the number of interfering BSs encountered at the users. This can be done through applying the p_{RB} and p_{tx} constraints. As shown in Fig. 4.6, under these constraints the outage probability is significantly reduced at the tagged femto user (note that the number of interfering macro-BSs at the tagged femto user is considered equal for all the curves in the figure). The goal is to see the effect of both p_{RB} and p_{tx} on the outage probability of the tagged femto user. As can be seen, for the case when $p_{RB} = 1$ and $p_{tx} = 1$, outage occurs with higher probability. In other words, when all the existing femto-BSs (except those who are inside the macro users' exclusion regions) pick the same RB as the tagged femto ($p_{RB} = 1$) and when they all have data to transmit in the current time slot ($p_{tx} = 1$), the tagged femto user will experience the maximum value for the outage probability derived for different SINR targets. Clearly, a significant reduction in the outage probability is occurred for the smaller values of p_{RB} and p_{tx} (see Fig. 4.6) (the smaller the values of p_{RB} and p_{tx}, the closer the outage probability curve becomes to the black curve which represents the outage probability in the case when the received interference at the tagged femto user is only the aggregate interference from the macro network). It can be seen that even for high values of p_{tx}, the outage probability is relatively less than that in the case where there is no constraint on the femto-BS's transmission schedule ($p_{tx} = 1$). Also, it is obvious that in the presence of multiple RBs where each RB is picked with probability p_{RB}, the outage probability is further decreased.

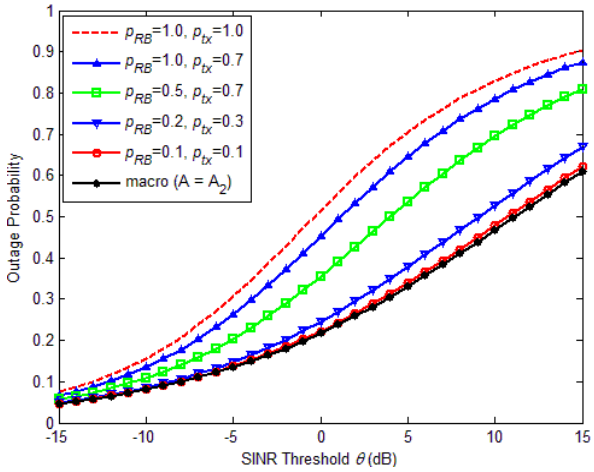

Fig. 4.6. Effect of p_{RB} and p_{tx} on outage probability of the tagged femto user. Effect of p_{RB} and p_{tx} (the defined parameters for the CR femto-BSs) on outage probability of the tagged femto user in the presence of both the macro and femto-BSs. The system parameters are set as $P_F = 23$ dBm, $P_M = 43$ dBm, $\alpha = 4$, $m_{d,F} = m_{I,F} = m_{I,M} = 1$, K = 1, $\lambda_F = 800$, $\lambda'_F = 700$ and $\lambda'_M = 10$.

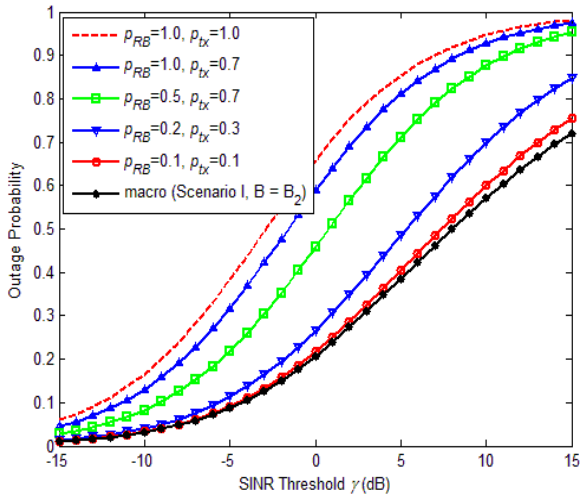

Fig. 4.7. Effect of p_{RB} and p_{tx} on outage probability of the tagged macro user. Effect of p_{RB} and p_{tx} (the defined parameters for the CR femto-BSs) on outage probability of the tagged macro user in the presence of both the macro and femto-BSs. The system parameters are set as $P_F = 23$ dBm, $P_M = 43$ dBm, $\alpha = 4$, $m_{d,F} = m_{I,F} = m_{I,M} = 1$, K = 1, $\lambda'_F = 700$, $\lambda_M = 50$ and $\lambda'_M = 10$.

The same story exists when the outage probability of the tagged macro user is investigated. Fig. 4.7 shows the effect of p_{RB} and p_{tx} on the outage probability of the tagged macro user. For instance, when all the active femto-BSs select the same RB as the tagged macro ($p_{RB} = 1$) and when they all have data to transmit (on this busy RB) in the current time slot ($p_{tx} = 1$), the tagged macro user will

experience the maximum value for the outage probability. It should be noted that the number of interfering macro-BSs at the tagged macro is considered equal for all curves in this figure.

Fig. 4.8 plots the outage probability versus the SINR threshold θ for the tagged femto user. As $m_{d,F} = m_{I,F}$ increases, the outage probability of the tagged femto user decreases. This is because as the fading becomes less severe (the bigger the Nakagami-m parameter, the smaller fading) for both the desired and interfering links of the femto network, the received power at the tagged femto user from its corresponding femto-BS increases more compared to the total received power from all the interfering femto-BSs. It should be noted that $\beta_F = \frac{\Omega_{d,F}}{m_{d,F}} = \frac{\Omega_{I,F}}{m_{I,F}}$ and $\beta_M = \frac{\Omega_{d,M}}{m_{d,M}} = \frac{\Omega_{I,M}}{m_{I,M}}$ (the scale parameters) are fixed for all the curves. The interference links between the interfering macro-BSs and the tagged femto user are more likely to be severe in terms of fading compared to the femto network's desired and interfering links. In other words, the interfering signals received at the tagged femto user originated by the macro-BSs suffer more serious fading than the received signals from the femto-BSs, in particular when we talk about indoor femto users. Similar arguments and statements can also be made about the outage probability of the tagged macro user observed in Fig. 4.9.

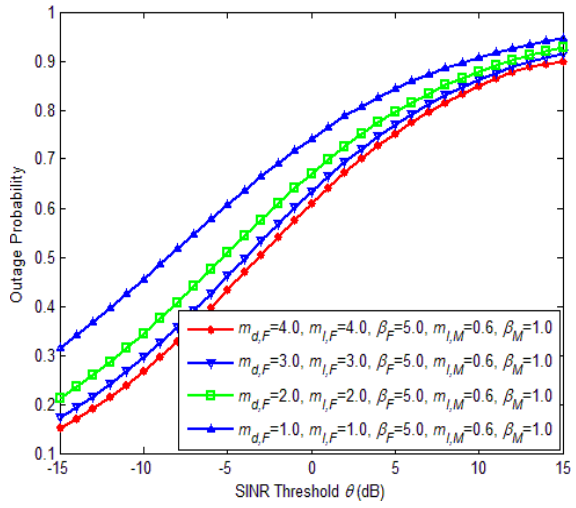

Fig. 4.8. Impact of Nakagami parameter of m on outage probability of the tagged femto user in the presence of both the macro and femto-BSs. The system parameters are set as $P_F = 23$ dBm, $P_M = 43$ dBm, $\alpha = 4$, $p_{RB} = 0.8$, $p_{tx} = 0.7$, K = 1, $\lambda_F = 800$, $\lambda'_F = 700$, $\lambda_M = 50$ and $\lambda'_M = 10$.

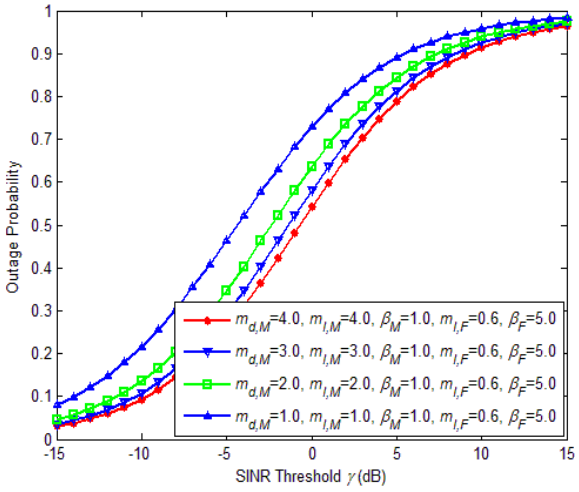

Fig. 4.9. Impact of Nakagami parameter of m on outage probability of the tagged macro user in the presence of both the macro and femto-BSs. The system parameters are set as $P_F = 23$ dBm, $P_M = 43$ dBm, $\alpha = 4$, $p_{RB} = 0.8$, $p_{tx} = 0.7$, K = 1, $\lambda_F = 800$, $\lambda'_F = 700$, $\lambda_M = 50$ and $\lambda'_M = 10$.

In Figs. 4.10 and 4.11, we analyze the performance of the authorized links (femto links) in terms of throughput (achievable with a simple ARQ scheme with error-free feedback) under both the perfect and imperfect sensing scenarios. The slotted ALOHA scheme, and the definitions for the probabilistic link throughput (τ) of a femto user and the femto link throughput (T) apply here as well (see Chapter 3 for more details).

In Fig. 4.10, the performance of half and full duplex systems are presented for the femto users. More specifically, the link throughput of any typical femto user (e.g. the link between the tagged femto user and its corresponding femto-BS) under perfect and imperfect spectrum sensing abilities for the CR femto-BSs is shown as a function of the transmission probability over a specific RB (i.e., $p = p_{RB}p_{tx}$). It can be seen that same as before the throughput achieved by the FD system is significantly higher, particularly when p is high. Regarding the performance of the HD system, for both the perfect and imperfect sensing cases, there is a unique optimal p which achieves the maximum throughput ($p = 0.3$ for the perfect and $p = 0.35$ for the imperfect sensing scenario). However, for high p, both throughput curves converge to zero due to over many transmissions and interferences on the RB. Obviously, for both the half and full duplex communications, a higher per-link throughput is achieved when the CR femto-BSs employ perfect sensing.

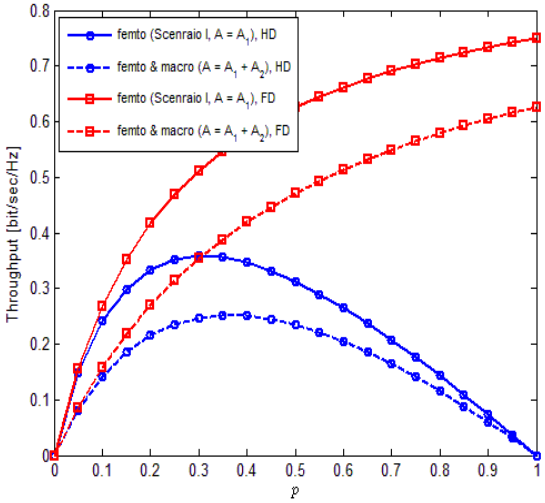

Fig. 4.10. The femto link throughput of half and full duplex systems as a function of the transmission probability. The femto link throughput of half and full duplex systems under perfect and imperfect sensing scenarios as a function of the transmission probability over a specific RB (p). The system parameters are set as $P_F = 23$ dBm, $P_M = 43$ dBm, $\alpha = 4$, $m_{d,F} = m_{I,F} = m_{I,M} = 1$, $\mathrm{K} = 1$, $\lambda'_M = 10$, $\lambda_F = 800$ and $\lambda'_F = 700$, and $\theta = 11$ dB.

In Fig. 4.11, the performance of half and full duplex systems are presented for femto users. More specifically, the link throughput of any typical femto user under perfect and imperfect spectrum sensing abilities for the CR femto-BSs is shown as a function of the target SINR θ. It can be seen again that the per-link throughput achieved by the FD system, for both the perfect and imperfect sensing scenarios, is significantly higher than the HD one. As it is seen, the link throughput curves are concave and there is an optimal point in each curve. With a high target SINR, we can transmit the user data with high spectral efficiency; however, the outage probability of this transmission is high, too. In contrast, with a low target SINR, we can send many packets that include little information. In other words, a high reliable transmission can be experienced at low target SINRs, while the minimum requirements for the transmission rate cannot be met.

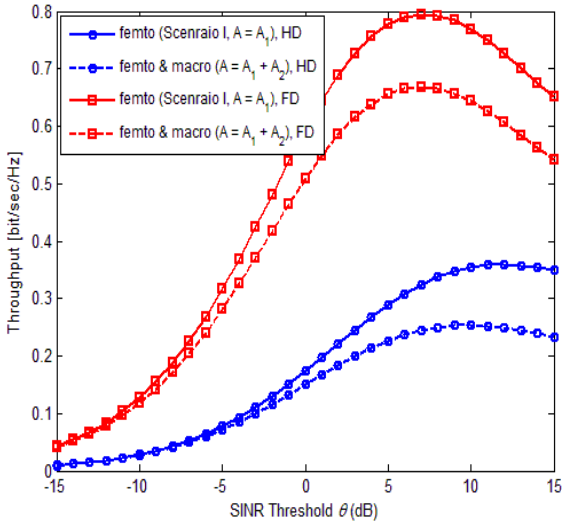

Fig. 4.11. The femto link throughput of half and full duplex systems as a function of the target SINR. The femto link throughput of half and full duplex systems under perfect and imperfect sensing scenarios as a function of the target SINR. The system parameters are set as $P_F = 23$ dBm, $P_M = 43$ dBm, $\alpha = 4$, $m_{d,F} = m_{I,F} = m_{I,M} = 1$, K = 1, $\lambda'_M = 10$, $\lambda_F = 800$ and $\lambda'_F = 700$, and for each curve the obtained optimal $\boldsymbol{p}$ in Fig. 4.10 is applied.

4.5 Conclusion

In this chapter, utilizing the spatial PPP theory, we presented a tractable model to derive the outage probability of a typical femto and macro user in a two-tier HetNet which provides insight into system design guidelines. In other words, for the case of the node locations modeled by a PPP and Nakagami-m fading channels, we demonstrated the use of the CR based framework to evaluate the outage probability at any arbitrary user. Exact closed-form expressions were obtained as a result. In addition, we observed that in the downlink analysis, the outage probability is a function of the network topology and several important system design parameters such as SINR target, exclusion regions, MAC mechanisms such as ALOHA ($\boldsymbol{p}_{tx}$), and the resource block (RB) selection constraint ($\boldsymbol{p}_{RB}$) which is controlled by the spectrum sensing measurements.

Chapter 5

Joint Interference Alignment and Power Allocation for Multi-User MIMO Interference Channels under Perfect and Imperfect CSI

5.1 Introduction

Although conventional approaches, such the orthogonal access schemes, power control, scheduling and antenna beamforming/nulling (and other mentioned approaches in the previous chapters) to deal with interference in both single and multi-tier communication systems can control interference without system overhead, it turns out that they are not optimal in most network configurations (except in certain special cases) because of their inefficient usage of the spectrum, and until recently, the sum-rate region of the IC was unknown while it has been shown in recent studies that the IC can be used in terms of providing linear scaling of the sum-rates [109]. Recently, a new paradigm for interference management techniques has emerged: interference shaping. This technique has shown to offer a better performance in the interference-limited communication regime than traditionally thought possible. The idea behind the concept of interference shaping is to create a certain interference pattern when transmitting

nodes propagate signals so that the aggregated interference effect is dramatically reduced or totally eliminated at each receiver. IA is considered as a representative interference shaping technique. IA has emerged as a viable transmission technique towards mitigating interference that can result in sum-rates that scale linearly with the number of users in the system for high SNR [109], [110]. In relation with the previous chapters, the IA, as another interference management technique, can be applied to the analysis of CR networks and cognitive cellular networks (or in general, HetNets). For example, in a MIMO CR system, multiple secondary users can coexist with the PU without generating any interference by using the IA technology. Or in HetNets, IA can be exploited to eliminate intra-tier (or inter-tier) and cross-tier interferences. However, in this chapter, we only introduce this interference management technique in MIMO systems, and possibly our future studies can cover heterogeneous MIMO CR wireless networks equipped with the IA technology.

The key idea of IA, as a linear precoding technique, is to align multiple interfering signals in time, frequency, or space in order to reduce the effective interference while still allowing the desired signals to be discerned. Thus, the maximum DoFs of the IC can be achieved. In other words, IA is a DoFs optimal approach, which means that it can reach the capacity of interference networks at very high SNR.

Such alignment in a K-user (K user-BS pairs in which each BS wishes to send d data streams) MIMO IC requires the knowledge of perfect and global CSI at each transmitting node (i.e., BS). In practice, this will potentially incur a significant increase in CSI overhead, because each user has to feed back its obtained CSI to all BSs using the feedback links resulting in overwhelming feedback overhead even if the quantized CSI is fed back [111]. Therefore, more efficient approaches and topologies are needed to reduce the requirement of global CSI as well as the sum feedback overhead for IA.

The design of an optimal feedback topology can be built upon closed-form IA solutions as in [53] and [112]. In other words, the IA transmit and receive filters (also respectively called IA precoding and suppression filters) can be designed through a closed-form solution of IA. However, the optimal IA solution in a closed-form does not seem trivial and exists only for some specific settings [53],

[112]. Thus, it is necessary to resort to iterative algorithms where the precoding and suppression filters are optimized progressively. Even though most of the IA iterative algorithms in the literature can indeed promise the maximum achievable DoFs in a MIMO IC, they still look for the perfect alignment solution as an ultimate objective; however, perfect IA solutions might also be suboptimal, because of the non-convex behavior of the alignment problem. Therefore, it is necessary to design iterative algorithms that directly or indirectly aim at maximizing the achievable sum-rate for users rather than seeking a perfect IA solution and meeting the IA feasibility conditions (see (5.4) and (5.5)).

As mentioned, iterative optimizations using the maximum sum-rate criterion have become more favorable for the implementation of IA. Unlike the traditional optimization schemes on Euclidean space, optimization algorithms on manifolds benefit from lower computational complexity and faster convergence [113], [114]. Indeed, utilizing the optimization on matrix manifolds makes it possible to design precoding (or suppression) filters for IA in terms of the sum-rate metric with an iterative process based on the simple steepest descent (SD) (also called gradient descent) method that converges to a local maximum due to the non-concavity of the objective function (sum-rate) [113]. Note that simpler optimization approaches based on the interference leakage minimization and SINR maximization criteria can also be used to design the filters.

Another important issue to consider is that unlike most of the studies on the IA MIMO IC (e.g., [53], and [109]-[112]) in which equal transmit powers are assumed for all user-BS pairs (ignoring the need for an optimal power allocation policy), optimal power allocation strategies can be performed to further optimize the sum-rate of a multi-user-BS network. Good reviews of different power allocation mechanisms in wireless networks can be found in [115]–[118]. They mostly formulated optimization problems for power allocation in different wireless network settings where interference is usually ignored or it is treated as noise [119]-[124], while in real scenarios where various BSs are operating in the same frequency band, ignoring interference can be a huge disadvantage in terms of system throughput.

In this chapter, which is an extension of [125], we propose three iterative IA algorithms for the problem of joint power allocation and transmit/receive filter design in a K-user MIMO IC based on three optimization approaches, including

the interference leakage minimization, max-SINR and sum-rate maximization. We design a centralized topology, where a CU (see Fig. 5.1) collects local CSI from all BSs, computes the IA transmit and receive filters, and makes the power allocation decisions. The information is then sent to the corresponding user-BS pairs. Note that unlike the conventional approaches in which the IA filters are designed under the assumption that CSI feedback is error-free (i.e., perfect CSI at each BS), in this chapter (see Section 5.3.3), we obtain the local CSI at BSs from the estimation of the channel states during the so-called uplink-training phase.

As we explain later, the proposed topology will lead to a significant decrease in CSI overhead compared to the conventional approaches where each user feeds back its own local CSI to all BSs using the feedback links so that the IA solution can be computed independently at each BS using the provided global CSI at each BS [111].

To design the IA filters at the CU, in addition to the well-known optimization approaches based on the interference leakage minimization and SINR maximization, we propose a new Riemannian optimization method on manifolds that solves the sum-rate maximization problem. We utilize the Riemannian optimization on matrix manifolds to design IA filters in terms of the sum-rate metric with an iterative process based on the SD method. We consider two related manifolds: the Stiefel manifold and the Grassmann manifold.

The Riemannian optimization scheme is employed on both the Stiefel and Grassmann manifolds based on geodesics with a variable step size. In other related studies (e.g., [126]), the updating rules obtained for the IA filters for the Grassmann manifold-based optimization greatly differ from the counterparts for the Stiefel manifold-based optimization. However, here we explain that the updating formulas given by the Riemannian optimization method on the Stiefel and Grassmann manifolds actually coincide since the chosen objective function (sum-rate) for optimization on the Stiefel manifold has a symmetry [113], [127].

We also study and apply a low-complexity iterative power allocation algorithm for sum-rate maximization over IA ICs under sum power constraint. In terms of the achievable sum-rate and DoFs, we compare the performance of our proposed methods with the conventional alternating leakage minimization, max-SINR (presented in [56]) and the proposed method in [57]. Simulation results show that

the proposed algorithms achieve promising sum-rate gains over the existing IA algorithms particularly at high SNRs and high-dimensional signal spaces.

In the following sections, we use lower case for scalars and upper case for vectors. We denote matrices with bold font. $\mathbf{A}^{\star d}$ represents the dth column of matrix $\mathbf{A}$. We represent a $d \times d$ identity matrix by $\mathbf{I}_d$. $\mathrm{Tr}[\mathbf{A}]$ is used to denote the trace of the matrix $\mathbf{A}$. Finally, $\mathbf{A}^H$ is the conjugate transpose (Hermitian) of matrix $\mathbf{A}$.

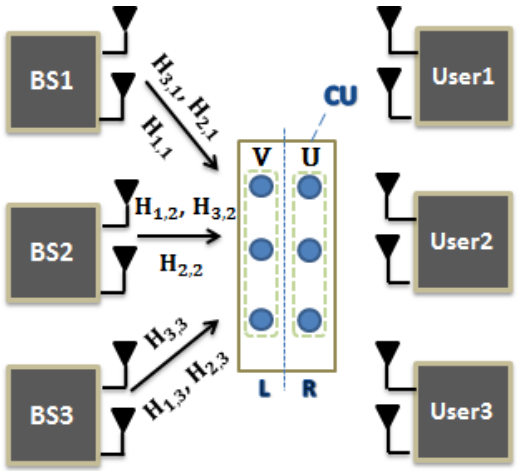

Fig. 5.1. An example model of the IA for a three-user IC with two antennas at each node ('CU' is a central unit, $\mathbf{V}$ and $\mathbf{U}$ are respectively the precoding and suppression filters, and 'L' and 'R' denote the left and right sides)

5.2 System Model

Consider a MIMO IC where K BSs intend to transmit data to K mobile users. The BSs and the users are respectively equipped with M and N antennas. Each user is to be associated to exactly one BS, and each BS only serves one user. A wireless channel links each user to each BS, but a given BS intends to have its signal decoded by its own specified user only. The transmitted signal vector of user k ($k \in \{1,2,\ldots,K\}$) from the associated BS l_k is given by

$$X_{k,l_k} = \sum_{d=1}^{d_k} \mathbf{V}_{k,l_k}^{\star d} S_{k,l_k}^{d} = \mathbf{V}_{k,l_k} S_{k,l_k},\ \forall k \in \{1,2,\dots,K\} \tag{5.1}$$

where S_{k,l_k} is the $d_k \times 1$ symbol vector to be transmitted by the l_kth BS, which is then beamformed with the corresponding precoding vector of $\mathbf{V}_{k,l_k}$ (an $M \times d_k$ unitary matrix). Inter-symbol interference is assumed to be managed perfectly using an OFDM transmission scheme. Mathematically, the received signal vector of user k is then given by

$$Y_k = \sum_{i=1}^{K} p_i \mathbf{H}_{k,l_i} \mathbf{V}_{i,l_i} S_{i,l_i} + Z_k,\ \forall k \in \{1,2,\dots,K\} \tag{5.2}$$

where $\mathbf{H}_{k,l_i}$ is the $N \times M$ matrix of channel coefficients between BS l_i and user k. Denote by p_k the power BS l_k uses to transmit the data intended for user k. Z_k is the $N \times 1$ circularly symmetric complex additive white Gaussian noise vector (AWGN) at user k.

Finally, the kth user uses the interference suppression matrix $\mathbf{U}_{k,l_k}$ (an $N \times d_k$ unitary matrix) to filter its received signal as follows

$$\begin{aligned} \overline{Y_k} &= \mathbf{U}_{k,l_k}^{H} Y_k \\ &= \underbrace{\mathbf{U}_{k,l_k}^{H} p_k \mathbf{H}_{k,l_k} \mathbf{V}_{k,l_k} S_{k,l_k}}_{desired\ signal} + \underbrace{\mathbf{U}_{k,l_k}^{H} \sum_{i=1, i\neq k}^{K} p_i \mathbf{H}_{k,l_i} \mathbf{V}_{i,l_i} S_{i,l_i}}_{interference} + \underbrace{\mathbf{U}_{k,l_k}^{H} Z_k}_{noise}. \end{aligned} \tag{5.3}$$

Assuming IA is feasible, the alignment is achieved when the precoding and suppression matrices satisfy the following conditions [56]:

$$\mathbf{U}_{k,l_k}^{H} \mathbf{H}_{k,l_i} \mathbf{V}_{i,l_i} = 0,\ \ \forall k, i \in \{1,\dots,K\}, i \neq k \tag{5.4}$$

$$\operatorname{rank}\left(\mathbf{U}_{k,l_k}^{H} \mathbf{H}_{k,l_k} \mathbf{V}_{k,l_k}\right) = d_k. \tag{5.5}$$

The aim of IA is to design precoding matrix $\mathbf{V}$ and suppression matrix $\mathbf{U}$ such that each user can decode its own desired signal by forcing interfering signals into a reduced-dimensional subspace of the received space. Therefore, each user can observe an interference-free desired signal.

In various studies (e.g., [56], [128]), iterative IA solutions have been proposed and shown to converge. These kinds of algorithms optimize the precoding and the interference suppression filters to minimize the interference leakage by alternating between forward and reverse links based on the assumption of channel reciprocity.

Iterative procedures based on the channel reciprocity assumption have a number of potential drawbacks. First, iterating over the air can incur a non-negligible overhead while iterations can be performed off-line at a central entity eliminating the need for over-the-air signaling. Second, reciprocity cannot be applied to all IA-based algorithms [43]. On the other hand, even though this property can be applied to time duplexed systems under the use of tightly calibrated RF devices, it does not hold in frequency duplexed systems [43], [112].

In this chapter, we utilize the topology of CSI exchange in the network as illustrated in Fig. 1. BS l_k ($k \in \{1,2,\dots,K\}$) obtains the knowledge of the local channel coefficients $\mathbf{H}_{i,l_k}$ ($\forall i \in \{1,2,\dots,K\}$) through the estimation of the channel states during the uplink-training phase explained in Section 5.3.3. Note that most of the previous studies on IA are based on the impractical assumption that perfect and global CSI is available at the BS sides. In this topology, as shown in the figure, CSI is conveyed from each BS to a CU where the optimal precoding and suppression filters as well as the power allocation decisions are designed (using our proposed algorithms in Section 5.3) and then sent to the corresponding user-BS pairs. In order to design the CU topology, we have assumed that each BS directly exchanges the estimated CSI from the uplink phase with the CU. This framework is feasible for the nodes that are located close together and linked with local area networks such as Wi-Fi. Moreover, the uplink coordinated multi-point (CoMP) system, which provides the high-capacity backhaul links between BSs can be applicable for this scenario. While a CU topology is an efficient scheme for the reduction in the CSI overhead, there exist some challenges regarding the implementation phase. The synchronization and organization of this kind of networks will be paramount in achieving the gains projected by IA. Moreover, central entity risks increasing the load on the backhaul network and risks missing delay constraints due to the transfer of CSI and computation time of IA solution.

As mentioned earlier, our proposed scheme has lower CSI overhead (particularly for large K) than the conventional approaches where each user feeds back its estimated local CSI to all BSs using the feedback links. Let's consider the scenario of designing the IA precoding filters. In the conventional approaches (e.g., [128]), a typical user has to feed back its estimated local CSI ($\mathbf{H}_{k,l_i}$ ($\forall i \in \{1,2,\dots,K\}$)) by broadcasting KNM complex coefficients to each BS

assuming no errors. Therefore, the number of coefficients sent by that user to all BSs is K^2NM. The total number of channel coefficients exchanged over the network (the total CSI overhead) is equal to K^3NM (i.e., the CSI overhead increases as $O(K^3NM)$). Meanwhile, under the same assumption, in the proposed method, each BS sends KNM complex coefficients to CU. Therefore, the number of coefficients exchanged by all BSs with CU is K^2NM. Then CU broadcasts a precoding matrix of Md coefficients to each of the BSs. Thus, the total CSI overhead for the proposed topology is computed as $K^2NM + KMd$ (i.e., the CSI overhead increases as $O(K^2NM)$).

5.3 Iterative Optimization (Mathematical Model)

5.3.1 Optimization Problems

In this section, we present several optimization problems used at the CU to determine the optimal precoding and suppression filters as well as the optimal power allocation for all user-BS pairs. We first formulate the optimization problem for power allocation in the network. The goal is to make power allocation decisions for sum-rate maximization subject to sum power constraint. We evaluate the sum power constrained problem (i.e., there is a constraint on the total power budget available for all BSs denoted by $\bar{p}_{TB}$) and propose a fixed point algorithm to solve it to global optima. Therefore, the optimization problem can be formulated as follows

Optimization I: max-min SINR based Power Allocation

$$\begin{aligned} \max_{\boldsymbol{p}} \min_{k=1,\dots,K} \mathrm{SINR}_{k,l_k} &= \frac{\frac{p_k}{d}\left|\mathbf{H}_{k,l_k}\mathbf{V}_{k,l_k}\right|^2}{\sum_{i=1,i\neq k}^{K}\frac{p_i}{d}\left|\mathbf{H}_{k,l_i}\mathbf{V}_{i,l_i}\right|^2 + {\sigma_k}^2} \\ \text{s.t. } 0 \le p_k \le \bar{p}_{l_k}, &\quad k = 1,\dots,K, \\ \{l_1,\dots,l_K\} &= \{1,\dots,K\}, \\ \sum_{k=1}^{K} p_k &\le \bar{p}_{TB}, \\ \boldsymbol{p} &= (p_1,\dots,p_K) \end{aligned} \tag{5.6}$$

The first constraint is individual power constraint per BS. We assume that each BS can adaptively vary its transmit power depending on the power allocation decisions and each BS can transmit with a power between 0 and the assigned power budget $\bar{p}_{l_k}$. An equal power budget is assumed for all BSs ($\bar{p}_{l_1} = \bar{p}_{l_2} = \cdots = \bar{p}_{l_K} = \bar{p}_{TB}$). The other constraint represents the sum power constraint that indicates the total power resource is constrained. ${\sigma_k}^2$ is the receive noise power at user k. It has been shown in [129] that the above max-min SINR problem developed for the power allocation problem in fact provides a provable approximation ratio to the sum-rate maximization objective.

We now want to solve the above max-min fairness power allocation problem: one way is to use a binary search strategy as in [130]. However, since the proposed binary search can be time-consuming, we present a fixed point algorithm that directly solves the max-min fairness power allocation problem.
Define

$$T_k(\boldsymbol{p}) \triangleq \frac{\sum_{i=1, i\neq k}^{K} \frac{p_i}{d} \left|\mathbf{H}_{k,l_i}\mathbf{V}_{i,l_i}\right|^2 + {\sigma_k}^2}{\frac{1}{d}\left|\mathbf{H}_{k,l_k}\mathbf{V}_{k,l_k}\right|^2},$$
$$T(\boldsymbol{p}) \triangleq \big(T_1(\boldsymbol{p}), \ldots, T_K(\boldsymbol{p})\big). \tag{5.7}$$

Notice that $T_k(\boldsymbol{p})$ is the minimum power needed by BS l_k to achieve an SINR value of 1 with fixed $p_j, \forall\, j \neq k$. The proposed algorithm simply picks a random positive power vector $\boldsymbol{p}(\mathbf{0})$ and updates the power vector as follows

$$\boldsymbol{p}\,(t+1) \leftarrow \frac{T\big(\boldsymbol{p}(t)\big)}{\sum_{i=1}^{K} T_i\big(\boldsymbol{p}(t)\big)}\bar{p}_{TB}. \tag{5.8}$$

and for user k

$$p_k(t+1) \leftarrow \frac{T_k\big(\boldsymbol{p}(t)\big)}{\sum_{i=1}^{K} T_i\big(\boldsymbol{p}(t)\big)}\bar{p}_{TB}. \tag{5.9}$$

We will next propose our algorithms to obtain the precoding and suppression filters of each user-BS pair through solving different optimization problems including sum-rate maximization, interference leakage minimization, and SINR maximization strategies. For example, in the first approach of the proposed algorithms (see Section 5.3.4), we present an iterative method at the central

coordinator to find the optimal interference suppression matrices $\mathbf{U}_{k,l_k}$ ($k \in \{1,2,\dots,K\}$) that minimize the leakage interference (from all undesired BSs) at each user, and compute the optimal precoding matrices $\mathbf{V}_{k,l_k}$ ($k \in \{1,2,\dots,K\}$) that maximize the sum mutual information. Thus, for the first approach of our proposed methods, we have the following optimization problems:

Optimization II: Interference Leakage Minimization

For each user k, we solve the following optimization problem

$$\min_{\mathbf{U}_{k,l_k}\mathbf{U}_{k,l_k}^H=\mathbf{I}_{d_k}} I_k \tag{5.10}$$

where I_k is the total interference leakage observed at user k (see Section 5.3.4). In other words, for each user we choose the unitary interference suppression filter $\mathbf{U}_{k,l_k}$ to minimize the leakage interference due to all undesired BSs (l_k is the corresponding BS of user k).

Optimization III: Sum-Rate Maximization

We want to find the best truncated unitary precoding matrices that maximize the sum-rate. Therefore, we have the following optimization problem

$$\begin{aligned} &\max_{\mathbf{V}_{1,l_1},\dots,\mathbf{V}_{K,l_K}} R_{sum} = \sum_{k=1}^{K} R_{k,l_k} \\ &\text{s.t. } \mathbf{V}_{k,l_k}\mathbf{V}_{k,l_k}^H = \mathbf{I}_{d_k},\ \forall k \in \{1,2,\dots,K\} \end{aligned} \tag{5.11}$$

where R_{k,l_k} is the mutual information between the BS l_k and its dedicated user k, and is expressed as follows [109], [131]

$$R_{k,l_k} = \log_2 \frac{\left|\mathbf{I} + \sum_{i=1}^{K} \frac{p_i}{d} \mathbf{H}_{k,l_i}\mathbf{V}_{i,l_i}\mathbf{V}_{i,l_i}^H\mathbf{H}_{k,l_i}^H\right|}{\left|\mathbf{I} + \sum_{i=1,i\neq k}^{K} \frac{p_i}{d} \mathbf{H}_{k,l_i}\mathbf{V}_{i,l_i}\mathbf{V}_{i,l_i}^H\mathbf{H}_{k,l_i}^H\right|}. \tag{5.12}$$

The optimization for the interference suppression matrix $\mathbf{U}$ (*Optimization II*) can be iteratively solved by obtaining the d_k eigenvectors corresponding to the d_k smallest eigenvalues of interference covariance matrix $\mathbf{W}_k$ (see Section 5.3.4) at each iteration [56]. Thus, the d_k columns of $\mathbf{U}_{k,l_k}$ are obtained as follows

$$\mathbf{U}_{k,l_k}^{\star d} = \nu_d[\mathbf{W}_k], \;\; d = 1, \dots, d_k \tag{5.13}$$

where $\nu_d[\mathbf{A}]$ indicates the eigenvector corresponding to the smallest eigenvalue of $\mathbf{A}$. It should be noted that we assume $d_k = d$ for all users.
The sum-rate maximization problem (*Optimization III*) under the unitary matrix constraint is addressed in the following subsection.

5.3.2 Riemannian Optimization Method for Sum-Rate Maximization Problem

In this section, we use the Riemannian optimization method to maximize R_{sum}. We obtain the updating rules for the precoding matrices $\mathbf{V}_{k,l_k}, (k \in \{1,2,\dots,K\})$ given by the Riemannian optimization method (on the two well-known manifolds Stiefel and Grassmann, and based on geodesics), which has been recently used in different research fields such as pattern recognition, neural networks, and numerical analysis. A geodesic is defined as a direct extension of a straight line in the Euclidean space to a manifold (a curved space). The major drawback of the classical optimization methods with a unitary matrix constraint that operate on the Euclidean space is that the unitary property of the matrix (here the precoding matrix $\mathbf{V}$) is lost after every iteration, and it needs to be restored in each step. In other words, the updated point $\mathbf{V}$ does not always remain on the manifold, while the Riemannian optimization approach updates a point on a manifold along a geodesic, therefore the updated points always satisfy the manifold constraint. Another potential drawback of the classical optimization methods on the Euclidean space is their slow convergence rate [113], [114], [126], [127].

When the above notations are considered, the updating rule of the precoding matrices $\mathbf{V}_{k,l_k}$ $(k \in \{1,2,\dots,K\})$ for the gradient descent method (a Riemannian optimization method) over the manifold T is described as follows [127]

$$\mathbf{V}_{k,l_k}^{t+1} = \phi_T\left(\mathbf{V}_{k,l_k}^{t}, \mathrm{grad}_{\mathbf{V}_{k,l_k}} R_{sum}, \mu\right) \tag{5.14}$$

where ϕ_T is the geodesic expression on manifold T emanating from $\mathbf{V}_{k,l_k} \in T$ in direction to $\mathrm{grad}_{\mathbf{V}_{k,l_k}} R_{sum}$. The natural gradient $\mathrm{grad}_{\mathbf{V}} R_{sum}$ of a function R_{sum} at

point $\mathbf{V}$ on a manifold T is intuitively the steepest direction the function R_{sum} ascends in T, and μ represents the step size. $\text{grad}_{\mathbf{V}} R_{sum}$ on Stiefel manifold ($\text{St}(M,d)$) is defined as follows

$$\text{grad}_{\mathbf{V}}^{\text{St}(M,d)} R_{sum} = \nabla R_{sum}(\mathbf{V}) - \mathbf{V}\nabla R_{sum}(\mathbf{V})^H \mathbf{V}. \tag{5.15}$$

The geodesic ϕ_T on $\text{St}(M,d)$ characterized by the matrix exponential maps, which in fact give geometrically simpler interpretations and expressions and are easier to analyze, is expressed as follows [113], [127]:

$$\begin{aligned}
&\phi_{\text{St}(M,d)}\left(\mathbf{V}, \text{grad}_{\mathbf{V}}^{\text{St}(M,d)} R_{sum}, \mu\right) \\
&\quad = \exp\left(\mu \text{grad}_{\mathbf{V}}^{\text{St}(M,d)} R_{sum} \mathbf{V}^H\right)\mathbf{V} \\
&\quad = \exp(\mu[\nabla R_{sum}(\mathbf{V})\mathbf{V}^H - \mathbf{V}\nabla R_{sum}(\mathbf{V})^H \mathbf{V}\mathbf{V}^H])\,\mathbf{V} \\
&\quad = \exp(\mu[\nabla R_{sum}(\mathbf{V})\mathbf{V}^H - \mathbf{V}\nabla R_{sum}(\mathbf{V})^H])\,\mathbf{V}.
\end{aligned} \tag{5.16}$$

For $R_{sum}(\mathbf{V})$ where $\mathbf{V}$ has complex components, and $R_{sum}(\mathbf{V})$ is a real-valued function, the gradient is defined as $\nabla R_{sum}(\mathbf{V}) = 2\frac{\delta(R_{sum}(\mathbf{V}))}{\delta \mathbf{V}^*} = 2\left(\frac{\delta(R_{sum}(\mathbf{V}))}{\delta \mathbf{V}}\right)^*$ [132]. For the user k, $\nabla R_{sum}(\mathbf{V})$ is derived and expressed as follows [109], [132]:

$$\nabla R_{sum}(\mathbf{V})_{k,l_k} = \frac{2}{\ln 2}\sum_{i=1}^{K} p_k \mathbf{H}_{i,l_k}^H \mathbf{X}_i^{-1} \mathbf{H}_{i,l_k} \mathbf{V}_{k,l_k} - \frac{2}{\ln 2}\sum_{i=1, i\neq k}^{K} p_k \mathbf{H}_{i,l_k}^H \mathbf{Y}_i^{-1} \mathbf{H}_{i,l_k} \mathbf{V}_{k,l_k} \tag{5.17}$$

where

$$\mathbf{X}_k = \mathbf{I} + \sum_{i=1}^{K} \frac{p_i}{d} \mathbf{H}_{k,l_i} \mathbf{V}_{i,l_i} \mathbf{V}_{i,l_i}^H \mathbf{H}_{k,l_i}^H \tag{5.18}$$

and

$$\mathbf{Y}_k = \mathbf{I} + \sum_{i=1, i\neq k}^{K} \frac{p_i}{d} \mathbf{H}_{k,l_i} \mathbf{V}_{i,l_i} \mathbf{V}_{i,l_i}^H \mathbf{H}_{k,l_i}^H. \tag{5.19}$$

A major advantage of our proposed solution is that the applied updating strategy and the obtained formulas corresponding to the SD algorithm along the geodesic give geometrically simpler interpretations and expressions (which are easier to analyze) making the implementation complexity very low. The update rules proposed for sum-rate maximization in [57] are shown to obtain higher sum-rate than the conventional alternating leakage minimization (for all SNR values)

and the max-SINR (in high SNR regime). However, it requires a series of both the eigenvalue decompositions and compact singular value decompositions (SVDs), which can lead to a significant increase in the computational complexity (the same problem applies to [131]). The authors in [57] propose an iterative alternating minimization algorithm that aims to find the best IA solution in terms of sum-rate in which the updating process for the filters (in contrast to our update formula, the geodesic $\boldsymbol{\phi}_T$, in (5.16)) requires the calculations of the compact SVD.

For further complexity reduction, the low dimensional Grassmann manifold is used to derive the corresponding geodesic equation $\boldsymbol{\phi}_T$. Similarly, the natural gradient $\mathbf{grad}_{\mathbf{V}} R_{sum}$ over the Grassmann manifold is expressed as [113]

$$\mathbf{grad}_{\mathbf{V}}^{\mathrm{Gr}(M,d)} R_{sum} = \nabla R_{sum}(\mathbf{V}) - \mathbf{V}\mathbf{V}^H \nabla R_{sum}(\mathbf{V}). \tag{5.20}$$

Before obtaining the updating rule of the precoding matrices $\mathbf{V}$ given by the gradient descent method over the Grassmann manifold ($\mathrm{Gr}(M,d)$), we consider the following important fact that says:

Note:
Our objective function for optimization on the Stiefel manifold has an $\mathbf{O}(d)$-symmetry ($\mathbf{O}(d)$ is the Lie group of unitary matrices)
i.e., $R_{sum}(\mathbf{VE}) = R_{sum}(\mathbf{V})$ (*for all* $\mathbf{V} \in \mathrm{St}(M,d)$, $\mathbf{E}$ *is a* $\mathrm{d} \times \mathrm{d}$ *unitary matrix, i.e.,* $\mathbf{E} \in \mathbf{O}(\mathrm{d})$) [127].

Notice that it is easy to show that our objective function (sum-rate) satisfies the above condition. Thus, based on the above fact, it can be proved that [127], [133]

$$\mathbf{grad}_{\mathbf{V}}^{\mathrm{Gr}(M,d)} R_{sum} = \mathbf{grad}_{\mathbf{V}}^{\mathrm{St}(M,d)} R_{sum} \tag{5.21}$$

which finally leads to

$$\phi_{\mathrm{Gr}(M,d)}\left(\mathbf{V}, \mathbf{grad}_{\mathbf{V}}^{\mathrm{Gr}(M,d)} R_{sum}, \mu\right) = \phi_{\mathrm{St}(M,d)}\left(\mathbf{V}, \mathbf{grad}_{\mathbf{V}}^{\mathrm{St}(M,d)} R_{sum}, \mu\right). \tag{5.22}$$

In other words, the updating rule given by the gradient descent method over the Stiefel manifold shown in (5.16) coincides with the one over the Grassmann manifold.

5.3.3 Uplink-Training Phase

In most of the IA studies that have been made, the IA filters were designed assuming that perfect knowledge of the channel matrices of all links is available in the network. However, in practice this assumption is unrealistic. Thus, in this subsection, we study common channel estimation techniques while employing reverse-link pilot sequences in a MIMO-OFDM scheme. In other words, we design an uplink channel-training phase using pilot symbols based on the least-squares (LS) and minimum mean square error (MMSE) estimators [134]-[137].

5.3.3.1 MIMO-OFDM Systems

Based on MIMO-OFDM systems ([136], [137]) and according to a specified modulation scheme (for example QAM), the binary information is first grouped and mapped to finite alphabet symbols. Next, pilot signals are inserted either into (i) certain subcarriers of each OFDM symbol or (ii) all sub-carriers of OFDM symbols with a specific period. Each OFDM symbol is then converted into a time-domain OFDM symbol via inverse discrete Fourier transform (IDFT). After adding the cyclic prefix (CP) (to eliminate *inter-carrier interference* and *inter-symbol interference*), the time-domain OFDM signal is transmitted through the transmit antennas (note that the CP inserted at the beginning of each OFDM symbol is usually equal to or longer than the expected delay spread). The transmit signals (the sum of complex exponentials, i.e., sine and cosine functions) are propagated through the MIMO channels. At the receiver, after the removal of the CP, data are transformed back to the frequency domain OFDM symbols via the DFT operation to start the next stage, which is the uplink channel estimation phase. Mathematically, the OFDM received signal can be written as

$$\mathbf{O} = DFT\big(IDFT(\mathbf{X}) \otimes \mathbf{G} + \widetilde{\mathbf{N}}\big) = \mathbf{HX} + \mathbf{N}, \tag{5.23}$$

where $\mathbf{O}$, $\mathbf{X}$, $\mathbf{G}$, $\widetilde{\mathbf{N}}$, and $\mathbf{N}$ are matrices respectively representing the received and transmitted symbols, channel impulse response, noise, and transformed noise. Furthermore, $\mathbf{H} = DFT(\mathbf{G})$ is the channel frequency response, and $\otimes$ represents circular convolution (note that $a \otimes b = b \otimes a$).

5.3.3.2 Channel Estimation for MIMO-OFDM Systems

In this subsection, channels are estimated at BSs using the observations of the pilot signals (pilot observations) in a local window.

We assume that the length of the uplink training period is equal to B (i.e., the total number of pilot observations in the window is equal to B), and all the users transmit the respective pilot sequences in the length of B simultaneously during the training period. We denote $\mathbf{X}_{\pi_i}$ (an $N \times B$ matrix) as the uplink pilot signal of user i. π_i is the index of the pilot sequence used by user i ($\pi_i \in \{1, \dots, B\},\ i \in \{1, \dots, K\}$). For simplicity, we have assumed that the maximum number of available orthogonal pilot sequences in the network is also equal to B.

The received signal (an $M \times B$ matrix) at BS l_k, ($l_k \in \{1, \dots, K\}, k \in \{1, \dots, K\}$) is expressed as follows

$$\mathbf{O}_{l_k} = \sum_{i=1}^{K} \sqrt{\bar{p}_i} d_{l_k}(\mathbf{r}_i) \overleftarrow{\mathbf{H}}_{i,l_k} \mathbf{X}_{\pi_i} + \mathbf{N}_{l_k} \tag{5.24}$$

where $\overleftarrow{\mathbf{H}}_{i,l_k}$ (an $M \times N$ matrix) is the channel between user i and BS l_k. $\bar{p}_i$ is the pilot signal power of user i. The vector $\mathbf{r}_i \in \mathbb{R}^2$ is the geographical position of user i and $d_{l_k}(\mathbf{r})$ is an arbitrary function that accounts for the channel attenuation (e.g., path loss and shadowing) between BS l_k and any user position $\mathbf{r}$, which is assumed to be constant and known to all BSs. $\mathbf{N}_{l_k}$ (an $M \times B$ matrix) is i.i.d. noise at BS l_k ($\mathbf{N}_l \sim CN(0, \sigma_z^2)$, σ_z^2 is the noise power).

Then, each BS can obtain the channel observation of all the users. Specifically, for the kth user, the BS l_k obtains the uplink channel observation as

$$\begin{aligned} \mathbf{Y}_{\pi_k,l_k} &= \mathbf{O}_{l_k} \mathbf{X}_{\pi_k}^H \\ &= \sum_{i=1}^{K} \sqrt{\bar{p}_i} d_{l_k}(\mathbf{r}_i) \overleftarrow{\mathbf{H}}_{i,l_k} \mathbf{X}_{\pi_i} \mathbf{X}_{\pi_k}^H + \mathbf{N}_{l_k} \mathbf{X}_{\pi_k}^H. \end{aligned} \tag{5.25}$$

Note: $\mathbf{X}_a \mathbf{X}_b^H = B\delta(a-b)$ (different pilot signals are assumed to satisfy the orthogonality condition)

$$\mathbf{Y}_{\pi_k,l_k} = \sum_{i=1}^{K} \sqrt{\bar{p}_i} d_{l_k}(\mathbf{r}_i) \overleftarrow{\mathbf{H}}_{i,l_k} B\delta(\pi_i - \pi_k) + \mathbf{N}_{l_k} \mathbf{X}_{\pi_k}^H$$

$$= \sum_{i \in S_{\pi_k}} \sqrt{\bar{p}_i} d_{l_k}(\mathbf{r}_i) \overleftarrow{\mathbf{H}}_{i,l_k} B + \mathbf{N}_{l_k} \mathbf{X}_{\pi_k}^H$$

$$= \sqrt{\bar{p}_k} d_{l_k}(\mathbf{r}_k) \overleftarrow{\mathbf{H}}_{k,l_k} B + \sum_{i \in S_{\pi_k} \setminus \{k\}} \sqrt{\bar{p}_i} d_{l_k}(\mathbf{r}_i) \overleftarrow{\mathbf{H}}_{i,l_k} B + \mathbf{N}_{l_k} \mathbf{X}_{\pi_k}^H. \quad (5.26)$$

where S_{π_k} is the set of those users using the same pilot as the kth user and "\" denotes the set subtraction operation.

LS estimate of the uplink channels: (assuming that $\bar{p}_i = \bar{p}$, $\forall i \in \{1, \dots, K\}$ and $\mathbf{N}_{l_k} = \mathbf{N}$, $\forall l_k \in \{1, \dots, K\}$)

$$\widehat{\mathbf{H}}_{k,l_k} = \frac{\mathbf{Y}_{\pi_k,l_k}}{B\sqrt{\bar{p}} d_{l_k}(\mathbf{r}_k)}$$

$$= \overleftarrow{\mathbf{H}}_{k,l_k} + \sum_{i \in S_{\pi_k} \setminus \{k\}} \frac{d_{l_k}(\mathbf{r}_i)}{d_{l_k}(\mathbf{r}_k)} \overleftarrow{\mathbf{H}}_{i,l_k} + \frac{\mathbf{N}\mathbf{X}_{\pi_k}^H}{B\sqrt{\bar{p}} d_{l_k}(\mathbf{r}_k)}. \quad (5.27)$$

It can be shown that $\frac{\mathbf{N}\mathbf{X}_{\pi_k}^H}{B\sqrt{\bar{p}} d_{l_k}(\mathbf{r}_k)} \sim CN(0, \frac{\sigma_z^2}{B\sqrt{\bar{p}} d_{l_k}(\mathbf{r}_k)})$. Denoting $p_e = \frac{\sqrt{\bar{p}}}{\sigma_z^2}$ as the uplink training SNR, we then have $\frac{\mathbf{N}\mathbf{X}_{\pi_k}^H}{B\sqrt{\bar{p}} d_l(\mathbf{r}_k)} \sim CN(0, \frac{1}{B p_e d_{l_k}(\mathbf{r}_k)})$. Therefore, (5.27) is rewritten as follows

$$\widehat{\mathbf{H}}_{k,l_k} = \overleftarrow{\mathbf{H}}_{k,l_k} + \underbrace{\sum_{i \in S_{\pi_k} \setminus \{k\}} \frac{d_{l_k}(\mathbf{r}_i)}{d_{l_k}(\mathbf{r}_k)} \overleftarrow{\mathbf{H}}_{i,l_k}}_{Pilot\ Interference} + \frac{\mathbf{N}_{\pi_k}}{\sqrt{B p_e d_{l_k}(\mathbf{r}_k)}} \quad (5.28)$$

where $\mathbf{N}_{\pi_k} \sim CN(0, \mathbf{I}_M)$ is the normalized additive noise. Finally, we assume that no users use the same pilot in the uplink-training phase; therefore, (5.28) is simplified to (5.29)

$$\widehat{\mathbf{H}}_{k,l_k} = \overleftarrow{\mathbf{H}}_{k,l_k} + \frac{\mathbf{N}_{\pi_k}}{\sqrt{B p_e d_{l_k}(\mathbf{r}_k)}}. \quad (5.29)$$

***MMSE estimate of the uplink channels*:**
Applying the MMSE estimator, we have

$$\widehat{\mathbf{H}}_{k,l_k} = \mathbf{R}_{k,l_k}\mathbf{Q}_{\pi_k,l_k}\mathbf{Y}_{\pi_k,l_k} \tag{5.30}$$

where

$$\mathbf{Q}_{\pi_k,l_k} = (\sum_{i\in S_{\pi_k}} \frac{d_{l_k}(\mathbf{r}_i)}{d_{l_k}(\mathbf{r}_k)}\mathbf{R}_{i,l_k} + \frac{1}{Bp_e d_{l_k}(\mathbf{r}_k)}\mathbf{I}_M)^{-1}$$

$$= (\mathbf{R}_{k,l_k} + \sum_{i\in S_{\pi_k}\setminus\{k\}} \frac{d_{l_k}(\mathbf{r}_i)}{d_{l_k}(\mathbf{r}_k)}\mathbf{R}_{i,l_k} + \frac{1}{Bp_e d_{l_k}(\mathbf{r}_k)}\mathbf{I}_M)^{-1}. \tag{5.31}$$

$\mathbf{R}_{i,l_k}$ (an $M \times M$ matrix) is the covariance matrix of the channel between the ith user and BS l_k. Under the same assumption made for (5.28), (5.31) is simplified to (5.32)

$$\mathbf{Q}_{\pi_k,l_k} = (\mathbf{R}_{k,l_k} + \frac{1}{Bp_e d_{l_k}(\mathbf{r}_k)}\mathbf{I}_M)^{-1}. \tag{5.32}$$

After the estimation of the channels corresponding to the pilot signals, the channels for the data signals are generated via proper interpolation among pilot channels. We assume that the uplink and downlink of each link are reciprocal (fulfilled in TDD mode), i.e., $\mathbf{H} = \overleftarrow{\mathbf{H}}^H$, which in fact indicates that the downlink channel $\mathbf{H}$ (applied at the CU) is equal to the transposition of uplink channel training $\overleftarrow{\mathbf{H}}$ in the coherence time.

Considering the above explanations, in the following subsection, we explain the detailed procedures of our three proposed SD-based algorithms for IA.

5.3.3.3 Proposed Algorithms on Different Strategies for IA

Proposed Algorithm-First Approach

At CU (see Fig. 1):

1. Start with random unitary matrices $\mathbf{V}_{k,l_k}$ ($k = 1, \dots, K$, and $l_k \in \{1, \dots, K\}$) at CU, pick random positive power vector $\boldsymbol{p}(0) = \big(p_1(0), \dots, p_K(0)\big)$, and initialize μ with 0.1.

2. Obtain the interference covariance matrix $\mathbf{W}_k$ for each user [56].

$$\mathbf{W}_k = \sum_{i=1, i\neq k}^{K} \frac{p_i}{d} \mathbf{H}_{k,l_i} \mathbf{V}_{i,l_i} \mathbf{V}_{i,l_i}^H \mathbf{H}_{k,l_i}^H$$

3. Calculate the interference suppression filter $\mathbf{U}_{k,l_k}$ for each user ($k \in \{1,2, \dots, K\}$) to minimize the leakage interference due to all undesired BSs using (5.13) (the interference leakage at user k can be obtained as $I_k = \mathrm{Tr}\big[\mathbf{U}_{k,l_k}^H \mathbf{W}_k \mathbf{U}_{k,l_k}\big]$).

4. Update the precoding filters $\mathbf{V}_{k,l_k}$ ($k \in \{1,2, \dots, K\}$) along the geodesic over the Stiefel (or Grassmann) manifold in the direction given by ∇R_{sum}:

$$\mathbf{V}_{k,l_k} = \exp\big(\mu\big[\nabla R_{sum}(\mathbf{V})_{k,l_k} \mathbf{V}_{k,l_k}^H - \mathbf{V}_{k,l_k} \nabla R_{sum}(\mathbf{V})_{k,l_k}^H\big]\big)\, \mathbf{V}_{k,l_k}$$

where $\nabla R_{sum}(\mathbf{V})$ was expressed in (5.17).

5. Update power allocation as follows

$$T_k(\boldsymbol{p}) \triangleq \frac{\sum_{i=1, i\neq k}^{K} \frac{p_i}{d} \big|\mathbf{H}_{k,l_i} \mathbf{V}_{i,l_i}\big|^2 + {\sigma_k}^2}{\frac{1}{d}\big|\mathbf{H}_{k,l_k} \mathbf{V}_{k,l_k}\big|^2}$$

$$T(\boldsymbol{p}) \triangleq (T_1(\boldsymbol{p}), \dots, T_K(\boldsymbol{p}))$$

$$p_k\,(t+1) \leftarrow \frac{T_k(\boldsymbol{p}(t))}{\sum_{i=1}^{K} T_i(\boldsymbol{p}(t))} \bar{p}_{TB}$$

6. Update the step size: $\mu = \mu \times 0.95$. Repeat Steps 2-6 until convergence.

7. Distribute all the obtained precoding and suppression filters as well as the power allocation decisions to the corresponding user-BS pairs.

Proposed Algorithm-Second Approach

At CU (see Fig. 1):

1. Start with random unitary matrices $\mathbf{V}_{k,l_k}$ ($k = 1, \dots, K$, and $l_k \in \{1, \dots, K\}$) at CU, pick random positive power vector $\boldsymbol{p}(0) = \big(p_1(0), \dots, p_K(0)\big)$, and initialize μ with 0.1.

2. Obtain the interference covariance matrix $\mathbf{W}_k$ for each user (see Step 2 in the first approach).

3. Calculate the interference suppression filter $\mathbf{U}_{k,l_k}$ for each user using (5.13).

4. Update the obtained suppression filter $\mathbf{U}_{k,l_k}$ ($k \in \{1,2,\dots,K\}$) in Step 3 along the geodesic over the Stiefel (or Grassmann) manifold in the direction given by ∇R_{sum} as follows

$$\mathbf{U}_{k,l_k} = \exp\left(\mu\left[\nabla R_{sum}(\mathbf{U})_{k,l_k}\mathbf{U}_{k,l_k}^H - \mathbf{U}_{k,l_k}\nabla R_{sum}(\mathbf{U})_{k,l_k}^H\right]\right)\mathbf{U}_{k,l_k}$$

where

$$\nabla R_{sum}(\mathbf{U})_{k,l_k} = \frac{2}{\ln 2}\sum_{i=1,}^{K} p_k \mathbf{H}_{i,l_k}\mathbf{X}_i^{-1}\mathbf{H}_{i,l_k}^H\mathbf{U}_{k,l_k} - \frac{2}{\ln 2}\sum_{i=1,i\neq k}^{K} p_k \mathbf{H}_{i,l_k}\mathbf{Y}_i^{-1}\mathbf{H}_{i,l_k}^H\mathbf{U}_{k,l_k}$$

where

$$\mathbf{X}_k = \mathbf{I} + \sum_{i=1}^{K}\frac{p_i}{d}\mathbf{H}_{k,l_i}^H\mathbf{U}_{i,l_i}\mathbf{U}_{i,l_i}^H\mathbf{H}_{k,l_i}$$

and

$$\mathbf{Y}_k = \mathbf{I} + \sum_{i=1,i\neq k}^{K}\frac{p_i}{d}\mathbf{H}_{k,l_i}^H\mathbf{U}_{i,l_i}\mathbf{U}_{i,l_i}^H\mathbf{H}_{k,l_i}.$$

5. Calculate the interference covariance matrix $\mathbf{W}_k$ in the reverse direction ('R' to 'L', see Fig. 1) as follows

$$\mathbf{W}_k = \sum_{i=1,i\neq k}^{K}\frac{p_i}{d}\mathbf{H}_{k,l_i}^H\mathbf{U}_{i,l_i}\mathbf{U}_{i,l_i}^H\mathbf{H}_{k,l_i}$$

6. Calculate the new $\mathbf{V}_{k,l_k}$ ($k \in \{1,2,\dots,K\}$) from the $\mathbf{W}_k$ obtained in Step 5 as follows

$$\mathbf{V}_{k,l_k}^{\star d} = \nu_d[\mathbf{W}_k], \quad d = 1,\dots,d_k.$$

7. Update the obtained precoding filters $\mathbf{V}_{k,l_k}$ in Step 6 along the geodesic over the Stiefel (or Grassmann) manifold in the direction given by ∇R_{sum} (see Step 4 in the first approach).

8. Update power allocation (see Step 5 in the first approach).

9. Update the step size ($\mu = \mu \times 0.95$). Repeat Steps 2-9 until convergence.

10. Distribute all the obtained precoding and suppression filters as well as the power allocation decisions to the corresponding user-BS pairs.

Proposed Algorithm-Third Approach

The third approach is exactly the same as the second one except for the following steps:

Step 3 in the second approach is replaced with:

The suppression filters are chosen to maximize SINR at the users instead of only minimizing the leakage interference. Thus, all the suppression filters are obtained in the following way [56].

$$\mathbf{U}_{k,l_k}^{\star s} = \frac{(\mathbf{B}_{ks})^{-1}\mathbf{H}_{k,l_k}\mathbf{V}_{k,l_k}^{\star s}}{\left\|(\mathbf{B}_{ks})^{-1}\mathbf{H}_{k,l_k}\mathbf{V}_{k,l_k}^{\star s}\right\|}$$

where

$$\mathbf{B}_{ks} = \sum_{j=1}^{K}\frac{p_j}{d_j}\sum_{d=1}^{d_j}\mathbf{H}_{k,l_j}\mathbf{V}_{j,l_j}^{\star d}\mathbf{V}_{j,l_j}^{\star d\,H}\mathbf{H}_{k,l_j}^{H} - \frac{p_k}{d_k}\mathbf{H}_{k,l_k}\mathbf{V}_{k,l_k}^{\star s}\mathbf{V}_{k,l_k}^{\star s\;H}\mathbf{H}_{k,l_k}^{H} + \mathbf{I}$$

(s stands for the stream number)

Similarly, Step 6 in the second approach is replaced with

$$\mathbf{V}_{k,l_k}^{\star s} = \frac{(\mathbf{B}_{ks})^{-1}\mathbf{H}_{k,l_k}^{H}\mathbf{U}_{k,l_k}^{\star s}}{\left\|(\mathbf{B}_{ks})^{-1}\mathbf{H}_{k,l_k}^{H}\mathbf{U}_{k,l_k}^{\star s}\right\|}$$

where

$$\mathbf{B}_{ks} = \sum_{j=1}^{K}\frac{p_j}{d_j}\sum_{d=1}^{d_j}\mathbf{H}_{k,l_j}^{H}\mathbf{U}_{j,l_j}^{\star d}\mathbf{U}_{j,l_j}^{\star d\,H}\mathbf{H}_{k,l_j} - \frac{p_k}{d_k}\mathbf{H}_{k,l_k}^{H}\mathbf{U}_{k,l_k}^{\star s}\mathbf{U}_{k,l_k}^{\star s\;H}\mathbf{H}_{k,l_k} + \mathbf{I}.$$

In [56], two famous algorithms, interference leakage minimization and Max-SINR, are proposed exploiting the reciprocity nature of channels. In the interference leakage minimization algorithm, at each iteration, the interference leakage is minimized at the users in the original network, and then minimized at the BSs in the reciprocal network. The iterations continue until it converges. This approach looks for the perfect alignment solution as an ultimate objective; however, perfect IA solutions might also be suboptimal, because of the non-convex behavior of the alignment problem. Moreover, this IA based approach will

fall short of the theoretical maximum at low SNR values, and the SINR of the received signal will decrease severely due to the inherent property of IA and channel fading, which is considered to be one of the most challenging issues of IA. This is because this IA based approach only attempts to eliminate the interferences, and does not consider the direct channel to maximize the received power of the desired signal of the users. Similar with the interference leakage minimization algorithm, the Max-SINR approach is also designed, and the difference lies in that the SINR of received signal is maximized in each direction instead of minimizing the interference leakage. By maximizing the SINR, the performance of MAX-SINR algorithm is better than that of interference leakage minimization algorithm due to the diversity gain it brings out. A Max-SINR algorithm for IA is defined to maximize the SINR of the received signal, which can consequently improve the sum-rate of interference networks especially at low SNR. However, its advantage tends to be lost in the high SNR regime. Recently, iterative optimizations using the maximum sum-rate criterion have become more favorable for the implementation of IA. Therefore, it is necessary to design iterative algorithms that directly or indirectly aim at maximizing the achievable sum-rate for users rather than seeking a perfect IA solution. Motivated by this insight, the first and second approaches of our proposed algorithms were presented as above to improve the sum-rate performance of the proposed interference leakage minimization in [56] (we combine both interference leakage minimization and sum-rate maximization in two different ways). The third proposed scheme was also presented to improve the sum-rate performance of the Max-SINR approach in [56].

5.4 Simulation Results

In this section, we evaluate the performance (in terms of the achievable sum-rate and average per user multiplexing gain) of our proposed schemes vis-a-vis the interference leakage minimization and max-SINR approaches discussed in [56] and the proposed method in [57]. Equal power allocation has been considered for all user-BS pairs in the mentioned studies. We consider a K-user MIMO IC as an $(N \times M, d)^K$ system ($d \leq \min(M, N)$ and $N + M - d(K + 1) \geq 0$, see [138]). In our evaluation we run simulations for a $(6 \times 6, d = 1,2,3)^3$, a $(8 \times 8, d = 1,3)^3$,

and a $(8 \times 8, d = 1)^7$ system. Unless stated otherwise, in the simulations, all results are averaged over 100 channel realizations where each channel matrix comprises i.i.d. elements drawn from a complex Gaussian distribution with zero mean and unit variance. We also set the noise power level to 1.

The parameter μ, which represents the step size, is initialized with a relatively large value at first (the starting point is $\mu = 0.1$ for all the proposed schemes). In each iteration we reduce the amount of the step size. In practice, an optimal value of the step size is difficult to compute and determine. This parameter trades off between high convergence speed, which requires a large step size, and good sum-rate performance, which requires a small step size [113]. In other words, an optimal parameter μ can help us achieve a desired sum-rate in a much smaller number of iterations. Thus, an adaptive step size is a desirable choice and the RL-based method developed in our previous work [139] can be considered for this matter.

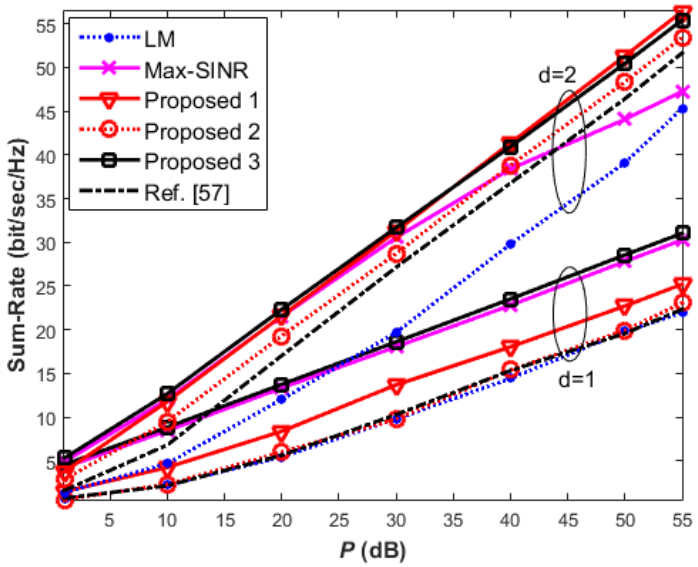

Fig. 5.2. Sum-rate versus P for a $(6 \times 6, d = 1,2)^3$ system

We compare the proposed algorithms presented in Section 5.3 with the other widely used algorithms for an equal number of iterations (500) unless stated otherwise, as shown in the following simulation examples. Note that we first consider perfect CSI in our evaluations, and the performance evaluation of the channel estimation techniques is presented in Figs. 5.8 and 5.9.

A. *Example I*

In Fig. 5.2, the sum-rate is plotted versus P (where P is the total power budget over the average noise power) considering a $(6 \times 6, d = 1, 2)^3$ system. It is observed that for $d = 1$, when using the third proposed approach and max-SINR solution, the rates approximately match for all SNRs. However, the first and third proposed schemes always offer a better sum-rate performance than the leakage minimization approach. Our approach to the problem in the second proposed solution differs from [57] in terms of the update expressions (the geodesics) for the precoding and suppression filters and in terms of the power allocation strategy, as mentioned before. As can be seen, the performance of the second proposed approach closely matches that of the proposed method in [57] and the leakage minimization approach for all SNR values; however, they all obtain less sum-rate than the first proposed method and particularly the third proposed and max-SINR methods. This is because the third proposed method and max-SINR make extra attempts to maximize the desired signal power within the desired signal subspace [57].

For $d = 2$ and SNRs up to 30 dB, the max-SINR sum-rate performance approximately matches the first and third proposed methods while it shows a higher sum-rate than the second proposed method and the method in [57]. However, as can be seen, there is a growing gap in the achievable sum-rate between our proposed algorithms (along with the proposed method in [57]) and the max-SINR approach for the SNRs greater than 30 dB. This is because the max-SINR cannot provide extra DoFs for only 500 iterations. On the other hand, the proposed algorithms along with the max-SINR and the proposed method in [57] always outperform the leakage minimization approach. In comparison with the leakage minimization approach, the improved sum-rate performance of the second proposed scheme is also observable from $d = 1$ to $d = 2$. A similar behavior (as the second proposed scheme) is also observed for the proposed method in [57]. All our proposed methods always offer (for $d = 2$) a better sum-rate performance than the method in [57].

B. *Example II*

In Fig. 5.3, we consider a $(8 \times 8, d = 1, 3)^3$ system. Similar arguments and statements that we produced for *Example I* apply here as well.

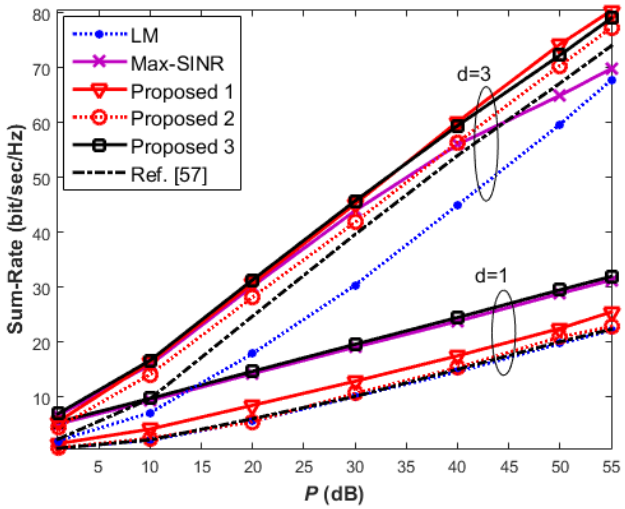

Fig. 5.3. Sum-rate versus P for a $(8 \times 8, d = 1,3)^3$ system

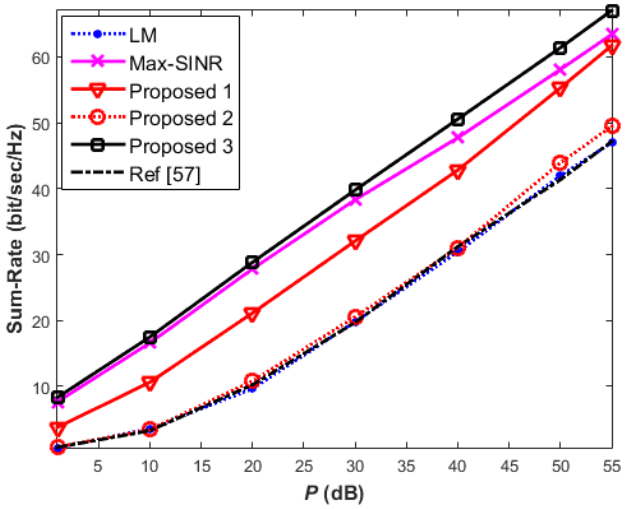

Fig. 5.4. Sum-rate versus P for a $(8 \times 8, d = 1)^7$ system

C. Example III

In a similar manner to that for the second example, we consider a $(8 \times 8, d = 1)^7$ system as shown in Fig. 5.4. From this figure, it can be seen that we observed almost the same trend as that for the $(8 \times 8, d = 1)^3$ system for the SNRs up to 30 dB (the first proposed approach showed a relatively more sum-rate performance improvement than the other approaches). However, for SNRs greater than 30 dB we observed sum-rate behavior different from that for the 3-

user case (for $d = 1$), and the benefits of our first and third proposed algorithms become more apparent.

In Figs. 5.5, 5.6, and 5.7, considering a $(6 \times 6, d = 1,2,3)^3$ system, we analyze the explained schemes in terms of multiplexing gain (or DoFs) defined as the number of interference free signaling dimensions at user k (i.e., $d_k = \text{rank}\left(\mathbf{U}_{k,l_k}^H \mathbf{H}_{k,l_k} \mathbf{V}_{k,l_k}\right) - \text{rank}(\mathbf{U}_{k,l_k}^H \sum_{i=1,i\neq k}^{K} \mathbf{H}_{k,l_i} \mathbf{V}_{i,l_i})$). For $d = 1$ (see Fig. 5.5), it is observed that all schemes except the third proposed scheme and max-SINR achieve exactly $d = 1$ average per user multiplexing gain for all SNRs. The third proposed and max-SINR methods represent almost the same behavior and more adaptive performance, which yields one interference free dimension at the high SNR values, where the multiplexing gain will become an important factor of the SINR metric.

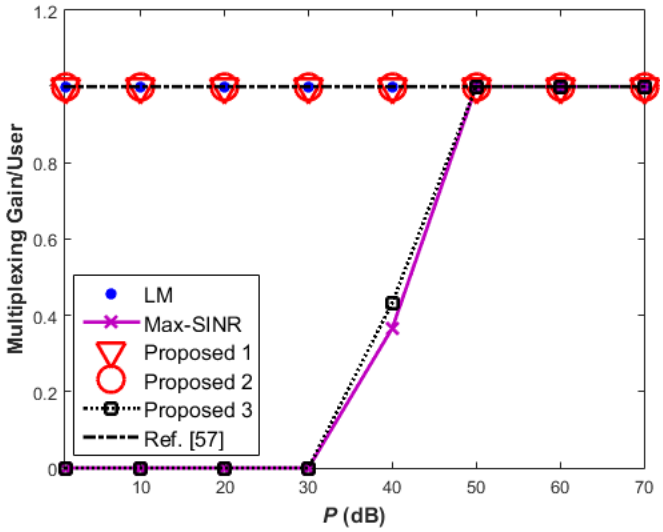

Fig. 5.5. Multiplexing gain per user versus P for a $(6 \times 6, d = 1)^3$ system, 3000 iterations, and over 10 channel realizations

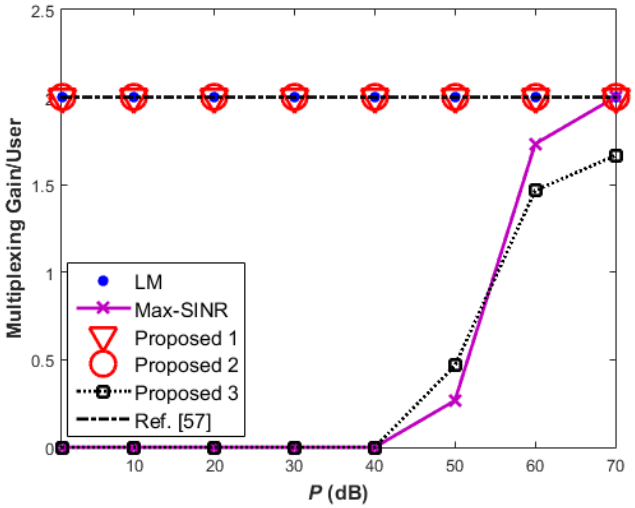

Fig. 5.6. Multiplexing gain per user versus P for a $(6 \times 6, d = 2)^3$ system, 3000 iterations, and over 10 channel realizations

A similar situation applies to the $d = 2$ case (see Fig. 5.6). Thus, we can say that when d is smaller than its maximum value ($[N + M]/[K + 1]$) in a proper system, all the schemes seem to get the maximum multiplexing gain (at least in the high SNR regime).

For $d = 3$ (Fig. 5.7), it is observed that the leakage minimization, our second proposed scheme, and the method in [57] achieve much more interference free dimensions than the other approaches, which results in higher achievable per user multiplexing gain. For this case, our first and third proposed methods along with the max-SINR perform worse and do not seem to achieve perfect IA even in the high SNR regime. There exists an oscillating behavior in the curves shown in Fig. 5.7, either because the number of iterations that we have used for $d = 3$ is insufficient or the initial value chosen for μ might not be proper. Thus, the existing schemes may not converge to an optimal solution for $d = 3$.

In Fig. 5.8, we compare the performance of the LS and MMSE estimation techniques. The estimation mean square error (MSE), which is proportional to $\|\mathbf{H} - \mathbf{H}_{est}\|_F^2$ (squared Frobenius norm error), is performed to evaluate the performance of both estimators ($\mathbf{H}_{est}$ is the estimated channel). We depict the estimation error (in dB) versus the uplink training SNR (p_e). It can be seen that as the uplink-training SNR increases, the remaining additive noise vanishes. Therefore, the estimation error of both methods decreases, which implies that the channel estimations tend to be perfect. As shown in this figure, the MMSE

estimator presents a better performance for all values of the training SNR. Note that the OFDM based estimation model is operating with 64 subcarriers (DFT/IDFT size). 16-QAM constellation is used here. The number of pilot subcarriers per symbol is $B = 3$, and a $\mathsf{CP} = 8$ is considered for a 6 tap channel.

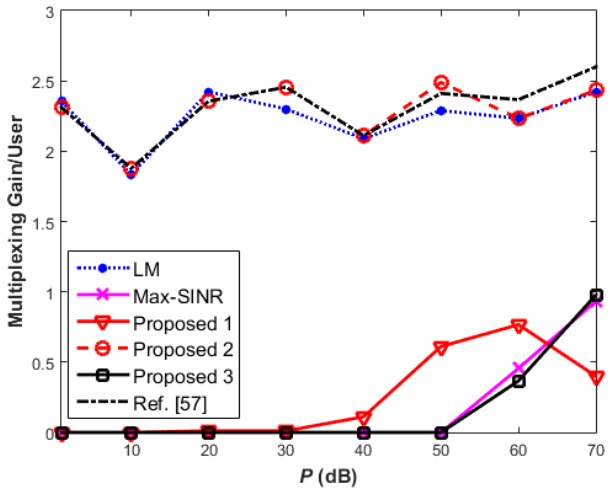

Fig. 5.7. Multiplexing gain per user versus P for a $(6 \times 6, d = 3)^3$ system, 3000 iterations, and 10 channel realizations

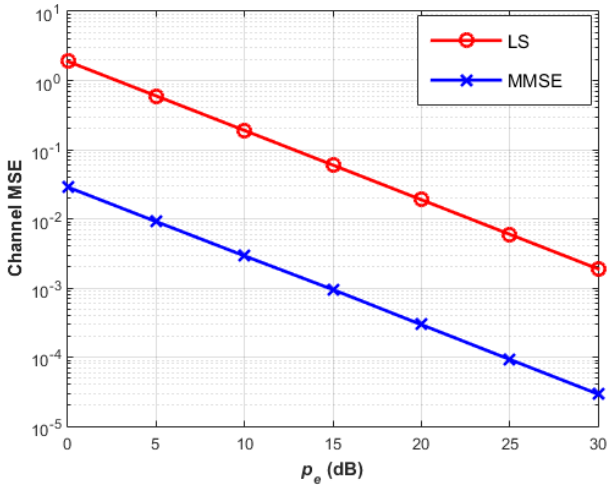

Fig. 5.8. Comparison of MSE versus p_e between LS and MMSE channel estimators, for the system parameters $M = N = 6$, $K = 3$, $B = 3$, $\frac{d_{l_k}(\mathbf{r}_i)}{d_{l_k}(\mathbf{r}_k)} = 1, \forall k \in \{1, \dots, K\}, i \neq k$

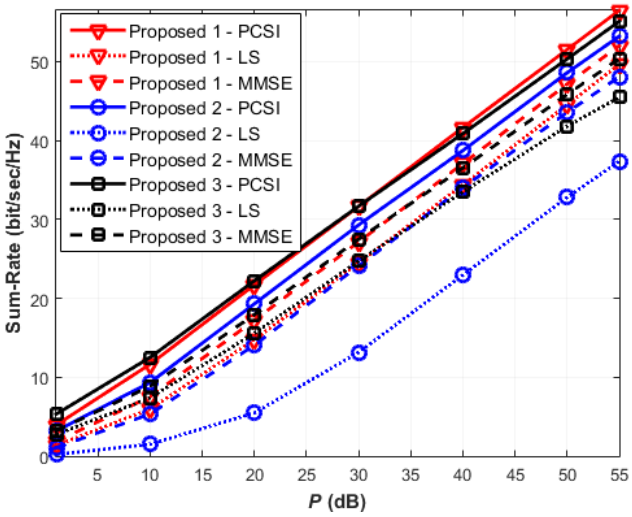

Fig. 5.9. Sum-rate versus P for a $(6 \times 6, d = 2)^3$ system and $p_e = 10$ dB.

Finally, in Fig. 5.9, we show the effect of channel estimation error on the sum-rate for our proposed methods over a $(6 \times 6, d = 2)^3$ system. If we consider the results shown in Fig. 5.8 and for the uplink-training SNR value of 20 dB, we find that the proposed methods with the MMSE channel estimator gain a higher sum-rate than that gained with an LS estimator. Obviously, the maximum sum-rate value is achieved when perfect CSI is available. It seems that compared with the first and third proposed approaches the second proposed approach is quite sensitive to the channel estimation error when the LS estimator is applied.

5.5 Conclusion

In this chapter, we proposed three iterative IA algorithms for the problem of joint power allocation and transmit/receive filter design in a K-user MIMO IC. They are based on three optimization approaches: interference leakage minimization, max-SINR, and sum-rate maximization. A new Riemannian optimization method based on the Stiefel and Grassmann manifolds was introduced to solve the sum-rate maximization problem. We also studied and applied a low complexity iterative power allocation algorithm for sum-rate maximization over IA ICs under a sum power constraint. An analysis of OFDM based channel estimation was also carried out, which is required for designing practical IA systems. In terms of the achievable sum-rate, we compared the

performance of our proposed methods with the conventional alternating leakage minimization, max-SINR (presented in [56]) and the proposed method in [57]. Simulation results showed that the proposed algorithms achieve promising sum-rate gains over the existing IA algorithms particularly at high SNRs and high-dimensional signal spaces.

Chapter 6

Conclusions and Future works

The objective of this research has been to improve performance on both user and network scales by proposing mechanisms and solutions to interference modeling, management and avoidance issues arising in different wireless communication environments. Results of this work can be used for several real world scenarios such as: wireless technologies operating in the industrial science medical (ISM) bands and maybe in the future in the TV bands by employing the machine-learning based cognitive short-range devices, the performance analysis of large wireless networks of future using stochastic geometry, and IA based Device-to-device (D2D) communication as one of the key technologies for the future 5G mobile communication systems.

In Chapter 2, we study the interference management issue in CR networks and propose a learning based scheme for channel sensing in partially-sensed CR network. In particular, the CR network's channel sensing scheme is formulated as a POMDP, and the optimal policy is determined by the FQL algorithm. Simulations show that the proposed sensing scheme allows the CR network to significantly improve its own spectral efficiency and reduce the probability of interfering with the PU. We have also shown, even in a very transient environment, it is quite possible to achieve reasonable estimates of channel state transition probabilities. In Chapters 3 and 4, we present a tractable model to derive the outage probability of a typical femto and macro user in a two-tier HetNet, which provides insight into system design guidelines. For the case of the node locations modeled by a PPP and when the desired and interfering channels are subject to Rayleigh (in Chapter 3) and Nakagami-m fading (in

Chapter 4), we demonstrate the use of the CR based framework to evaluate the outage probability at any arbitrary user. As a result, exact closed-form expressions are obtained. In addition, we discuss that in the downlink analysis, the outage probability is a function of the network topology and several system design parameters such as SINR target, exclusion regions, MAC mechanisms such as ALOHA, and the RB selection constraint controlled by the spectrum sensing measurements. In these two chapters, we derive a tight closed-form expression of outage probability for users in the network in order to evaluate the outage performance of users and as a contribution to define a benchmark to assess our analysis and future studies. Outage probability is considered an important performance metric to assess users QoS and due to its huge impact on the network performance and power consumption. Our derivations can have several applications in 4G and beyond broadband networks. For example, outage probability can be considered as a QoS metric to meet a specific connection data rate requirement, or it can be utilized as a performance measure to evaluate the level of meeting the total demands of users in a cellular network. Thus, the availability of accurate analytic expression is of paramount importance for system analysis and optimization purposes. Another typical example is found in the radio power control problems, where the powers must be minimized under outage probability constraints. For the future work, we can think of the possible ways and directions to expose our analytical results for the implementation purposes. For example, our analytical expressions can provide useful insights to the network design and can be adapted to optimize the deployment of BSs, density of BSs, frequency sharing/partitioning for multi-tier cellular networks, frequency reuse, transmission rate, etc.

Finally, in Chapter 5, the IA technique, which has been recently used as an alternative interference management method, is applied to the MIMO IC networks. In particular, we propose iterative IA algorithms for the problem of joint power allocation and transmit/receive filter design in a K-user MIMO IC. They are based on different optimization approaches including: interference leakage minimization, max-SINR, and sum-rate maximization. A novel Riemannian optimization method based on the Stiefel and Grassmann manifolds is introduced to solve the sum-rate maximization problem. We also study a low complexity iterative power allocation algorithm for sum-rate maximization over

IA ICs under a sum power constraint. At the end, an analysis of OFDM based channel estimation is also carried out, which is required for designing practical IA systems. Simulation results show that the proposed algorithms achieve promising sum-rate gains over the existing IA algorithms particularly at high SNRs and high-dimensional signal spaces.

During this work, great effort was made to provide useful techniques and solutions which would lead to higher data rates and more reliable communications considering the limiting nature of radio communication resources and the most challenging phenomena: interference. Now, we will briefly describe some general but interesting directions for future work aimed at improving and completing our proposed constructions.

Recently, energy-efficient communication has sparked tremendous interest as one of the most important design goals of future wireless networks. Thus, a paradigm shift of current operation from data oriented to energy-efficient oriented networks is obviously expected. In this context, a green CR (GCR), which is aware of sustainable development and takes it as an additional constraint in the decision making engine of the cognitive cycle, can be considered as an interesting extension for Chapter 2. In other words, the GCR can decide actions which decrease the total power (energy) consumption in the network while satisfying QoS constraints. Regarding the Chapters 3 and 4, a green HetNet can be also an alternative for the proposed model. In the near future, the cellular network is expected to become increasingly heterogeneous to improve the spectral efficiency. As a result, the deployment of massive small cells in the macrocells can increase the total power consumption of the 5G HetNets. Thus, it is important to jointly manage the power consumption of both macrocells and small cells for more energy-efficient operation with traffic sharing. Finally, in Chapter 5, power allocation techniques can be also leveraged to optimize the energy efficiency of the IA-based network. However, our proposed power allocation algorithm as well as those seen in the existing IA works focus only on optimizing the sum-rate, i.e., spectrum efficiency, instead of energy efficiency, and the energy efficiency issue is totally ignored. Thus, an adaptive energy-efficient IA algorithm for green IA-based wireless networks can be considered as an interesting direction, too.

Appendices

Appendix A

Appendix A.1

Derivation Of $M(\theta,\alpha)$

Proof: From the expression of $M(\theta,\alpha)$ in (3.13), we have

$$M(\theta,\alpha)=\int_0^{\infty}\left[(g)^{\frac{d}{\alpha}}\left(\Gamma\left(-\frac{d}{\alpha},\mu\theta g\right)-\Gamma\left(-\frac{d}{\alpha}\right)\right)\right]\mu e^{-\mu g}\,\mathrm{d}g$$

We know that $\Gamma(a,x)+\gamma(a,x)=\Gamma(a)$, and $\gamma(a,x)=x^{a}\Gamma(a)e^{-x}\sum_{k=0}^{\infty}\frac{x^{k}}{\Gamma(a+k+1)}$, therefore, the above equation is simplified as follows

$$=-\Gamma\left(-\frac{d}{\alpha}\right)\mu(\mu\theta)^{-\frac{d}{\alpha}}\int_0^{\infty}e^{-g(\mu+\mu\theta)}\left[\sum_{k=0}^{\infty}\frac{(\mu\theta)^{k}g^{k}}{\Gamma\left(-\frac{d}{\alpha}+k+1\right)}\right]\mathrm{d}g$$

$$=-\Gamma\left(-\frac{d}{\alpha}\right)\mu(\mu\theta)^{-\frac{d}{\alpha}}\int_0^{\infty}e^{-g(\mu+\mu\theta)}\left[\frac{(\mu\theta)^{0}g^{0}}{\Gamma\left(1-\frac{d}{\alpha}\right)}+\frac{(\mu\theta)^{1}g^{1}}{\Gamma\left(2-\frac{d}{\alpha}\right)}+\frac{(\mu\theta)^{2}g^{2}}{\Gamma\left(3-\frac{d}{\alpha}\right)}+\cdots\right]\mathrm{d}g$$

$$=-\Gamma\left(-\frac{d}{\alpha}\right)\mu(\mu\theta)^{-\frac{d}{\alpha}}\left[\int_0^{\infty}\frac{(\mu\theta)^{0}(g)^{(1)-1}e^{-g(\mu+\mu\theta)}}{\Gamma\left(1-\frac{d}{\alpha}\right)}\mathrm{d}g+\int_0^{\infty}\frac{(\mu\theta)^{1}(g)^{(2)-1}e^{-g(\mu+\mu\theta)}}{\Gamma\left(2-\frac{d}{\alpha}\right)}\mathrm{d}g+\cdots\right]$$

$$=-\Gamma\left(-\frac{d}{\alpha}\right)\mu(\mu\theta)^{-\frac{d}{\alpha}}\left[\frac{(\mu\theta)^{0}}{\Gamma\left(1-\frac{d}{\alpha}\right)(\mu+\mu\theta)}\Gamma(1)+\frac{(\mu\theta)^{1}}{\Gamma\left(2-\frac{d}{\alpha}\right)(\mu+\mu\theta)^{2}}\Gamma(2)+\cdots\right]$$

Hence, we have

$$M(\theta,\alpha)=\left(-\Gamma\left(-\frac{d}{\alpha}\right)\mu(\mu\theta)^{-\frac{d}{\alpha}}\right)\left[\sum_{k=0}^{\infty}\frac{(\mu\theta)^{k}}{\Gamma\left(k+1-\frac{d}{\alpha}\right)(\mu+\mu\theta)^{k+1}}\Gamma(1+k)\right]$$

Appendix B

Appendix B.1
Proof Of Equation 4.5

Proof: From (4.4), we have

$$P[\text{SINR} > \theta] = \int_0^\infty \left[e^{-\left(\frac{m_{d,F}\theta {r_F}^\alpha}{\Omega_{d,F}\ P_F}\right)I} \left[1 + \left(\frac{m_{d,F}}{\Omega_{d,F}}\frac{\theta {r_F}^\alpha}{P_F}\right) I + \frac{1}{2}\left(\frac{m_{d,F}}{\Omega_{d,F}}\frac{\theta {r_F}^\alpha}{P_F}\right)^2 I^2 + \cdots \right] \right] f_I(i)\, di$$

We then have

$$\left[\left[\left(\frac{m_{d,F}}{\Omega_{d,F}}\frac{\theta {r_F}^\alpha}{P_F}\right)^0 \int_0^\infty [e^{-sI}(I^0 f_I(i))]\, di \right] + \left[\left(\frac{m_{d,F}}{\Omega_{d,F}}\frac{\theta {r_F}^\alpha}{P_F}\right)^1 \int_0^\infty [e^{-sI}(I^1 f_I(i))]\, di \right] + \left[\frac{1}{2}\left(\frac{m_{d,F}}{\Omega_{d,F}}\frac{\theta {r_F}^\alpha}{P_F}\right)^2 \int_0^\infty [e^{-sI}(I^2 f_I(i))]\, di \right] + \cdots \right]$$

where s in each integral is equal to $\frac{m_{d,F}}{\Omega_{d,F}}\frac{\theta {r_F}^\alpha}{P_F}$.

In each part, we have to calculate the Laplace transform of $(I^n f_I(i))$. We also know that $x^n f(x) \overset{\mathcal{L}}{\Leftrightarrow} (-1)^n \frac{d^n \mathcal{L}_f(s)}{ds^n}$. Therefore, we have

$$\left[\left[\left(\frac{m_{d,F}}{\Omega_{d,F}}\frac{\theta {r_F}^{\alpha}}{P_F}\right)^{0}(-1)^{0}\frac{d^{0}\mathcal{L}_I(s)}{ds^{0}}\right]+\left[\left(\frac{m_{d,F}}{\Omega_{d,F}}\frac{\theta {r_F}^{\alpha}}{P_F}\right)^{1}(-1)^{1}\frac{d^{1}\mathcal{L}_I(s)}{ds^{1}}\right]\right.$$
$$\left.+\left[\frac{1}{2}\left(\frac{m_{d,F}}{\Omega_{d,F}}\frac{\theta {r_F}^{\alpha}}{P_F}\right)^{2}(-1)^{2}\frac{d^{2}\mathcal{L}_I(s)}{ds^{2}}\right]+\cdots\right]$$

Hence, we have

$$P[\text{SINR}>\theta]=\left[\sum_{k=0}^{m_{d,F}-1}\frac{(s)^{k}}{k!}(-1)^{k}\frac{d^{k}\mathcal{L}_I(s)}{ds^{k}}\right]$$

Appendix B.2
Proof Of Equation 4.10

Proof: From (4.9), we have

$$M(\theta,\alpha)=\int_0^{\infty}\left[(g)^{\frac{d}{\alpha}}\left(\Gamma\left(-\frac{d}{\alpha},\frac{m_{d,F}}{\Omega_{d,F}}\theta g\right)\right.\right.$$
$$\left.\left.-\Gamma\left(-\frac{d}{\alpha}\right)\right)\right]\frac{{m_{I,F}}^{m_{I,F}}}{{\Omega_{I,F}}^{m_{I,F}}\Gamma\left(m_{I,F}\right)}g^{m_{I,F}-1}e^{-\frac{m_{I,F}g}{\Omega_{I,F}}}\,\mathrm{d}g$$

We know that $\Gamma(a,x)+\gamma(a,x)=\Gamma(a)$, and $\gamma(a,x)=x^{a}\Gamma(a)e^{-x}\sum_{k=0}^{\infty}\frac{x^{k}}{\Gamma(a+k+1)}$, therefore, the above equation is simplified as follows

$$=\frac{-\Gamma\left(-\frac{d}{\alpha}\right){m_{I,F}}^{m_{I,F}}\left(\frac{m_{d,F}}{\Omega_{d,F}}\theta\right)^{-\frac{d}{\alpha}}}{{\Omega_{I,F}}^{m_{I,F}}\Gamma\left(m_{I,F}\right)}\int_0^{\infty}(g)^{m_{I,F}-1}e^{-g\left(\frac{m_{I,F}}{\Omega_{I,F}}+\frac{m_{d,F}\theta}{\Omega_{d,F}}\right)}\left[\sum_{k=0}^{\infty}\frac{\left(\frac{m_{d,F}}{\Omega_{d,F}}\theta\right)^{k}g^{k}}{\Gamma\left(-\frac{d}{\alpha}+k+1\right)}\right]\mathrm{d}g$$

$$= \frac{-\Gamma\left(-\frac{d}{\alpha}\right) {m_{I,F}}^{m_{I,F}} \left(\frac{m_{d,F}}{\Omega_{d,F}}\theta\right)^{-\frac{d}{\alpha}}}{{\Omega_{I,F}}^{m_{I,F}}\Gamma\left(m_{I,F}\right)} \int_0^{\infty} (g)^{m_{I,F}-1} e^{-g\left(\frac{m_{I,F}}{\Omega_{I,F}}+\frac{m_{d,F}\theta}{\Omega_{d,F}}\right)} \left[\frac{\left(\frac{m_{d,F}}{\Omega_{d,F}}\theta\right)^0 g^0}{\Gamma\left(1-\frac{d}{\alpha}\right)} + \frac{\left(\frac{m_{d,F}}{\Omega_{d,F}}\theta\right)^1 g^1}{\Gamma\left(2-\frac{d}{\alpha}\right)} + \frac{\left(\frac{m_{d,F}}{\Omega_{d,F}}\theta\right)^2 g^2}{\Gamma\left(3-\frac{d}{\alpha}\right)} + \cdots \right] \mathrm{d}g$$

$$= \frac{-\Gamma\left(-\frac{d}{\alpha}\right) {m_{I,F}}^{m_{I,F}} \left(\frac{m_{d,F}}{\Omega_{d,F}}\theta\right)^{-\frac{d}{\alpha}}}{{\Omega_{I,F}}^{m_{I,F}}\Gamma\left(m_{I,F}\right)} \left[\int_0^{\infty} \frac{(g)^{m_{I,F}-1} e^{-g\left(\frac{m_{I,F}}{\Omega_{I,F}}+\frac{m_{d,F}\theta}{\Omega_{d,F}}\right)}}{\Gamma\left(1-\frac{d}{\alpha}\right)} \mathrm{d}g + \int_0^{\infty} \frac{\left(\frac{m_{d,F}}{\Omega_{d,F}}\theta\right)^1 (g)^{(m_{I,F}+1)-1} e^{-g\left(\frac{m_{I,F}}{\Omega_{I,F}}+\frac{m_{d,F}\theta}{\Omega_{d,F}}\right)}}{\Gamma\left(2-\frac{d}{\alpha}\right)} \mathrm{d}g + \cdots \right]$$

$$= \frac{-\Gamma\left(-\frac{d}{\alpha}\right) {m_{I,F}}^{m_{I,F}} \left(\frac{m_{d,F}}{\Omega_{d,F}}\theta\right)^{-\frac{d}{\alpha}}}{{\Omega_{I,F}}^{m_{I,F}}\Gamma\left(m_{I,F}\right)} \left[\frac{\left(\frac{m_{d,F}}{\Omega_{d,F}}\theta\right)^0 \left(\frac{\Omega_{I,F}\Omega_{d,F}}{m_{I,F}\Omega_{d,F}+\Omega_{I,F}m_{d,F}\theta}\right)^{m_{I,F}}}{\Gamma\left(1-\frac{d}{\alpha}\right)} \Gamma\left(m_{I,F}\right) + \frac{\left(\frac{m_{d,F}}{\Omega_{d,F}}\theta\right)^1 \left(\frac{\Omega_{I,F}\Omega_{d,F}}{m_{I,F}\Omega_{d,F}+\Omega_{I,F}m_{d,F}\theta}\right)^{m_{I,F}+1}}{\Gamma\left(2-\frac{d}{\alpha}\right)} \Gamma\left(m_{I,F}+1\right) + \cdots \right]$$

Hence, we have

$$M(\theta,\alpha)$$

$$= \left(\frac{-\Gamma\left(-\frac{d}{\alpha}\right) {m_{I,F}}^{m_{I,F}} \left(\frac{m_{d,F}}{\Omega_{d,F}}\theta\right)^{-\frac{d}{\alpha}}}{{\Omega_{I,F}}^{m_{I,F}}\Gamma\left(m_{I,F}\right)} \right) \left[\sum_{k=0}^{\infty} \frac{\left(\frac{m_{d,F}}{\Omega_{d,F}}\theta\right)^k \left(\frac{\Omega_{I,F}\Omega_{d,F}}{m_{I,F}\Omega_{d,F}+\Omega_{I,F}m_{d,F}\theta}\right)^{m_{I,F}+k}}{\Gamma\left(k+1-\frac{d}{\alpha}\right)} \Gamma\left(m_{I,F}+k\right) \right]$$

Appendix B.3

Outage Probability Expression For Non-Integer $m_{d,F}$

Proof: From Section 4.3

For non-integer $m_{d,F}$, by using the infinite series representation of incomplete gamma function presented in Appendix B.2 ($\frac{\Gamma(a,x)}{\Gamma(a)} = 1 - \frac{\gamma(a,x)}{\Gamma(a)}$, and $\gamma(a,x) = x^a\Gamma(a)e^{-x}\sum_{k=0}^{\infty}\frac{x^k}{\Gamma(a+k+1)}$), and following the exact procedure as that in Section 4.3 (from (4.1) to (4.14))) to obtain the closed-form outage probability expression for the tagged femto user, we obtain an exact but infinite summation expression for the outage probability. In other words, we use the infinite series representation of incomplete gamma not only for the interfering links calculations but also for the desired link to obtain an expression in which the Nakagami-m parameters of all the communication links ($m_{d,F}$, $m_{I,F}$ and $m_{I,M}$) can take any values (integer or non-integer) bigger than 0.5. Thus, considering the above explanations we have

$$p_{OF} = \sum_{k=0}^{\infty} \frac{(z)^{k+m_{d,F}}}{\Gamma\left(k+m_{d,F}+1\right)}(-1)^{k+m_{d,F}} \frac{d^{k+m_{d,F}}\left(\exp\left(l(z)\right)\right)}{dz^{k+m_{d,F}}}$$

where

$$\exp\left(l(z)\right) = e^{[\mathrm{A}]z^{\frac{d}{\alpha}} - \frac{m_{d,F}\theta_6{}^2}{\Omega_{d,F}P_F}z}, \text{ and } z = r_F{}^{\alpha}$$

Operating in an interference-limited regime and using the Taylor Series Expansions of Exponential Functions, the above expression is simplified as follows

$$p_{OF} = \sum_{k=0}^{\infty} \frac{(z)^{k+m_{d,F}}}{\Gamma\left(k+m_{d,F}+1\right)}(-1)^{k+m_{d,F}} \frac{d^{k+m_{d,F}}\left(\sum_{n=0}^{\infty}\frac{\mathrm{A}^n z^{n\left(\frac{d}{\alpha}\right)}}{n!}\right)}{dz^{k+m_{d,F}}}$$

$$p_{OF} = \sum_{k=0}^{\infty} \frac{(z)^{k+m_{d,F}}}{\Gamma\left(k+m_{d,F}+1\right)}(-1)^{k+m_{d,F}} \frac{d^{k+m_{d,F}}\left(\frac{\mathrm{A}^0 z^0}{0!} + \frac{\mathrm{A}^1 z^{\left(\frac{d}{\alpha}\right)}}{1!} + \frac{\mathrm{A}^2 z^{2\left(\frac{d}{\alpha}\right)}}{2!} + \cdots\right)}{dz^{k+m_{d,F}}}$$

The fractional derivative, the arbitrary order derivative, is used here to simplify the above expression [140] (the notation $D^{\mu}\big(f(z)\big) = \frac{d^{\mu}(f(z))}{dz^{\mu}}$ denotes the μth order fractional derivative of the function $f(z)$ where $\mu > 0$). According to [140], $D^{\mu}(z^{\gamma})$ (where $\gamma > -1$) is equal to $\frac{\Gamma(\gamma+1)}{\Gamma(\gamma-\mu+1)} z^{\gamma-\mu}$, and we also have $D^{\mu}\big(cf(z)\big) = cD^{\mu}\big(f(z)\big)$ (c is a constant value). Thus, we can write

$$p_{OF} = \sum_{k=0}^{\infty} \frac{(z)^{k+m_{d,F}}}{\Gamma\big(k+m_{d,F}+1\big)} (-1)^{k+m_{d,F}} \Big[\frac{\mathrm{A}^{0}\Gamma\left(0\left(\frac{d}{\alpha}\right)+1\right) z^{0\left(\frac{d}{\alpha}\right)-(k+m_{d,F})}}{0!\,\Gamma\left(0\left(\frac{d}{\alpha}\right)-\big(k+m_{d,F}\big)+1\right)} + \frac{\mathrm{A}^{1}\Gamma\left(1\left(\frac{d}{\alpha}\right)+1\right) z^{1\left(\frac{d}{\alpha}\right)-(k+m_{d,F})}}{1!\,\Gamma\left(1\left(\frac{d}{\alpha}\right)-\big(k+m_{d,F}\big)+1\right)} + \frac{\mathrm{A}^{2}\Gamma\left(2\left(\frac{d}{\alpha}\right)+1\right) z^{2\left(\frac{d}{\alpha}\right)-(k+m_{d,F})}}{2!\,\Gamma\left(2\left(\frac{d}{\alpha}\right)-\big(k+m_{d,F}\big)+1\right)} + \cdots \Big]$$

and finally,

$$p_{OF} = \sum_{k=0}^{\infty} \frac{(z)^{k+m_{d,F}}}{\Gamma\big(k+m_{d,F}+1\big)} (-1)^{k+m_{d,F}} \sum_{n=0}^{\infty} \frac{\mathrm{A}^{n}}{n!} \frac{\Gamma\left(n\left(\frac{d}{\alpha}\right)+1\right)}{\Gamma\left(n\left(\frac{d}{\alpha}\right)-\big(k+m_{d,F}\big)+1\right)} z^{n\left(\frac{d}{\alpha}\right)-(k+m_{d,F})}$$

where A is given by (4.15).

Similar expression can be obtained for the outage probability of the tagged macro user.

Appendix C

List of Author's Publications and Awards

C.1 Journals

[1] Fereidoun H. Panahi and T. Ohtsuki, "Optimal Channel-Sensing Scheme for Cognitive Radio Systems Based on Fuzzy Q-Learning," *IEICE Transactions on Communications*, Vol. E97-B, no. 2, pp.283-294, Feb. 2014.

[2] Fereidoun H. Panahi and T. Ohtsuki, "Analytical Modeling of Cognitive Heterogeneous Cellular Networks over Nakagami-m Fading," *EURASIP Journal on Wireless Communications and Networking*, Volume 2015, Issue 1, 2015:61, DOI: 10.1186/s13638-015-0277-6.

[3] Fereidoun H. Panahi and T. Ohtsuki, "Stochastic Geometry Modeling and Analysis of Cognitive Heterogeneous Cellular Networks," *EURASIP Journal on Wireless Communications and Networking*, Volume 2015, Issue 1, 2015:141. DOI: 10.1186/s13638-015-0363-9.

[4] Fereidoun H. Panahi, T. Ohtsuki, W. Jiang, T. Takatori, and K. Uehara, "Joint Interference Alignment and Power Allocation for Multi-User MIMO Interference Channels under Perfect and Imperfect CSI," (*to be submitted*), 2016.

C.2 Full Articles on International Conferences Proceedings

[1] Fereidoun H. Panahi, T. Ohtsuki, W. Jiang, T. Takatori, and K. Uehara, "Interference Alignment and Power Allocation for Multi-User MIMO Interference Channels," in *IEEE International Conference on Communications (ICC)*, Kuala Lumpur, Malaysia, May 2016.

[2] Fereidoun H. Panahi, T. Ohtsuki, Wenjie Jiang and Tasushi Takatori, "Interference Alignment for Multi-User MIMO Interference Channels via a Riemannian Optimization Approach," in *IEEE 25th International Symposium on Personal, Indoor and Mobile Radio Communications (PIMRC)*, pp. 287-292, Hong Kong, China, August 2015.

[3] Fereidoun H. Panahi and T. Ohtsuki, "Analytical Evaluation of Coverage Probability in Two-tier Cognitive Femto Networks," in *IEEE Vehicular Technology Conference (VTC)*, pp. 1-6, Glasgow, Scotland, May 2015.

[4] Fereidoun H. Panahi and T. Ohtsuki, 'Analytical Modeling of Cognitive Heterogeneous Cellular Networks over Nakagami-m Fading," in *IEEE Global Communications Conference (GLOBECOM)*, pp. 3628-3634, Austin, TX, USA, Dec. 2014.

[5] Fereidoun H. Panahi and T. Ohtsuki, "Stochastic Geometry Based Analytical Modeling of Cognitive Heterogeneous Cellular Networks," in *IEEE International Conference on Communications (ICC)*, pp. 5281-5286, Sydney, Australia, June 2014.

[6] Fereidoun H. Panahi and T. Ohtsuki, "Optimal Channel-Sensing Policy Based on Fuzzy Q-Learning Process over Cognitive Radio Systems," in *IEEE International Conference on Communications (ICC)*, pp. 2677-2682, Budapest, Hungary, June 2013.

[7] Fereidoun H. Panahi, T. Ohtsuki, W. Jiang, T. Takatori, and K. Uehara, "Joint Interference Alignment and Power Allocation under Perfect and Imperfect CSI," in *IEEE Global Communications Conference (GLOBECOM)*, (*accepted*), Washington DC, USA, Dec. 2016.

[8] H. Moridveisi, Fereidoun H. Panahi, F. H. Panahi, Parvin Farhadi, Morteza Mehrnush, "Multi-rate STBC Transmission Based on a New Fuzzy Method over Dynamic Fading Channels," in *Second International Conference on Computer and Electrical Engineering (ICCEE)*, pp. 573 - 577, Dubai, UAE, Dec. 2009.

[9] F. H. Panahi, A. Falahati, F. N. Mohammadi, and Fereidoun H. Panahi, "Probability-Based Rake Receiver in Ultra-Wideband Multiple Access Systems," in *IEEE International Conference on Circuit and Systems for Communications, (ICCSC)*, pp. 507 - 511, Shanghai, China, May 2008.

[10] F. H. Panahi, A. Falahati, F. N. Mohammadi, and Fereidoun H. Panahi, "A New Full Diversity Super High Rate Transmission with OSTBCs," in *16th Iranian Conference on Electrical Engineering (ICEE)*, pp. 588-592, Tehran, Iran, May 2008.

[11] F. H. Panahi, A. Falahati, F. N. Mohammadi, and Fereidoun H. Panahi, "A Novel Detection in FH-SS-LPI Wireless Systems," in *16th Iranian Conference on Electrical Engineering (ICEE)*, pp. 582-587, Tehran, Iran, May 2008.

[12] Ali Alshikh, Fereidoun H. Panahi, and T. Ohtsuki, "Q-learning Based Superposed Band Detection" in *IEEE Global Communications Workshop (GLOBECOM)*, (*submitted*), Washington DC, USA, Dec. 2016.

C.3 Articles on Domestic Conference Proceedings

[1] Fereidoun H. Panahi, T. Ohtsuki, W. Jiang, T. Takatori, and K. Uehara, "A Riemannian Optimization Based Filter Designs for Interference Alignment in Multi-User MIMO Interference Channels," in *IEICE-Society*, Sendai, Sept., 2015.

[2] Fereidoun H. Panahi and T. Ohtsuki, "A Fuzzy Q-Learning Based Sensing Policy for Cognitive Radio Systems ," in *IEICE. RCS*, Fukuoka, October, 2012.

[3] Fereidoun H. Panahi and T. Ohtsuki, "A Reinforcement Learning Based Sensing Policy for Cognitive Radio Systems," in *IEICE. RCS*, Tokyo, Feb., 2013.

[4] Fereidoun H. Panahi and T. Ohtsuki, "Coverage Probability Analysis of Cognitive Heterogeneous Cellular Networks Based on Stochastic Geometry," in *IEICE. RCS*, Hamamatsu, July, 2013.

[5] Fereidoun H. Panahi, T. Ohtsuki, W. Jiang, and T. Takatori, "A Riemannian Optimization Based Interference Alignment for Multi-User MIMO Interference Channels," in *IEICE. RCS*, Hokkaido, June , 2015.

[6] Fereidoun H. Panahi, T. Ohtsuki, W. Jiang, T. Takatori, and K. Uehara, "A Centralized Interference Alignment (IA) Design for Multi-User MIMO Interference Channels," in *IEICE-BCT*, Hokkaido, Feb., 2016.

[7] Fereidoun H. Panahi, T. Ohtsuki, W. Jiang, T. Takatori, and K. Uehara, "Interference Alignment for Multi-User MIMO Interference Channels Based on Estimated Uplink Channels," in *IEICE-RCS*, Tokyo, March, 2016.

[8] Fereidoun H. Panahi, T. Ohtsuki, W. Jiang, T. Takatori, and K. Uehara, "Joint Interference Alignment Transceiver Filter Design and Power Allocation for Downlink Multi-User MIMO Interference Channels," in *IEICE-RCS*, Tokyo, March, 2016.

C.4 Awards

[1] IEEE VTS Japan 2015 Young Researchers Encouragement Award (Awarded paper: Fereidoun H. Panahi and T. Ohtsuki, "Analytical Evaluation of Coverage Probability in Two-tier Cognitive Femto Networks," in Proceedings of the 2015 IEEE Vehicular Technology Conference (VTC2015-Spring), pp. 1-6, Glasgow, Scotland, May 2015)

C.5 Others

[1] JSPS Research Fellow (DC2) – JSPS Research Fellowship for Young Scientists (April 2016 - September 2016)

[2] JSPS Post-doctoral Research Fellow (PD) – JSPS Post-doctoral Research Fellowship for Young Scientists (September 2016 - March 2018)

[3] PhD Scholarship from Japan's Ministry of Education and Technology (Monbukagakusho-MEXT)

[4] Master Scholarship from JGC-S Scholarship Foundation (Nikki Saneyoshi/Daisanshu), Japan

[5] NEC C&C Research Grant 2014 from NEC C&C Foundation (Japan)

[6] NEC C&C Research Grant 2013 from NEC C&C Foundation (Japan)

[7] Graduate School Doctoral Student Grant-in-Aid Program 2015, Keio University (selection among all graduate schools)

[8] Graduate School Doctoral Student Grant-in-Aid Program 2014, Keio University (graduate school recommendation)

[9] Keio Graduate School Scholarship 2013 (Administered by the Student Affairs Center, Keio University)

[10] Keio Graduate School Scholarship 2011 (Administered by the Student Affairs Center, Keio University)

[11] Research Assistant (RA), Keio University, Japan (December 2013 - March 2014)

[12] Honors Scholarship (JASSO)

Bibliography

[1] P. Cardieri. "Modeling Interference in Wireless Ad Hoc Networks," *IEEE Communications Surveys & Tutorials*, vol. 12, no.4, 4th 2010.

[2] J. Mitola III and G. Q. Maguire, Jr., "Cognitive radio: making software radios more personal," *IEEE Pers. Commun.*, vol. 6, no. 4, pp. 13 –18, Aug. 1999.

[3] J. Mitola, "Cognitive radio: An integrated agent architecture for software defined radio," Ph.D. dissertation, Royal Institute of Technology (KTH), Stockholm, Sweden, 2000.

[4] L. Giupponi, A. Galindo-Serrano, P. Blasco, and M. Dohler, "Docitive networks: an emerging paradigm for dynamic spectrum management [dynamic spectrum management]," *IEEE Wireless Commun.*, vol. 17, no. 4, pp. 47 –54, Aug. 2010.

[5] S. K. Jayaweera and C. G. Christodoulou, "Radiobots: Architecture, algorithms and real time reconfigurable antenna designs for autonomous, self-learning future cognitive radios," University of New Mexico, Technical Report EECE-TR-11-0001, Mar. 2011. [Online]. Available: http://repository.unm.edu/handle/1928/12306

[6] S. Haykin, "Cognitive radio: brain-empowered wireless communications," *IEEE J. Sel. Areas Commun.*, vol. 23, no. 2, pp. 201–220, Feb. 2005.

[7] N. Devroye, M. Vu, and V. Tarokh, "Cognitive radio networks," *IEEE Signal Processing Mag.*, vol. 25, pp. 12–23, Nov. 2008.

[8] A. Goldsmith, S. A. Jafar, I. Maric, and S. Srinivasa, "Breaking spectrum gridlock with cognitive radios: An information theoretic perspective," *Proc. IEEE*, vol. 97, no. 5, pp. 894–914, May 2009.

[9] J. G. Proakis, Digital Communications, 4th ed. McGraw-Hill, 2001.

[10] H. Urkowitz, "Energy detection of unknown deterministic signals," *Proc. of the IEEE*, vol.55, no.4, pp. 523- 531, April 1967.

[11] J. Lunden, V. Koivunen, A. Huttunen, and H. Poor, "Collaborative cyclostationary spectrum sensing for cognitive radio systems," *IEEE Trans. Signal Process.*, vol. 57, no. 11, pp. 4182 –4195, Nov. 2009.

[12] Z. Tian and G. B. Giannakis, "A wavelet approach to wideband spectrum sensing for cognitive radios," in *Proc. IEEE Int. Conf. Cognitive Radio Oriented Wireless Networks and Commun.*, pp. 1-5, 2006.

[13] Y. Zeng and Y.-C. Liang, "Covariance based signal detections for cognitive radio," in *Proc. IEEE Int. Symposium on New Frontiers in Dynamic Spectrum Access Networks*, Dublin, Ireland, pp. 202–207, Apr. 2007.

[14] T. Yucek and H. Arslan, "A survey of spectrum sensing algorithms for cognitive radio applications," *IEEE Commun. Surveys Tutorials*, vol. 11, no. 1, pp. 116 –130, quarter 2009.

[15] K. Shin, H. Kim, A. Min, and A. Kumar, "Cognitive radios for dynamic spectrum access: from concept to reality," *IEEE Wireless Commun.*, vol. 17, no. 6, pp. 64 –74, Dec. 2010.

[16] A. De Domenico, E. Strinati, and M.-G. Di Benedetto, "A survey on MAC strategies for cognitive radio networks," *IEEE Commun. Surveys Tutorials*, vol. 14, no. 1, pp. 21 –44, quarter 2012.

[17] R. S. Sutton, and A.G. Barto, "Reinforcement learning: An Introduction," MIT Press, Cambridge, MA, 1998.

[18] M. Bkassiny, S. K. Jayaweera, and K. A. Avery, "Distributed reinforcement learning based MAC protocols for autonomous cognitive secondary users," in *20th Annual Wireless and Optical Communications Conference (WOCC '11)*, Newark, NJ, pp. 1 –6, Apr. 2011.

[19] M. L. Puterman, Markov Decision Processes: Discrete Stochastic Dynamic Programming. New York: John Wiley and Sons, 1994.

[20] X. Dong, Y. Li, C. Wu, and Y. Cai, "A learner based on neural network for cognitive radio," in *12th IEEE International Conference on Communication Technology (ICCT '10)*, Nanjing, China, pp. 893 –896, Nov. 2010.

[21] M. M. Ramon, T. Atwood, S. Barbin, and C. G. Christodoulou, "Signal classification with an SVM-FFT approach for feature extraction in cognitive radio," in *SBMO/IEEE MTT-S International Microwave and Optoelectronics Conference (IMOC '09)*, Belem, Brazil, pp. 286 –289, Nov. 2009.

[22] B. Hamdaoui, P. Venkatraman, and M. Guizani, "Opportunistic exploitation of bandwidth resources through reinforcement learning," in *IEEE Global Telecommunications Conference (GLOBECOM '09)*, Honolulu, HI, pp. 1 –6, Dec. 2009.

[23] K.-L. A. Yau, P. Komisarczuk, and P. D. Teal, "Applications of reinforcement learning to cognitive radio networks," in *IEEE International Conference on Communications Workshops (ICC), 2010*, Cape Town, South Africa, pp. 1 –6, May 2010.

[24] Y. Reddy, "Detecting primary signals for efficient utilization of spectrum using Q-learning," in *Fifth International Conference on Information Technology: New Generations (ITNG '08)*, Las Vegas, NV, pp. 360 –365, Apr. 2008.

[25] R. Sutton, D. Mcallester, S. Singh, and Y. Mansour, "Policy gradient methods for reinforcement learning with function approximation," in *Proc. 12th conference on Advances in Neural Information Processing Systems (NIPS '99)*. Denver, CO: MIT Press, pp. 1057–1063, 2001.

[26] M. Kumarasamy, and A.J. Ratnakumar, "An Implementation of Machine Learning Systems using Fuzzy Distributed Artificial Intelligent Systems," *Int. J. of Eng. and Technol.*, vol. 2, No. 8, August, 2012.

[27] M.J. Er, and C. Deng, "Online tuning of fuzzy inference systems using dynamic fuzzy Q-learning," *IEEE Trans. Systems, Man, and Cybernetics, Part B: Cybernetics*, vol.34, no.3, pp. 1478-1489, June 2004.

[28] D.F. Sameh, and S.M. Howard, "Q(λ)-learning fuzzy logic controller for differential games," *Int. Conf. on Intelligent Systems Design and Applications (ISDA)*, pp. 109-114, Dec. 2010.

[29] "More Than 50 Billion Connected Devices", Ericsson White Paper, February 2011.

[30] J. Andrews, H. Claussen, M. Dohler, S. Rangan, and M. Reed, "Femtocells: Past, Present, and Future," *IEEE Journal on Sel. Areas in Comm.*, vol. 30, no. 3, pp. 497–508, 2012.

[31] H. ElSawy, E. Hossain, and D. I. Kim, "HetNets with cognitive small cells: User offloading and Distributed channel allocation techniques," *IEEE Communications Magazine, Special Issue on "Heterogeneous and Small Cell Networks (HetSNets)"*, vol. 51, no. 6, 2013.

[32] D. Cao, S. Zhou, and Z. Niu, "Improving the energy efficiency of two-tier heterogeneous cellular networks through partial spectrum reuse," *IEEE Trans. on Wireless Comm.*, vol. 12, no. 8, pp. 4129-4141, 2013.

[33] K. Gilhousen, I. Jacobs, R. Padovani, A. J. Viterbi, L. Weaver, and C. Wheatley, "On the Capacity of a Cellular CDMA System," *IEEE Trans. on Veh. Tech.*, vol. 40, no. 2, pp. 303–312, 1991.

[34] H. ElSawy, E. Hossain, M. Haenggi, "Stochastic Geometry for Modeling, Analysis, and Design of Multi-Tier and Cognitive Cellular Wireless Networks: A Survey," *IEEE Comm. Surveys & Tutorials*, vol. 15, no.3, pp. 996-1019, 2013.

[35] K. Gilhousen, I. Jacobs, R. Padovani, A. J. Viterbi, L. Weaver, and C. Wheatley, "On the Capacity of a Cellular CDMA System," *IEEE Trans. on Veh. Tech.*, vol. 40, no. 2, pp. 303–312, 1991.

[36] J. Xu, J. Zhang, and J. G. Andrews, "On the Accuracy of the Wyner Model in Cellular Networks," *IEEE Trans. on Wireless Comm.*, vol. 10, no. 9, pp. 3098–3109, 2011.

[37] J. G. Andrews, F. Baccelli, R. K. Ganti, "A Tractable Approach to Coverage and Rate in Cellular Networks," *IEEE Trans. on Comm.*, vol.59, no.11, pp.3122-3134, 2011.

[38] S. A. R. Zaidi, D. C. McLernon, M. Ghogho, "Outage probability analysis of cognitive radio networks under self-coexistence constraint," *44th Annual Conference on Information Sciences and Systems (CISS)*, pp.1-6, 17-19, 2010.

[39] R. K. Ganti and M. Haenggi, "Interference and Outage in Clustered Wireless Ad Hoc Networks," *IEEE Trans. on Information Theory*, vol. 55, pp. 4067–4086, 2009.

[40] A. Hasan and J. G. Andrews, "The Guard Zone in Wireless Ad hoc Networks," *IEEE Trans. on Wireless Comm.*, vol. 4, no. 3, pp. 897–906, 2007.

[41] C.-H.Lee and M. Haenggi, "Interference and Outage in Poisson Cognitive Networks," *IEEE Trans. on Wireless Comm.*, vol. 11, pp. 1392–1401, 2012.

[42] V. R. Cadambe and S. A. Jafar, "Interference alignment and degrees of freedom of the K-user interference channel," *IEEE Trans. Inf. Theory*, vol. 54, no. 8, pp. 3425–3441, Aug. 2008.

[43] O. El Ayach, S. W. Peters, and R. W. Heath, Jr., "The practical challenges of interference alignment," *IEEE Wirel. Commun.*, vol. 20, no. 1, pp. 35–42, Feb. 2013.

[44] F. L. Blasco, F. Rossetto, and G. Bauch, "Time interference alignment via delay offset for long delay networks," *IEEE Trans. Commun.*, vol. 62, no. 2, pp. 590–599, Feb. 2014.

[45] B. Da and R. Zhang, "Exploiting interference alignment in multi-cell cooperative OFDMA resource allocation," in *Proc. IEEE Globecom'11*, pp. 1–5, Houston, TX, Dec. 2011.

[46] H. Huang, V. K. N. Lau, Y. Du, and S. Liu, "Robust lattice alignment for K-user MIMO interference channels with imperfect channel knowledge," *IEEE Trans. Signal Process.*, vol. 59, no. 7, pp. 3315–3325, Jul. 2011.

[47] S. M. Perlaza, N. Fawaz, S. Lasaulce, and M. Debbah, "From spectrum pooling to space pooling: Opportunistic interference alignment in MIMO cognitive networks," *IEEE Trans. Signal Process.*, vol. 58, no. 7, pp. 3728–3741, Jul. 2010.

[48] H. J. Yang, W.-Y. Shin, B. C. Jung, and A. Paulraj, "Opportunistic interference alignment for MIMO interfering multiple-access channels," *IEEE Trans. Wireless Commun.*, vol. 12, no. 5, pp. 2180–2192, May 2013.

[49] B. Guler and A. Yener, "Selective interference alignment for MIMO cognitive femtocell networks," *IEEE J. Sel. Areas Commun.*, vol. 32, no. 3, pp. 439–450, Mar. 2014.

[50] F. Pantisano, M. Bennis, W. Saad, M. Debbah, and M. Latva-aho, "Interference alignment for cooperative femtocell networks: A game theoretic approach," *IEEE. Trans. Mob. Comput.*, vol. 12, no. 11, pp. 2233–2246, Nov. 2013.

[51] R. Tandon, S. Mohajer, H. V. Poor, and S. Shamai, "Degrees of freedom region of the MIMO interference channel with output feedback and delayed CSIT," *IEEE Trans. Inf. Theory*, vol. 59, no. 3, pp. 1444–1457, Mar. 2013.

[52] B. Rankov and A. Wittneben, "Spectral efficient protocols for half duplex fading relay channels," *IEEE J. Sel. Areas Commun.*, vol. 25, no. 2, pp. 379–389, Feb. 2007.

[53] R. K. Mungara, G. George, A. Lozano, "Overhead and Spectral Efficiency of Pilot-Assisted Interference Alignment in Time-Selective Fading Channels," *IEEE Trans. on Wireless Commun.*, vol.13, no.9, pp.4884-4895, 2014.

[54] Cho Sungyoon, H. Kaibin, K. K. Dong, V.K.N. Lau, C. Hyukjin, S. Hanbyul, K. Byoung-Hoon, "Feedback-Topology Designs for Interference Alignment in MIMO Interference Channels," *IEEE Trans. on Signal Processing*, vol.60, no.12, pp.6561-6575, Dec. 2012.

[55] N. Zhao, F. R. Yu, and V. C. M. Leung, "Opportunistic communications in interference alignment networks with wireless power transfer," *IEEE Wireless Commun.*, vol. 22, no. 1, pp. 88–95, Feb. 2015.

[56] K. Gomadam, V.R. Cadambe, S.A. Jafar, "A Distributed Numerical Approach to Interference Alignment and Applications to Wireless Interference Networks," *IEEE Trans. on Information Theory*, June 2011.

[57] I. Santamaria, O. Gonzalez, R. Heath, and S. Peters, "Maximum sum rate interference alignment algorithms for MIMO channels," in *Proc. IEEE GLOBECOM*, 2010, pp. 1–6.

[58] Y. C. Liang, Y. Zeng, E. Peh, and A. T. Hoang, "Sensing-throughput tradeoff for cognitive radio networks," IEEE Trans. Wireless Commun., vol. 7, no. 4, pp. 1326-1337, Apr. 2008.

[59] A. Ghasemi, E.S. Sousa, "Spectrum sensing in cognitive radio networks: requirements, challenges and design trade-offs," *IEEE Commun. Mag.*, Vol. 46, no.4, pp. 32-39, April 2008.

[60] B. Razavi, "Cognitive Radio Design Challenges and Techniques," *IEEE Journal of Solid-State Circuits*, vol.45, no.8, pp. 1542-1553, Aug. 2010.

[61] S. Geirhofer, L. Tong, and B. M. Sadler, "Cognitive medium access: Constraining interference based on experimental models," *IEEE J. Sel. Areas Commun.*, vol. 26, no. 1, pp. 95âĂŞ105, Jan. 2008.

[62] Q. Zhao, and Y. Chen, "Decentralized cognitive MAC for opportunistic spectrum access in ad hoc networks: A POMDP framework," *IEEE J. Sel. Areas Commun.*, vol. 25, no. 3, pp. 589-600, Apr. 2007.

[63] K. W. Choi, "Adaptive Sensing Technique to Maximize Spectrum Utilization in Cognitive Radio," *IEEE Trans. Veh. Tech.*, vol.59, no.2, pp.992-998, Feb. 2010.

[64] G. E. Monahan, "A survey of partially observable Markov decision processes: theory, models, and algorithms," *Management Science*, vol. 28, no. 1, pp. 1-16, Jan. 1982.

[65] Z. Enlu, M.C. Fu, S.I. Marcus, "Solving Continuous-State POMDPs via Density Projection," *IEEE Trans. Automatic Control*, vol.55, no.5, pp.1101-1116, May 2010.

[66] Z. Weidong, Y. Baozong, "Trainbot: A spoken dialog system using partially observable Markov Decision Processes," *Wireless, Mob. and Multimedia Net. (ICWMNN 2010), IET 3rd Int. Conf.*, pp.381-384, 26-29 Sept. 2010.

[67] D. Braziunas, "POMDP solution methods," 2003.

[68] C. Watkins, P. Dayan, "Q-learning, Machine Learning," pp. 279-292, 1992.

[69] C. Ghosh, C. Cordeiro, D. P. Agrawal, and M. B. Rao, "Markov chain existence and hidden Markov models in spectrum sensing," *IEEE Pervasive Computing and Commun.*, pages 1-6, March 2009.

[70] S. Geirhofer, L. Tong, and B. Sadler, "Dynamic spectrum access in the time domain: Modeling and exploiting white space," *IEEE Commun. Mag.*, vol. 45, no. 5, pp. 66-72, May 2007.

[71] S. Geirhofer, L. Tong, and B. Sadler, "A measurement-based model for dynamic spectrum access in WLAN channels," in *Proc. IEEE Military Commun. Conf.*, Washington, D.C., USA, Oct. 2006.

[72] K. Murphy, "A survey of POMDP solution techniques," tech. rep., 2000. Technical Report, UC Berkeley.

[73] D. Bertsekas and J. Tsitsiklis, "Neural Dynamic Programming," Athena Scientific, Belmont, MA, 1996.

[74] T. Takagi and M. Sugeno, "Fuzzy identification of systems and its applications to modeling and control," *IEEE Trans. Systems, Man and Cybernetics*, SMC-15(1), pp. 116-132. 1985.

[75] R. Pfeifer and C. Scheier, "Understanding Intelligence," MIT Press, 1999.

[76] A. Akbulut, T. Adiguzel, A. E. Yilmaz, "Estimation of Time-Varying Channel State Transition Probabilities for Cognitive Radio Systems by means of Particle Swarm Optimization," *Radio engineering*, vol. 21, no. 1, pp. 104-109, 2012.

[77] X. Long, X. Gan, Y. Xu, J. Liu, M. Tao, "An Estimation Algorithm of Channel State Transition Probabilities for Cognitive Radio Systems, " *Cognitive Radio Oriented Wireless Net. and Commun., CrownCom. 3rd Int. Cont.,* pp.1-4, 15-17 May 2008.

[78] L. R. Rabiner, "A tutorial on hidden Markov models and selected applications in speech recognition," *Proc. IEEE*, vol. 77, no. 2, pp. 257-286, Feb. 1989.

[79] Sun Zhanwei, G.J. Bradford, J.N. Laneman, "Sequence Detection Algorithms for PHY-Layer Sensing in Dynamic Spectrum Access Networks," *Selected Topics in Sig. Proc., IEEE Journal*, vol.5, no.1, pp. 97-109, Feb. 2011.

[80] N.M. Laird, "Nonparametric Maximum Likelihood Estimation of a Mixing Distribution," *J. Amer. Stat. Asso.73*, pp. 805-811, 1978.

[81] Brian G.Leroux, "Maximum-Penalized-Likelihood Estimation for Independent and Markov Dependent Mixture Models," *Biometerics 48*, pp. 545-558, 1992.

[82] R. K. Sharma and J. W. Wallace, "Indoor shadowing correlation measurements for cognitive radio studies," in *Proc. 2009 IEEE Antennas and Propag. Society Intl. Symp*, Charleston, SC, USA, June 2009, pp. 1-4.

[83] F. Ye, N. Yi, Y. Wang, "EM Algorithm for Training High-order Hidden Markov Model with Multiple Observation Sequences," *Journal of Information and Computational Science*, 8(10), 1761-1777 (2011).

[84] S. Cheng, S. Lien, F. hu, and K. Chen, "On Exploiting Cognitive Radio to Mitigate Interference in Macro/Femto Heterogeneous Networks," *IEEE Wireless Comm. Mag*, vol. 18, no. 3, pp. 40–47, 2011.

[85] V. Chandrasekhar, J.G. Andrews, Tarik Muharemovict, Zukang Shen, and Alan Gatherer, "Power control in two-tier femtocell networks," *IEEE Trans. on Wireless Comm.*, 8(8):4316–4328, 2009.

[86] H.S. Jo, C. Mun, J. Moon, and J.G. Yook, "Interference mitigation using uplink power control for two-tier femtocell networks," *IEEE Trans. on Wireless Comm.*, vol. 8, no 10, pp. 4906–4910, 2009.

[87] V. Chandrasekhar and J.G. Andrews, "Spectrum allocation in tiered cellular networks," *IEEE Trans. on Comm.*, vol. 57, no. 10, pp. 3059-3068, 2009.

[88] J. Xiang, Y. Zhang, T. Skeie, and L. Xie, "Downlink spectrum sharing for cognitive radio femtocell networks," *IEEE Sys. Journal*, vol. 4, no. 4, pp. 524-534, 2010.

[89] Y. Shi, Y. T. Hou, H. Zhou, and S. F. Midkiff, "Distributed cross-layer optimization for cognitive radio networks," *IEEE Trans. On Veh. Tech.*, vol. 59, no. 8, pp. 4058-4069, 2010.

[90] H. Dhillon, R. Ganti, F. Baccelli, and J. Andrews, "Modeling and Analysis of K-Tier Downlink Heterogeneous Cellular Networks," *IEEE J. Selected Areas in Comm.*, vol. 30, no. 3, pp. 550-560, 2012.

[91] H. Jo, Y. Sang, P. Xia, and J. Andrews, "Outage Probability for Heterogeneous Cellular Networks with Biased Cell Association," *Proc. IEEE GlobeCom*, 2011.

[92] T. Novlan, R. Ganti, A. Ghosh, and J. Andrews, "Analytical Evaluation of Fractional Frequency Reuse for OFDMA Cellular Networks," *IEEE Trans. Wireless Comm.*, vol. 10, no. 12, pp. 4294-4305, Dec. 2011.

[93] T. Novlan, R. Ganti, A. Ghosh, and J. Andrews, "Analytical Evaluation of Fractional Frequency Reuse for Heterogeneous Cellular Networks," *IEEE Trans. Comm.*, vol. 60, no. 7, pp. 2029-2039, July 2012.

[94] F. H. Panahi, T. Ohtsuki, "Stochastic geometry based analytical modeling of cognitive heterogeneous cellular networks," *IEEE International Conf. on Comm. (ICC)*, pp. 5281-5286, 2014.

[95] H. ElSawy and E. Hossain, "Two-tier HetNets with cognitive femtocells: Downlink performance modeling and analysis in a multi-channel environment," *IEEE Trans. on Mobile Computing*, vol.13, no.3, pp.649-663, 2014.

[96] H. ElSawy and E. Hossain, "Channel assignment and opportunistic spectrum access in two-tier cellular networks with cognitive small cells," in *Proc. IEEE Global Communications Conference (Globecom)*, 2013.

[97] H. ElSawy and E. Hossain, "On cognitive small cells in two-tier heterogeneous networks," Workshop on Spatial Stochastic Models for Wireless Networks (SpaSWiN), in conjunction with 11th Intl. Symposium on Modeling and Optimization in Mobile, Ad Hoc, and Wireless Networks (WiOpt), 2013.

[98] M. Haenggi and R. K. Gant, Interference in Large Wireless Networks. Foundations and Trends in Networking, NOW Publisher, 2008, vol. 3, no. 2.

[99] IEEE Instrumentation and Measurement Society, "IEEE 1588 standard for a precision clock synchronization protocol for networked measurement and control systems," in *IEEE Std 1588*, 2008.

[100] Q. Wu, G. Ding, J. Wang, and Y.-D. Yao, "Spatial-temporal opportunity detection in spectrum-heterogeneous cognitive radio networks: Two dimensional sensing," *IEEE Trans. on Wireless Comm.*, vol. 12, no. 2, pp. 516–526, Feb. 2013.

[101] Y. Chen, Q. Zhao, and A. Swami, "Joint design and separation principle for opportunistic spectrum access in the presence of sensing errors," *IEEE Trans. Inf. Theory*, vol. 54, no. 5, pp. 2053-2071, 2008.

[102] F. Paisana, N. Marchetti, and L. A. Dasilva, "Radar , TV and Cellular Bands : Which Spectrum Access Techniques for which Bands?" *IEEE Comm. Surveys & Tutorials*, vol.16, no.3, pp.1193-1220, Third Quarter 2014.

[103] Q. Chen, M. Motani, W.-C.Wong, and Y.-C. Liang, "Opportunistic spectrum access protocol for cognitive radio networks," in *Proc. IEEE International Conference on Comm. (ICC)*, pp. 1–6, 2011.

[104] Li. Xiaofan, Liu Hui, S. Roy, Zhang Jianhua, Zhang Ping, C. Ghosh, "Throughput Analysis for a Multi-User, Multi-Channel ALOHA Cognitive Radio System, " *IEEE Trans. on Wireless Comm.*, vol. 11, no. 11, pp. 3900-3909, 2012.

[105] L. Luo, C. Ghosh, and S. Roy, "Joint optimization of spectrum sensing for cognitive radio networks," in *Proc. IEEE Global Telecommunications Conference (GLOBECOM)*, pp. 1 –5, 2010.

[106] L. Wang and V. Fodor, "On the gain of primary exclusion region and vertical cooperation in spectrum sharing wireless networks," *IEEE Trans. Veh. Tech.*, vol. 61, no. 8, pp. 3746–3758, 2012.

[107] M. Haenggi: Outage, local throughput, and capacity of random wireless networks. *IEEE Trans. on Wireless Comm.*, 8(8), 4350–4359 (2009).

[108] J-M.Dricot, G. Ferrari, A. Panahandeh, Fr. Horlin and Ph. De Doncker: Probabilistic Coexistence and Throughput of Cognitive Dual-Polarized Networks. *EURASIP Journal on Wireless Comm. and Networking*, 2010:387625.

[109] Y. Fadlallah, K. Amis, A. Aïssa-El-Bey and R. Pyndiah "Interference alignment for a multi-user SISO interference channel," *EURASIP Journal on Wireless Communications and Networking*, 10.1186/1687-1499-2014-79.

[110] O. El Ayach, S. W. Peters, and R. W. Heath Jr., "The Feasibility of Interference Alignment Over Measured MIMO-OFDM Channels," *IEEE Trans. on Vehicular Technology*, vol.59, no.9, pp.4309-4321, Nov. 2010.

[111] T. Gou and S. A. Jafar, "Degrees of freedom of the K user$M \times N$ MIMO interference channel," *IEEE Trans. on Inform. Theory*, vol. 56, no. 12, pp. 6040-6057, Dec. 2010.

[112] Cho Sungyoon, H. Kaibin, K. K. Dong, V.K.N. Lau, C. Hyukjin, S. Hanbyul, K. Byoung-Hoon, "Feedback-Topology Designs for Interference Alignment in MIMO Interference Channels," *IEEE Trans. on Signal Processing*, vol.60, no.12, pp.6561-6575, Dec. 2012.

[113] T.E. brudan, J. Eriksson, V. Koivunen, "Steepest Descent Algorithms for Optimization Under Unitary Matrix Constraint," *IEEE Trans. on Signal Processing,* vol.56, no.3, pp.1134-1147, Mar. 2008.

[114] Y. Nishimori, S. Akaho, and M. D. Plumbley, "Riemannian optimization method on the flag manifold for independent subspace analysis," in *Proc. 6th Int. Conf. Independent Compon.Anal. Blind Signal Separat.*, vol. 3889, pp. 295–302. Mar. 2006.

[115] M. Chiang, P. Hande, T. Lan and C. W. Tan, "Power Control in Wireless Cellular Networks," *Foundations and Trends in Networking*, vol. 2, pp. 381-533, Apr. 2008.

[116] V. G. Douros and G. C. Polyzos, "Review of some fundamental approaches for power control in wireless networks," *Elsevier Computer Communications*, vol. 34, no. 13, 2011.

[117] M. Hong and Z.-Q.Luo, "Signal processing and optimal resource allocation for the interference channel," in Library in Signal Processing. New York: Academic Press, 2013, vol. 2, *Communications and Radar Signal Processing*, ch. 8, pp. 409–462.

[118] E. Bjornson and E. Jorswieck, "Optimal resource allocation in coordinated multi-cell systems," *Foundations and Trends in Communications and Information Theory*, vol. 9, no. 2-3, pp. 113-181, 2013.

[119] C. Y. Wong, R. S. Cheng, K. B. Letaief and R. D. Murch, "Multiuser OFDM with adaptive subcarrier, bit and power allocation," in *IEEE Journal on Selected Areas in Communications*, vol. 17, pp. 1747-1758, Oct. 1999.

[120] W. Rhee and J. M. Cioffi, "Increase in capacity of multiuser OFDM system using dynamic subchannel allocation," in *Proc. IEEE Vehicular Technology Conference*, vol. 2, pp. 1085-1089, 2000.

[121] H. Yin and H. Liu, "An Efficient Multiuser Loading Algorithm for OFDM-based Broadband Wireless Systems," in *Proc. IEEE GLOBECOM*, vol. 1, pp. 103-107, 2000.

[122] N. U. Hassan and M. Assaad, "Dynamic resource allocation in multiservice OFDMA systems with dynamic queue control," *IEEE Trans. on Commun.*, vol. 59, issue 6, pp. 1664-1674, Jun. 2011.

[123] X. Chen and C. Yuen, "Performance analysis and optimization for interference alignment over MIMO interference channels with limited feedback," *IEEE Trans. Signal Process.*, vol. 62, no. 7, pp. 1785-1795, Apr. 2014.

[124] N. U. Hassan and M. Assaad, "Resource Allocation in Multiuser OFDMA System: Feasibility and Optimization Study," in *Proc. IEEE Wireless Commun. and Networking Conference*, pp. 1-6, Apr. 2009.

[125] F.H. Panahi, T. Ohtsuki, W. Jiang, Y. Takatori, "Interference alignment for multi-user MIMO interference channels via a Riemannian optimization approach, " in *Proc. PIMRC*, pp.287-292, Sep. 2015.

[126] A. Edelman, T.A. Arias, and S.T. Smith, "The Geometry of algorithms with orthogonality constraints," *SIAM Journal on Matrix Analysis and Applications*, 20 (2), pp.303-353, 1998.

[127] Y. Nishimori, S. Akaho, "Learning algorithms utilizing quasi-geodesic flows on the stiefel manifold," *Neuro computing* 67, 106–135 (2005).

[128] J. Thukral and H. Bolcskei, "Interference alignment with limited feedback," in *Proc., IEEE Int. Symp. Inform. Theory*, June. 2009.

[129] C. W. Tan, M. Chiang, and R. Srikant, "Maximizing sum rate and minimizing MSE on multiuser downlink: Optimality, fast algorithms and equivalence via max-min SIR," in *Proc. IEEE Int. Symp. Inf. Theory*, Jun. 2009, pp. 2669–2673.

[130] R. Sun and Z.-Q.Luo, "Globally optimal joint uplink base station association and power control for max-min fairness," in *Proc. IEEE Int. Conf. Acoust., Speech, Signal Process.(ICASSP).*

[131] H. Sung, S. H. Park, K. J. Lee, I. Lee, "Linear precoder designs for K user interference channels," *IEEE Trans. on Wireless Commun.,* vol. 9, no. 1, pp. 291-301, Jan. 2010.

[132] Ye Sigen, R.S. Blum, "Optimized signaling for MIMO interference systems with feedback," *IEEE Trans. on Signal Processing*, vol.51, no.11, pp.2839-2848, Nov. 2003.

[133] Y. Nishimori, "A Note on Riemannian Optimization Methods on the Stiefel and the Grassmann Manifolds," *International Symposium on Nonlinear Theory and its Application (NOLTA2005)*, Oct. 2005.

[134] J. Jose, A. Ashikhmin, T. L. Marzetta, and S. Vishwanath, "Pilot contamination and precoding in multi-cell TDD systems," *IEEE Trans. Wireless Commun.*, vol. 10, no. 8, pp. 2640–2651, Aug. 2011.

[135] L. You, X. Gao, X.-G. Xia, N. Ma, and Y. Peng, "Pilot reuse for massive MIMO transmission over spatially correlated Rayleigh fading channels," *IEEE Trans. Wireless Commun.*, vol. 14, no. 6, pp. 3352–3366, June 2015.

[136] S. Coleri, M. Ergen, A. Puri, and A. Bahai, "Channel estimation techniques based on pilot arrangement in OFDM systems," *IEEE Trans. Broadcast.*, vol. 48, no. 3, pp. 223–229, Sep. 2002.

[137] S. Park, B. Shim, and J. Choi, "Iterative channel estimation using virtual pilot signals for MIMO-OFDM systems," *IEEE Trans. Signal Process.*, vol. 63, no. 12, pp. 3032–3045, Jun. 2015.

[138] C.M. Yetis, G. Tiangao, S.A. Jafar, A.H. Kayran, "On Feasibility of Interference Alignment in MIMO Interference Networks," *IEEE Trans. on Signal Processing*, vol.58, no.9, pp.4771-4782, Sept. 2010.

[139] F.H. Panahi and T. Ohtsuki, "Optimal channel-sensing policy based on fuzzy q-learning process over cognitive radio systems," in *IEEE International Conf. on Commun. (ICC)*, pp. 2677–2682, June 2013.

[140] A.A. Kilbas, H.M. Srivastava, J.J. Trujillo: Theory and Applications of Fractional Differential Equations. Elsevier B.V, Netherlands (2006).